

**RELIABILITY ANALYSIS OF
STATIC SEALED JOINTS**

Thesis submitted for the degree of
Doctor of Philosophy
at the University of Leicester

by

HONG YUE BSc. MSc.
Department of Engineering
University of Leicester

October 1995

UMI Number: U543225

All rights reserved

INFORMATION TO ALL USERS

The quality of this reproduction is dependent upon the quality of the copy submitted.

In the unlikely event that the author did not send a complete manuscript and there are missing pages, these will be noted. Also, if material had to be removed, a note will indicate the deletion.



UMI U543225

Published by ProQuest LLC 2015. Copyright in the Dissertation held by the Author.
Microform Edition © ProQuest LLC.

All rights reserved. This work is protected against
unauthorized copying under Title 17, United States Code.



ProQuest LLC
789 East Eisenhower Parkway
P.O. Box 1346
Ann Arbor, MI 48106-1346

Reliability Analysis of Static Sealed Joints

(PhD Thesis)

HONG YUE

Abstract

Leaking, friction and wear of seals are concerns for machine designers and users everywhere. Although perfect sealing may be the general aim, in practice, considering apparently identical seals in the same application, some may seal while some may not. This is due, at least in part, to surface-related random phenomena. Therefore, the importance of considering the reliability of sealed joints cannot be overemphasized. Up to now, there is no paper in the published literature about the reliability analysis of static sealed joints.

All of these facts provide the motivation for the current research work. A computer simulation model for the leakage analysis of static sealed joints has been developed based on the percolation theory. The features of the leakage simulation model can be concluded as follows:

- (1) It reveals the effect of random properties of rough surfaces on the sealing performance and makes it possible to apply the statistical concepts in discussing the sealing reliability of static sealed joints;
- (2) It provides much simpler and more economic tool for the statistical analysis of leakage by computer simulation than by experiments;
- (3) It makes it possible to describe the leakage phenomenon more accurately using the leakage path model instead of the clearance between surface centre-lines;
- (4) It eliminates the need for individual asperity model of rough surfaces, because the actual digitized surface is used directly.

The relationship between the leakage probability and the applied load, which is of great general interest to the designers of static sealed joints, has been predicted by the leakage simulation model. The simulated results show that for a given leakage probability, the required load will increase as the value of RMS height σ increases or the value of correlation length λ^* decreases. It is confirmed that a certain value of contact ratio can be used as the criterion for identifying the reliability of static sealed joints with a certain confidence level. The contact ratio criterion provides a simple, inexpensive and useful tool to evaluate the effects of rough surfaces, material properties and applied load on the sealing reliability of static sealed joints. However, in order to be of practical use, experimental work is required to evaluate its validity.

Acknowledgement

I am deeply indebted to my supervisor, Dr. W. Manners for his constant guidance and encouragement. He kept me on the right track and gave me overall support throughout the research.

Members of the Department of Engineering provided me with much assistance. Special thanks are due to Dr. D.A. Kelly for his advice and assistance.

I would like to thank Leicester of University which provided me with excellent research environment. Some of the technical inquiries about the computer problems and software support offered by the staff of the computer centre in Leicester of University is also acknowledged.

No words can express my gratitude towards my family, who supported me financially and morally all the way through this lengthy, hard and challenging work and gave me the opportunity to explore and to fulfil my dreams, without asking for anything in return.

I would like to thank you all from the bottom of my heart.

Declaration

This thesis is the result of my own work. Any reference to the work of other researchers is clearly indicated in the text.

None of the material contained in this thesis has been submitted in support of an application for another degree or qualification of this or any other university or institute of learning.

This thesis is 231 pages in length.

.....
HONG YUE

Contents

<i>Abstract</i>	i
<i>Acknowledgement</i>	ii
<i>Declaration</i>	iii
<i>List of Tables</i>	xi
<i>List of Figures</i>	xiii
<i>Nomenclature</i>	xvii
 <i>CHAPTER 1.</i>	
<i>Introduction</i>	1
1.1 Research Objectives	1
1.2 Research Background	5
1.3 Thesis Overview	10

CONTENTS

CHAPTER 2.

<i>Characterisation and Topography of Engineering Surfaces</i>	16
2.1 Introduction	16
2.2 Measurement of Surface Topography	18
2.3 Analytical Methods of Surface Characterisation	19
2.3.1 Average Roughness Parameters	21
2.3.1.1 Centre Line Average	21
2.3.1.2 Root Mean Square (RMS)	22
2.3.2 Statistical Analysis - Probability Density Function (PDF)	23
2.3.3 Random Process Methods	25
2.3.3.1 Autocorrelation Function	25
2.3.3.2 Power Spectral Density Function	29
2.4 Topography of Engineering Surfaces	30
2.4.1 Typical Average Roughness	30
2.4.2 Isotropic and Anisotropic Surfaces	32
2.4 Summary	34

CHAPTER 3.

<i>Random Rough Surfaces Numerical Simulation</i>	36
3.1 Introduction	36
3.2 Numerical Simulation Algorithm	38
3.2.1 Input Matrix of Random Numbers	39
3.2.2 Linear Transformation on Input Matrix	40
3.2.2.1 Autocorrelation Matrix	41
3.2.2.2 Linear Transformation Coefficients	41

CONTENTS

3.3	Numerical Simulation Parameters	44
3.3.1	Correlation Length	44
3.3.2	Sampling Interval	45
3.3.3	Surface Anisotropy	47
3.4	Computer Program Structure	50
3.5	Numerical Examples	53
3.5.1	Generated Rough Surfaces	53
3.5.2	Comparison of Numerical Simulation and Theoretical Results	62
3.6	Conclusion	69

CHAPTER 4.

<i>Contact of Rough Surfaces</i>	71	
4.1	Introduction	71
4.2	Contact Models of Rough Surfaces	72
4.2.1	Stochastic Contact Model	72
4.2.2	Numerical Contact Model	76
4.3	Contact Geometry	82
4.3.1	Modified Original Surface Profile	84
4.3.2	Gap between Two Surfaces	86
4.3.3	Deformed Surface Shape	88
4.4	Boundary Condition of Contact	89
4.4.1	Displacement Boundary Condition	89
4.4.2	Pressure Boundary Condition	89
4.5	Deformation of Rough Surface Contact	91

CONTENTS

CHAPTER 5.

Two-dimensional Numerical Model for the Elastic Contact of Rough

<i>Surfaces</i>	96
5.1 Introduction	96
5.2 Statement of Contact Problem	97
5.2.1 Constrains and Assumptions	97
5.2.2 Distributed normal tractions	98
5.3 Numerical Solution	99
5.3.1 Types of Pressure Elements	100
5.3.2 Contact Pressure Element Equations	102
5.3.3 Formulation of Numerical Solution	104
5.4 Numerical Solution Techniques	106
5.4.1 Variational Methods	107
5.4.2 Quadratic Programming Formulation	110
5.5 Algorithm and Computer Programm	114
5.6 Numerical Examples	119
5.6.1 Contact of Two Elastic Smooth Cylindrical Bodies	119
5.6.2 Contact of Rough Surfaces	122
5.7 Comparison of Numerical and Stochastic Results	126

CHAPTER 6.

Three-dimensional Numerical Model for the Elastic Contact of Rough

<i>Surfaces</i>	131
6.1 Introduction	131
6.2 Statement of Contact Problem	132

CONTENTS

6.2.1	Constrains and Assumptions	132
6.2.2	Generalized Boussinesq Solution	133
6.3	Numerical Method	134
6.3.1	Contact Pressure Element Equation	135
6.3.2	Formulation of Numerical Solution	136
6.3.3	Quadratic Programming Formulation	140
6.4	Numerical Examples	141
6.4.1	Contact of Two Elastic Smooth Spheres	141
6.4.2	Contact of Rough Surfaces	144
6.5	Comparison of Numerical and Stochastic Results	147
6.6	Conclusions	153

CHAPTER 7.

<i>Prediction of Leakage Probability and Criteria for Identifying Reliability of Static Sealed Joints</i>	155	
7.1	Introduction	155
7.2	Theoretical Background - Percolation Theory	156
7.3	Simulation Analysis of Leakage of Static Sealed Joints	160
7.3.1	Simulation Model of Static Sealed Joints	160
7.3.2	Production of Contact Map	162
7.3.3	Computer Check of Leakage Paths	164
7.4	Prediction of Leakage and Sealing Probability	170
7.4.1	Simulation Procedure of Prediction of Leakage Probability	170
7.4.2	Leakage Probability-v-Load Relationship	173
7.4.2.1	Effect of Rough Surfaces	174

CONTENTS

7.4.2.2	Effect of Simulation Parameters . . .	180
7.4.2.2.1	Effect of Sampling Interval . .	181
7.4.2.2.2	Effect of Number of Sampling Points	183
7.5	Criteria for Identifying Sealing Reliability of Static Sealed Joints	185
7.5.1	Relationship between Sealing Reliability and Sealing Probability	185
7.5.2	Criteria for Identifying Sealing Reliability of Static Sealed Joints with Isotropic Surfaces	186
7.5.3	Effect of Surface Anisotropy on Contact Ratio Criteria	192
7.6	Conclusion	195

CHAPTER 8.

<i>Summary and Further Work</i>	198
8.1 Conclusion	198
8.1.1 Overall Conclusions	198
8.1.2 Numerical Simulation of Random Rough Surface	202
8.1.3 Numerical Contact Models of Rough Surfaces	203
8.1.4 Computer Check of Leakage Paths	205
8.2 Suggestions for Further work	206
8.2.1 Numerical Simulation of Random Rough Surfaces	206
8.2.2 Numerical Contact of Rough Surfaces	207
8.2.3 Reliability Analysis of Static Sealed Joints	209

CONTENTS

APPENDIX A.

Quadratic Programming Routine - E04NAF 211

APPENDIX B.

Calculation of Bandwidth Parameter 213

APPENDIX C.

Simulated Results of Leakage Probability of Static Sealed Joints 216

REFERENCES 223

List of Tables

Table 3.1	ACF values of the expected and the generated surface in Figure 3.4(a)	65
Table 3.2	ACF values of the expected and the generated surface in Figure 3.4(b)	66
Table 4.1	Material properties of typical static sealed joints	93
Table 4.2	Values of the plasticity index ψ_c for typical sealed joints	94
Table 5.1	Comparisons between Hertzian and numerical solution . .	121
Table 5.2	Results comparing numerical and stochastic values of P_d/A_c	128
Table 5.3	Results comparing numerical and stochastic values of P_d/A_c showing the effect of sampling interval	129
Table 6.1	Bandwidth parameters and second moment of PSD	149
Table 6.2	Results comparing numerical and stochastic values of P_d/A_c	150
Table 6.3	Parameters used in GW model	151
Table 6.4	Results comparing numerical and stochastic values of P_d/A_c	152

TABLES

Table 7.1	Selected percolation thresholds for two- and three-dimensional lattices	159
Table 7.2	Average contact area ratio for different values of sealing probability, showing the effect of rough surfaces	188
Table 7.4	Average contact area ratio for different values of sealing probability, showing the effect of sampling interval	190
Table 7.5	Average contact area ratio for different values of sealing probability, showing the effect of number of sampling points	191
Table C.1 (a)	Predicted variation of leakage probability as a function of load, showing the effect of rough surfaces	216
Table C.1 (b)	Predicted variation of leakage probability as a function of load, showing the effect of rough surfaces	218
Table C.1 (c)	Predicted variation of leakage probability as a function of load, showing the effect of rough surfaces	219
Table C.1 (d)	Predicted variation of leakage probability as a function of load, showing the effect of rough surfaces	220
Table C.2	Predicted variation of leakage probability as a function of load, showing the effect of sampling interval	221
Table C.3	Predicted variation of leakage probability as a function of load, showing the effect of number of sampling points	222

List of Figures

Figure 2.1	A general typology of surfaces	17
Figure 2.2	The principle of operation of a simple stylus profilometer	19
Figure 2.3	A measured surface profile	20
Figure 2.4	Height density function $f(z)$	24
Figure 2.5	Profiles with (a) 'closed' and (b) 'open' textures and their corresponding autocorrelation functions.	26
Figure 2.6	Construction of the autocorrelation function	27
Figure 2.7	Surface roughness produced by common production methods	31
Figure 2.8	Directional pattern of surfaces generated in various manufacturing processes	33
Figure 3.1	Correlation length λ_x^* Criteria	45
Figure 3.2	Typical contact areas for longitudinally oriented ($\gamma < 1$), isotropic ($\gamma = 1$) and transversely oriented ($\gamma > 1$)	49
Figure 3.3	Flow chart for numerical simulation of a random rough surface	52
Figure 3.4	Generated rough surfaces with Gaussian statistics	56
Figure 3.5	Profiles of generated isotropic rough surfaces with Gaussian statistics, but different RMS height σ	57

FIGURES

Figure 3.6	Profile of generated isotropic rough surfaces with Gaussian statistics, but different correlation length λ^* . . .	58
Figure 3.7	Profiles of generated rough surfaces with Gaussian statistics and same statistical parameters but different surface forms	59
Figure 3.8	Profiles of generated surfaces with Gaussian statistics and same statistical parameters but different values of simulation parameter	60
Figure 3.9	Typical x and y directional profiles of the generated surface in Figure 3.4(b)	61
Figure 3.10	Comparison of probability density functions with respect to nondimensional height (z/σ)	63
Figure 3.11	x and y profile ACFs of the generated surface in Figure 3.4 (a)	67
Figure 3.12	x and y profile ACFs of the generated surface in Figure 3.4 (b)	68
Figure 4.1	Configuration of elastic rough surface contact	83
Figure 4.2	Deformation due to removal of the pressure in the rigid plane region	86
Figure 5.1	Possible traction elements for use in two-dimensional contact problems	102
Figure 5.2	Vertical displacement on the surface due to uniform normal pressure element	103
Figure 5.3	Computer program flow chart for two-dimensional numerical contact model	118
Figure 5.4	Comparison of pressure distribution for the contact of	

FIGURES

	smooth cylinders	120
Figure 5.5	Simulated results for an equivalent rough surface loaded against a rigid plane	124
Figure 5.6	Predicted variation of contact length with applied load for two-dimensional contact of rough surfaces, showing the effect of rough surfaces	125
Figure 6.1	Discretization of the contact boundary	137
Figure 6.2	Pressure distribution for the contact of smooth spheres	143
Figure 6.3	Comparison of pressure distribution for the contact of smooth spheres	143
Figure 6.5	Predicted variation of the real contact area with applied load, showing the effect of rough surfaces	146
Figure 7.1	Definition of percolation and its cluster.	158
Figure 7.2	Simulation model for static sealed joints	161
Figure 7.3	Results of computer check of leakage paths for typical patterns of contact	166
Figure 7.4	Simulation procedure of leakage analysis of static sealed joints	169
Figure 7.5	Simulation procedure for the prediction of leakage probability	172
Figure 7.6	Predicted variation of leakage probability as a function of load, showing the effect of RMS height σ	175
Figure 7.7	Predicted variation of sealing probability as a function of load, showing the effect of RMS height σ	176
Figure 7.8	Predicted variation of leakage probability as a function of load, showing the effect of correlation length λ^*	178

FIGURES

Figure 7.9	Predicted variation of sealing probability as a function of load, showing the effect of correlation length λ^*	178
Figure 7.10	Surface model to show relation separation and correlation length at constant normal stress	180
Figure 7.11	Predicted variation of leakage probability as a function of load, showing the effect of sampling interval	182
Figure 7.12	Predicted variation of sealing probability as a function of load, showing the effect of sampling interval	183
Figure 7.13	Predicted variation of leakage probability as a function of load, showing the effect of number of sampling points . .	184
Figure 7.14	Predicted variation of sealing probability as a function of load, showing the effect of number of sampling points . .	184
Figure 8.1	Contact model of layer elastic bodies with rough surfaces	208

Nomenclature

a, b	semi-width of a rectangular element in three-dimensional contact
a_{kl}	linear transformation coefficients in rough surface simulation
A_c	real contact area
A_e	surface area of elements in contact simulation
A_n	nominal area of contact
$b(x,y), b_y$	gap in the undeformed state
C_{ij}, C_{yij}	influence coefficient in contact simulation
d	normal mean separation
d_c	threshold normal separation defined in Equation (4.2)
D_{sum}	area density of summits
$E\{ \}$	average value denotation
E'	equivalent Young's modulus
E_1, E_2	Young's modulus
$f(z)$	height density function
$F_1(t)$	integral defined in Equation (6.18)
$F_{3/2}(t)$	integral defined in Equation (6.20)
$g(x,y), g_y$	gap in the deformed state
h	uniform clearance between two surfaces
H	indentation hardness of rough surface
$I(i), I(i, j)$	index matrix to record the position of non-contacting elements
$J(k), J(k, l)$	index matrix to record the position of contacting elements

NOMENCLATURE

k	defined in Equation (5.36)
k'	defined in Equation (5.37)
k_r	constant defined in Equation (5.13)
K_e	elastic parameter defined in Equation (6.3)
$K(k)$	complete elliptical integral of the first kind given by Equation (5.38)
L	contact simulation segment length in two-dimensional contact
m	nondimensional distance in two-dimensional contact
m_0	zero moment of power spectral density function
m_2, m_{02}, m_{20}	second moments of power spectral density function
m_4, m_{04}, m_{40}	fourth moments of power spectral density function
M, M_x, M_y	number of elements in contact simulation
M', M'_x, M'_y	number of elements in contact
M'', M''_x, M''_y	number of elements in non-contact
n_L	a population in probability analysis
n_S	number of failure seals in a population
n_x, n_y	nondimensional sampling interval in rough surface simulation
N, N_x, N_y	number of sampling points in rough surface simulation
$p(x), p(x,y)$	contact pressure distribution
p_1, p_y	elemental contact pressure
p_m	average contact pressure
p_{max}	maximum contact pressure
$\frac{P}{P}$	dimensionless contact load defined in Equation (7.3)
P_1	system pressure
P_2	environmental pressure
P_3	atmosphere pressure
P_a	applied load
P_c	calculated load
P_L	leakage probability of static sealed joints
P_S	sealing probability of static sealed joints

NOMENCLATURE

r	contact half length in Hertzian normal contact
r_i	inner radii of seal ring surface
r_o	outer radii of seal ring surface
R_1, R_2	radius of cylinder or sphere in Hertzian normal contact
R	equivalent radius of cylinder or sphere in Hertzian normal contact
R_a	centre-line average in rough surface measurement
R_q	root-mean-square roughness in rough surface measurement
$R(\lambda), R_{p,q}$	autocorrelation function
$[R_{p,q}]$	$n_x \times n_y$ autocorrelation matrix
x_r	vertical distance at which zero vertical displacement is assumed in two
u	elastic displacement of body surface
U_E	elastic strain energy of two stressed bodies
U_E^*	internal complementary energy of two stressed bodies
V^*	total complementary energy of two stressed bodies
Y	uniaxial yield strength
$z(x,y), z_y$	rough surface heights measured from the mean plane
$[z_{ij}]$	rough surface height matrix
α	bandwidth parameter
β	curvature radius of summits
γ	anisotropy parameter
δ	approach between two bodies
$\delta_o(x), \delta_o(x,y)$	elastic displacement due to average pressure
ΔL	elemental length in two-dimensional contact
$\Delta x, \Delta y$	sampling interval in rough surface simulation
$[\eta_{ij}]$	input matrix in rough surface simulation
κ	curvature of summits
$\lambda_x, \lambda_y, \lambda_\theta$	delay length
$\lambda_\theta^*, \lambda_x^*, \lambda_y^*$	correlation length
μ	fluid viscosity

NOMENCLATURE

ν	poission's ratio
ξ	defined in Equation (5.34)
σ	standard deviation of surface height distribution
σ_s	standard deviation of summit height distribution
φ_f	pressure flow factor derived by Patir and Cheng (1978)
φ_m	multiplying coefficient defined by Shimomura et al. (1989)
ψ	plasticity index defined by Greenwood et al. (1966)
ψ_c	plasticity index defined by Ogilvy (1992)
Ω_c	real contact region
Ω_n	nominal region

CHAPTER 1.

Introduction

1.1 Research Objectives

Leaking, friction and wear of seals are concerns for machine designers and users everywhere. Although perfect sealing may be the general aim, in practice there is usually infiltration of fluid through imperfections in the sealing surfaces. Therefore, the importance of the reliability of sealed joints cannot be overemphasized.

Societies are undergoing rapid changes. The population growth is coupled to the high growth of information and communication systems, leading to an explosion of knowledge. The consequence of this is the speeding up of the rate of technological breakthroughs but also more sophisticated and demanding customers and end users. When the above is coupled to the intense competition in today's markets, it follows that products (and, by implication, their components such as seals) are required to have higher reliability in order that they fulfil the "trouble-free operation" demands of the end user. Moreover, the protection of our fragile environment is today

CHAPTER 1.

of global concern. In many cases, it is therefore necessary to provide the reverse protection, that is, protect the environment from fluid used in machinery and various installations. This is another reason for increasing demands for effective sealing.

The static sealed joints are widely used in practices. Static sealing performance is of obvious interest in cases of long stationary periods. In this thesis, it is concerned only with static seals involving solid materials. It does not concern itself with the seals used between moving parts, e.g. faces seals and lip seals, where the greatest concerns are usually wear and the escape of lubricating oil. The sort of situation envisaged is that of seals in flanged joints, but static seal and gaskets used in a wide range of situation will be influenced by very similar concerns. The main concern in such joints is the creation of a barrier to the flow of fluid from one side of the sealed area to the other; the barrier being formed by contact between the two materials due to the application of external force. The creation and integrity of this barrier can be discussed at two very different scales, termed for convenience macroscopic and microscopic views of the problem.

The macroscopic view is concerned with the overall distribution of stresses throughout the joint and whether this creates compressive stresses over the area of the seal. Thus, for example, the shape of the flanges and the location of bolts in a flanged joint are primary interests for design, and as far as integrity and reliability are concerned, major concerns would be the quality of the jointing material and the cleanliness of the joint where debris might prevent proper contact being made.

CHAPTER 1.

The microscopic view looks at the surface roughness of the contacting materials which is apparent if their surfaces are magnified sufficiently, and considers whether the compressive stresses do in fact bring sufficient area into contact to form a barrier. There may be situations in which failure to form a seal at the microscopic level is unimportant. However, ever increasing concerns over environmental pollution mean that for toxic or radioactive materials, for example, the demands made on the design of seals can only get more severe as time goes on.

The work in this thesis is limited to considering the microscopic view; it is considered appropriate to investigate the nature of the sealing process at this scale before progressing to the macroscopic view, since the microscopic view will determine the criterion that should be adopted in a macroscopic analysis.

This thesis is concerned with the situation of two "rough" surfaces which are compressed together. Flitney, Nau and Reddy (1984) have shown that the characteristics of rough surfaces determine the nature of leakage paths at interface. When two surfaces are in contact the roughness provides a path through which fluid flow may take place. The leakage route is inevitably affected by the way in which the surface roughness asperities are deformed when the two surfaces are loaded together. Rough surfaces produce a multitude of relatively large leakage paths and will require higher applied load to seal effectively. Smooth surfaces on the other hand produce smaller leakage paths which offer high resistance to leakage flow and require less contact pressure at the interface. Therefore, the more important factors on the

CHAPTER 1.

sealing performance of static sealed joints are surface characteristics and the face loading or face contact pressure. Assuming ideally flat faces, leakage can be reduced by improving surface finish and by increasing the contact pressure.

A number of works have considered the effect of surface roughness on the sealing performance of static sealed joints (Rathbun 1963; Tsukizoe and Hisakado 1965; Mitchell and Rowe, 1967/1969; Thomas 1973; Shimomura, Kiryu, Hirabayshi and Nakajima 1989; Etsion and Front 1994), and several surface criteria have been proposed for the effectiveness of such seals. All of these researches have achieved certain successes but also with some limitations on each of the solution methods. A survey will be given in the next section.

An important fact observed in practice is that for apparently identical seals in the same application, some may seal while some not. This is partly due to surface-related random phenomena. It therefore is the most reasonable to apply statistical concepts in discussing sealing reliability. Since the existing work deals only with average properties, it cannot therefore model the possible variations of surface-related random phenomena. Up to now, there is not a paper in the published literature about the reliability analysis of static sealed joints. The lack of a reliable model that predicts the effects of influential parameters on the sealing reliability of static sealed joints necessitates the use of test. This may be a tedious procedure and can not satisfy the need that the market competition requires faster product development.

All of these facts have provided the motivation for the current research work. This research aims at present a new simulation model of leakage that

CHAPTER 1.

can reveal the effect of random properties of rough surfaces on the sealing performance so that it is possible to apply the statistical concepts, i.e. leakage probability or sealing probability, in discussing the sealing reliability of static sealed joints. Computer simulation is not only the most reasonable approach in light of the complexity of the problem, but also is much simpler and more economic for the statistical analysis of leakage than experiments. The computer simulation of random rough surfaces and the numerical contact model of rough surfaces make it possible to develop such a simulation model of leakage.

Considering the variables controlling the leakage, if one were to write a mathematical formula for leakage probability P_L , it would look like this:

$$P_L = F\{S_1 \text{ \& } S_2 \text{ surface roughness, } S_1 \text{ \& } S_2 \text{ material properties, } S_1 \text{ \& } S_2 \text{ face loading}\}$$

where S_1 & S_2 are the sealing surfaces.

1.2 Research Background

A number of equations have been put forward for the calculation of leakage rate through seals operating in the full fluid lubrication regime. These are all based on the Poiseuille equation for laminar flow through a simple annular gap. The Poiseuille flow formula applied to parallel sealing faces is written in the form (Summers-Smith 1988):

CHAPTER 1.

for incompressible fluid

$$Q = \frac{\pi (P_1 - P_2) h^3}{6\mu \ln(r_0/r_i)} \quad (1.1)$$

or for compressible fluid:

$$Q = \frac{\pi (P_1^2 - P_2^2) h^3}{12\mu P_3 \ln(r_0/r_i)} \quad (1.2)$$

where:

Q : flow rate [m³/s]

h : uniform clearance [m]

μ : fluid viscosity [Pa.s]

r_0 and r_i : outer and inner radii of the seal ring surface [m]

P_1 and P_2 : system pressure and environmental pressure for testing machine
[Pa]

P_3 : atmospheric pressure [Pa].

Equation (1.1) and (1.2) also assumes perfectly smooth surfaces, but gives very good results when the clearance h is large enough compared to the surface roughness. From Equation (1.1) and (1.2), the clearance h is an important parameter controlling the fluid flow and the effect of this parameter on the sealing performance is very strong, since leakage is proportional to h^3 .

Rathbun et al. (1963) and Tsukizoe and Hisakado (1965) had analyzed profilometer traces and derived expressions for fluid leakage when surface are

CHAPTER 1.

loaded against a perfectly flat surface. The analysis of Rathbun et al, who used an effective mean gap weighted according to the point-to-point variation of flow rate, would predict an even larger range of variation in leak rate. Both these solutions were based on plastic deformation and assumed a constant pressure for individual asperity deformation.

Mitchell and Rowe (1967) studied face seal performance based on the parameters of a statistical representation of surface roughness. They derived the load-compression and load-leakage relationships for wedge-shaped asperities of constant apex semi-angle when the distributions of peak and valley levels were defined as Gaussian in form. The results suggested that a convenient quantity for specifying the form of a surface profile is the ratio of the distance between the mean peak and mean valley levels to the standard deviation of the distributions (d/σ). For the best sealing performance d/σ should be as large as possible, whilst the centre-line average, which provided a measure of the scale of the roughness should be as small as possible. Mitchell and Rowe (1969) extended further their analysis by taking account of the influence of asperity deformation mode on gas leakage between contacting surfaces. In their analysis, full account was taken of the effect of displaced material on the deformation pressure and on the rate of fluid leakage between the contacting surfaces. The expressions for fluid leakage between two contacting surfaces was derived based on the plastic deformation of wedge-shaped model.

Thomas (1973) studied the influence of roughness on the deformation of metal surfaces in static contact. The effect of correlation length on the

CHAPTER 1.

separation of the contacting surfaces was taken into account. The theory of statistical geometry was applied to predict the mode of surface elastic deformation, and clearance and mean gap at a given load were calculated for steel surfaces as function of nominal stress. The clearance at a given load was shown to decrease with increasing correlation length of the surface profile, the best and worst finishing being cylindrical lapping and horizontal grinding respectively: the ratio of their resistances to viscous leakage under the same nominal load is calculated as 8:1.

Shimomura, Hirabayshi and Nakajima (1989) studied the relationship between sealing performance and surface characteristics of end face seals by experiments. The Poiseuille formula was applied to calculate the leakage rates past the sealing surfaces under static conditions, where the average clearance h was replaced by the RMS roughness of the cover plate. In order to compensate for the large deviation from a uniform parallel clearance between the sealing surface, a modification to the Poiseuille formula was introduced in the form of a multiplying coefficient φ_m , where Q_c denotes the actual leakage rate between the sealing surfaces and it took the form:

$$Q_c = \frac{\pi(P_1 - P_2)R_q^3}{6\mu \ln(r_o/r_i)} \cdot \varphi_m \quad (1.3)$$

The coefficient φ_m was experimentally determined for each fluid with results that indicate reasonable correlation of the varying surface topographies. Their analysis first combined the problems of topographies and flow between two surfaces by experiments. The experimental results for the modification

CHAPTER 1.

coefficient φ_m are limited to the material combination and test conditions of the experiments. This limits the prediction model within a certain range.

Etsion and Front (1994) developed a model for static sealing performance of end face seals considering the effect of face loading, surface roughness and material properties. Although the Poiseuille formula was still applied as the basic formula to calculate the leakage rates past the sealing surfaces under static conditions, the average clearance h was, however, dependent on the nature of the contact between the seal surfaces, and was determined by using the contact model of rough surfaces (McCool, 1987). The analysis first combined the problems of elastic-plastic contact and flow between two rough surfaces. The effect of the pressure-induced flow between rough surfaces was taken into account in the model by introducing the pressure flow factor φ_f derived by Patir and Cheng (1978). For isotropic roughness the pressure flow factor is given by:

$$\varphi_f = 1 - 0.9e^{-0.56h/\sigma} \quad (1.4)$$

and σ is the composite standard deviation of the surface heights: $\sigma = (\sigma_1^2 + \sigma_2^2)^{1/2}$. Therefore, the actual leakage rate between the sealing surfaces took the form:

$$Q_c = \frac{\pi(p_1 - p_2)\sigma^3}{6\mu \ln(r_o/r_i)} \cdot Q_n \quad (1.5)$$

where the dimensionless leakage Q_n is:

CHAPTER 1.

$$Q_n = \phi_f \left(\frac{h}{\sigma} \right)^3 \quad (1.6)$$

The dimensionless leakage depends on h/σ . According to the numerical results of the contact model, an empirical expression was found that relates the dimensionless leakage to the dimensionless load $P_d/A_n H$ based on the assumption that the plasticity index defined by Greenwood and Williamson (1966) is greater than 3, which means that the surface asperities will deform plastically. Thus, a model, which can predict the sealing performance of static sealed joints as a function of roughness σ , material hardness H , and face contact pressure P_d/A_n , has been obtained.

As can be seen from the survey above, all of these researches have certain successes. Since the existing work deals only with average properties, it is not suitable to discuss the reliability of static sealed joints, which is a surface-related random problem.

1.3 Thesis Overview

This section gives a presentation overview of the thesis. This thesis is organized in such a way as to produce a coherent and unifying theme representing the main features of the reliability analysis of static sealed joints, which may be divided into the following three topics:

- (1) Characterisation and numerical simulation of random rough surfaces

CHAPTER 1.

(Chapter 2. and Chapter 3.);

- (2) Contact of rough surfaces (Chapter 4., Chapter 5. and Chapter 6.);
- (3) Simulation model of leakage and reliability analysis of static sealed joints (Chapter 7.).

Chapter 1 (the current chapter) introduces the nature, scope and objectives of the research topic undertaken and makes a survey of the existing works on the subject on the effect of the contact of rough surfaces on the performance of static sealed joints. It also gives an overview of the thesis.

Chapter 2 introduces the analytical methods of surface characterisation and topography of engineering surfaces. A measured surface may be comprehensively described by two statistical functions: the probability density function and the autocorrelation function. The probability density function describes the distribution of surface heights, and the *RMS* height is a measure of the deviation of the surface from the mean plane; the autocorrelation function gives the information on the shapes or spacings of the surface irregularities, and the correlation length measures the rate of the change of the roughness along the surface. Different manufacturing processes produce various directional patterns of the surfaces. It is proposed that two types of rough surfaces should be classified: isotropic surface and anisotropic surface.

Chapter 3 presents a numerical simulation algorithm for generating

CHAPTER 1.

random rough surfaces with Gaussian statistical properties. Based on the algorithm, the computer program has been written in FORTRAN. The desired probability density of the roughness heights is obtained by controlling the probability density of the random numbers in the input matrix. Because linear transformations of independent Gaussian random variables result in Gaussian variables, the roughness heights having the desired autocorrelation function are then obtained through a linear transformation on the input matrix. These coefficients are determined by solving a system of non-linear equations constructed by autocorrelation matrix. For each set of values (i.e. RMS height and correlation length) there are an infinite number of possible surface forms, which facilitates the simulation of surface-related random phenomena. The numerical simulation program has been verified through a series of comparisons. The close agreement between the theory and simulation validates the use of this procedure to numerically simulate a random surface.

Chapter 4 makes a survey of the existing models for the contact of rough surfaces. The numerical contact model of rough surfaces can provide important information about the real contact situation at the interface of sealed joints, therefore it is suitable for the analysis of leakage by simulation. The geometric relationship and the boundary condition of contact have been derived. The values of plasticity index for typical sealed joints has been calculated based on the conventional plasticity index. The results show that making the assumption of elastic deformation for the contact of static sealed joints is reasonable although it is not strictly true for all static sealed joints. The contact model developed based on the assumption of purely elastic deformation to be used in the reliability analysis of static sealed joints is on

CHAPTER 1.

the safe side for design.

Chapter 5 derives the numerical relationship between contact pressure and surface displacement for two-dimensional elastic frictionless contact based on the corrected Timoshenko's solution for vertical surface displacements due to an arbitrary pressure distribution. The numerical solution technique based on variational principles has been applied successfully to the numerical contact of rough surfaces so that the problems involved in Matrix Inversion Method, such as the iteration of solution procedure and the distortion of solution caused by the difficult of convergence, have been eliminated. Using the variational method, the contact problem becomes a quadratic programming problem. The computer algorithm and program in FORTRAN for two-dimensional numerical elastic contact problems have been completed. The program has been compared with the Hertzian solution for the contact of two smooth cylinders. The results show that it gives excellent agreement with the Hertzian solution for both the contact length and the pressure distribution. Comparison with an existing stochastic contact model for highly anisotropic rough surfaces has been attempted. The results obtained from the stochastic and numerical models show an encouraging agreement.

Chapter 6 derived the numerical relationship between contact pressure and surface displacement for three-dimensional elastic frictionless contact based on the Boussinesq solution for a normal point load. Three-dimensional elastic contact model of rough surfaces is presented based on the numerical solution technique of variational principles. The computer algorithm and computer program in FORTRAN for three-dimensional elastic frictionless

CHAPTER 1.

contact problems has been completed. To verify the accuracy of the program, the contact of two elastic smooth spheres has been studied. The results show that it would yield accuracy pressure distribution and would give reasonable results in calculating the real contact area. Comparison with an existing stochastic contact model for isotropic rough surfaces has been attempted. The results obtained from the stochastic and numerical models show an encouraging agreement.

Chapter 7 develops a computer simulation model for the leakage analysis of static sealed joints based on the percolation theory. Introducing the concept of contact map and the assumption of zero-leakage makes it possible to describe more accurately the leakage phenomenon by means of leakage paths instead of an average clearance. The computer algorithm and program in FORTRAN for determining if any leakage paths exist or not for a typical pattern of contact have been completed. The program along with the numerical simulation of random rough surfaces and the numerical contact model of rough surfaces make it is possible to develop the leakage simulation model, by which we can apply the statistical concepts in discussing sealing reliability. The relationship between the leakage probability and the applied load, which is of great general interest to the designers of static sealed joints, has been predicted by the leakage simulation model. The simulated results also makes good conditions for further studying the sealing reliability of static sealed joints. By statistics and comparison of simulated results, it is confirmed that a certain value of contact ratio can be used as the criteria for identifying the reliability of static sealed joints with a certain confidence level. The effect of surface anisotropy on the sealing reliability has been investigated.

CHAPTER 1.

Comparing the isotropic rough surfaces with the anisotropic ones, the value of contact ratio criteria would increase apparently. The results suggest that to insure a good performance of a static sealed joint, it may be more important to control and inspect the surface-finish profile across the direction of fluid flow than in the direction of fluid flow. The contact ratio criteria would provide a simple, inexpensive and useful tool to evaluate the effects of rough surfaces, material properties and applied load on the sealing reliability of static sealed joints. However, in order to practical use, experimental work is required to evaluate its validity.

Chapter 8 gives a summary and overall conclusions of this research project. It also gives a summary of the main contributions resulting from this research, and a suggestion for further work.

CHAPTER 2.

Characterisation and Topography of Engineering Surfaces

2.1 Introduction

"When studied on a sufficiently fine scale, all solid surfaces are found to be uneven. In the limit, the surface irregularities will be on the scale of individual atoms or molecules; it is possible, for example, to prepare carefully cleaved specimens of the mineral mica which are truly smooth on a molecular scale over areas of several square centimetres. However, the surface of even the most highly polished engineering components show irregularities appreciably larger than atomic dimensions, and many different methods have been employed to study their topography. Some involve examination of the surface by electron or light microscopy, or by other optical methods, while others employ the contact of a fine stylus, electrical or thermal measurements, or rely on the leakage of a fluid between the surface and a precision-machined surface. Perhaps the highest resolution can be achieved by the techniques of scanning tunnelling microscopy or atomic force microscopy, which can resolve

CHAPTER 2.

individual atoms; but for most engineering surfaces less sensitive methods are adequate to study their topography (Hutchings 1992)."

A very general typology of solid surfaces (Nayak 1971) is shown in Figure 1.1. Surfaces that are deterministic may be studied by relatively simple analytical and empirical methods; their detailed characterization is straightforward. However, many engineering surfaces are random; and it is these that have been subjected to a great deal of study in the past decade. In the thesis, attention is concentrated on random rough surfaces.

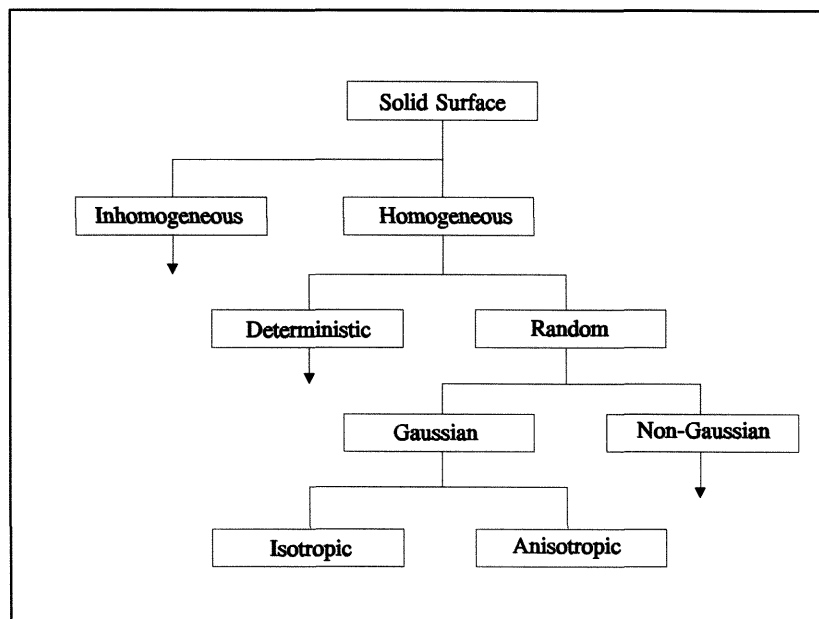


Figure 2.1 A general typology of surfaces

CHAPTER 2.

2.2 Measurement of Surface Topography

A number of instruments for measuring surface characteristics have been devised. The majority of instruments in use for measuring surface roughness depend on electrical processing of the signal produced by the motion of a stylus perpendicular to the surface over which the stylus is traversed. The principle of operation of a simple stylus profilometer is illustrated in Figure 2.2 (from Thomas T R (Ed), *Rough Surfaces*, Longman, 1982). A fine stylus profilometer is dragged smoothly and steadily across the surface under examination. As the stylus travels over the surfaces it rises and falls. Its vertical displacement is converted by a transducer into an electrical signal which is amplified and in the simplest form of the instrument, moves the pen of a chart recorder. The graph drawn by the pen represents the vertical displacement of the stylus as a function of the distance travelled along the surface.

A profile graph represents a section through the surface in only one direction. It is possible, however, by making a large number of profilometer traverses across a specimen and displacing the specimen slightly between each traverse, to generate a three-dimensional picture of the surface. Some stylus profilometers will do this automatically.

CHAPTER 2.

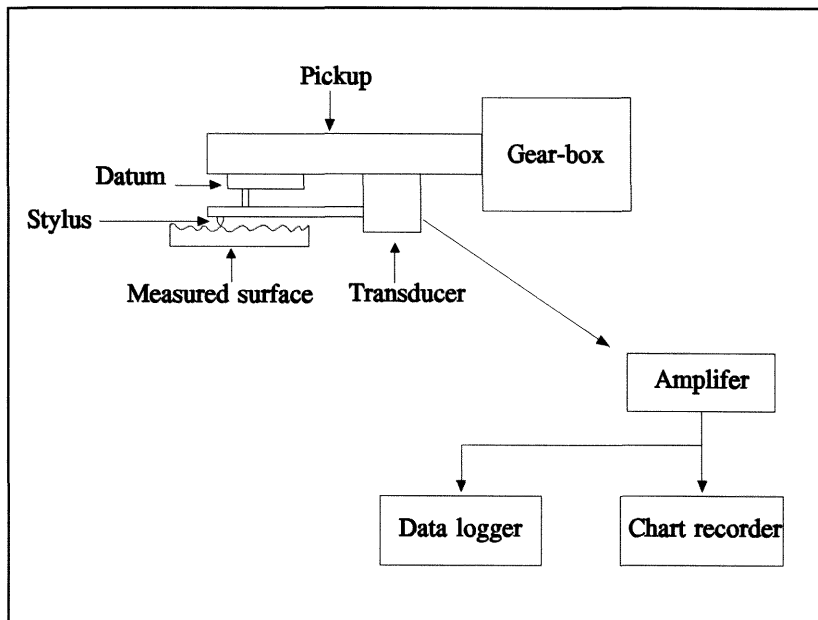


Figure 2.2 The principle of operation of a simple stylus profilometer

2.3 Analytical Methods of Surface Characterisation

We will now discuss briefly the topographical characteristics of random rough surfaces which are relevant to their behaviour when pressed into contact, which refer mainly to Hutchings (1992).

A measured surface profile generated by a stylus or optical profilometer, which is a graph of surface height z plotted against distance shown as in Figure 2.3, contains most of the information needed to describe the topography of the surface along a single direction. Note that the graph is a much distorted image of the actual profile through using a larger

CHAPTER 2.

magnification in the normal than in the tangential direction. The profile graph itself, however, does not provide a sufficiently simple and readily interpreted means of describing surface roughness; several quantities derived from the profile, which are often automatically computed by the profilometer instrument, are used for this purpose. Actually, most manufactures need a combination of no more than two to four parameters to define the surface characteristics.

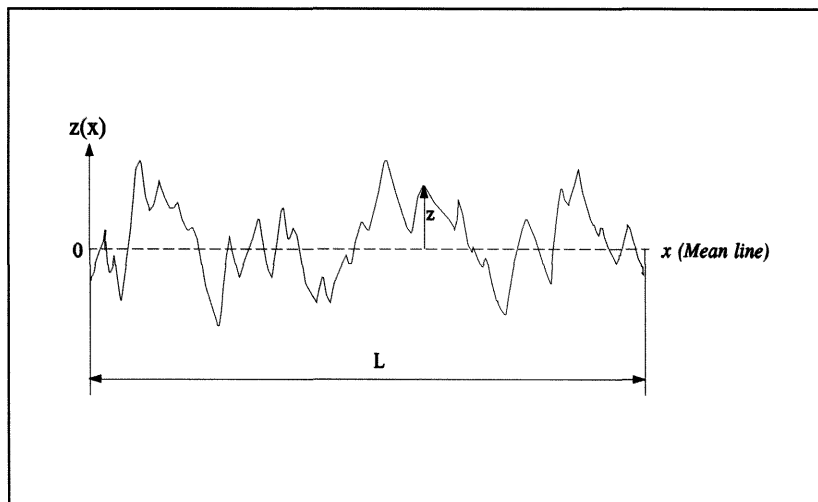


Figure 2.3 A measured surface profile

CHAPTER 2.

2.3.1 Average Roughness Parameters

Two measures widely used in industry, mainly for quality control purposes, are the centre-line average R_a or the arithmetic average and the root-mean square (*RMS*). As a mathematical technique, each can be used to define the mean line or mean plane, and in fact they are equivalent. The *RMS* technique which involves minimizing the sum of the squares defines the same mean as the R_a condition of equal areas or volumes of surface and void, above and below the mean.

2.3.1.1 Centre Line Average

The R_a , *c.l.a.* for "centre line average" or *AA* for "arithmetic average" is the most universally used roughness parameter because of its ease of measurement; this is defined by

$$R_a = \frac{1}{L} \int_0^L |z(x)| dx \quad (2.1)$$

where $z(x)$ is the height of the surface above the mean line at a distance x from the origin and L is the overall length of the profile under examination.. Alternatively, the centre-line average mean line is defined as the line such that the area of the solid above is equal to the area of void below.

CHAPTER 2.

2.3.1.2 Root Mean Square (RMS)

The root-mean-square roughness (symbol R_q or σ) is defined as the root mean square deviation of the profile from the mean line:

$$R_q = \sqrt{\frac{1}{L} \int_0^L z^2(x) dx} \quad (2.2)$$

For many surfaces, the values of R_q and R_a are interchangeable; for a Gaussian distribution of surface heights, $R_q \approx 1.25 R_a$.

In a modern profilometer, the integrals above are often carried out numerically by sampling the trace at intervals and using the approximations

$$R_a \approx \frac{1}{N} \sum_{i=1}^N |z_i| \quad (2.3)$$

or

$$R_q \approx \sqrt{\frac{1}{N} \sum_{i=1}^N z_i^2} \quad (2.4)$$

If this method is used care must be taken to ensure that the sampling interval is sufficiently small to give a good approximation to the integrals.

CHAPTER 2.

2.3.2 Statistical Analysis - Probability Density Function (PDF)

It is inevitable that in attempting to describe a profile by a single number, some important information about the surface topography will be lost. R_a and R_q for example, convey no indication of the probability of finding surface heights within certain limits, and given no information on the shapes or spacings of the surface irregularities. For a fuller description of the topography of the surface, information is needed about the probability distribution of surface heights and the spatial distribution of peaks and valleys across the surface.

If the surface or profile heights are considered as random variables, then their statistical representation in terms of the probability density function $f(z)$ is known as the height distribution. The height distribution is a means of representing all surface heights, which in some cases and applications is necessary.

The height density function, $f(z)$, is the value of which, for any height z , is proportional to the probability of finding a point on the surface at height z above the mean line. The quantity $f(z)\Delta z$ is the fraction of the surface profile which lies at heights between z and $z + \Delta z$ above the mean line, as shown in Figure 2.4. A symmetrical profile, such as sine curve, leads to an height density curve which is symmetrical about the position of the mean line. Asymmetry of the surface profile leads to skewing of the height density function, which therefore contains some information about the shapes of

CHAPTER 2.

surface irregularities as well as their vertical extent. In terms of the height density function $f(z)$, the *RMS* roughness, R_q , is the standard deviation σ , i.e. it is the square root of the variance or second moment of $f(z)$.

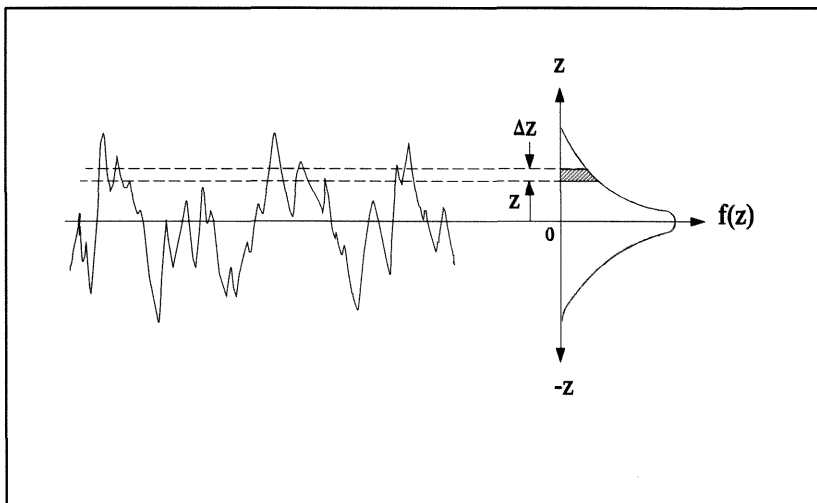


Figure 2.4 Height density function $f(z)$

There is considerable evidence (Greenwood and Williamson 1966, Williamson 1967/1968, Williamson, Pullen and Hunt 1970) that the height distribution of many common engineering surfaces are Gaussian or normal. Therefore, making the general assumption that surfaces have Gaussian height distribution is reasonable, although it is not strictly true for all possible applications.

When the height distribution is Gaussian the height probability density function is

CHAPTER 2.

$$f(z) = \frac{1}{\sqrt{2\pi}} \exp\left(-\frac{z^2}{2\sigma^2}\right) \quad (2.5)$$

2.3.3 Random Process Methods

2.3.3.1 Autocorrelation Function

The necessity for a spatial representation of topography is obvious from Figure 2.5 which shows two surfaces with the same roughness parameters, but clearly the spatial arrangement of surface heights is very different. This might represent an important function difference in many practical engineering cases. The outstanding problem in surface analysis is the representation of spatial variation, i.e. how height, slopes, etc. vary with distance in the plane of the surface. Two methods may be used to extract this information from a surface: autocorrelation and spectral analysis.

Autocorrelation function (ACF) has been the most popular way of representing spatial variation. It contains useful spatial information. With reference Figure 2.6, the autocorrelation function of a profile is defined as the following form by Peklenik (1967-1968):

$$R(\lambda_x) = \lim_{L \rightarrow \infty} \frac{1}{L} \int_0^L z(x)z(x + \lambda_x) dx \quad (2.6)$$

CHAPTER 2.

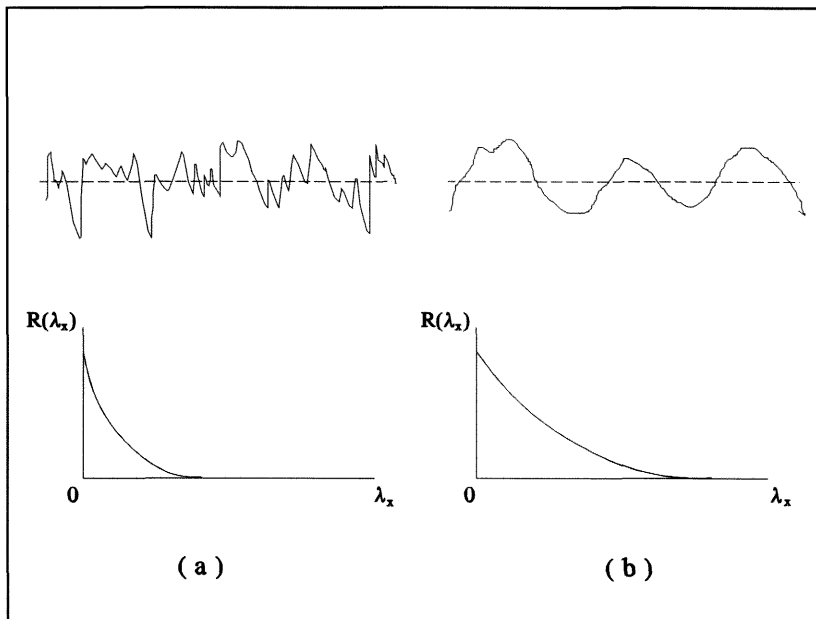


Figure 2.5 Profiles with (a) 'closed' and (b) 'open' textures and their corresponding autocorrelation functions.

In a more statistical form:

$$R(\lambda_x) = E\{z(x)z(x + \lambda_x)\} \quad (2.7)$$

where $E\{ \}$ denotes an expectation, i.e. an average value of $z(x)z(x + \lambda_x)$ and λ_x is the delay length or the displacement along the x direction.

The value of the autocorrelation function for some displacement λ_x along the surface is therefore derived by shifting the profile a distance λ_x along the surface, multiplying the shifted profile function by the corresponding unshifted value, and calculating the area beneath the resultant product curve.

CHAPTER 2.

When the displacement is zero, the value of the autocorrelation function is a maximum and represents the variance σ^2 of the surface profiles $z(x)$.

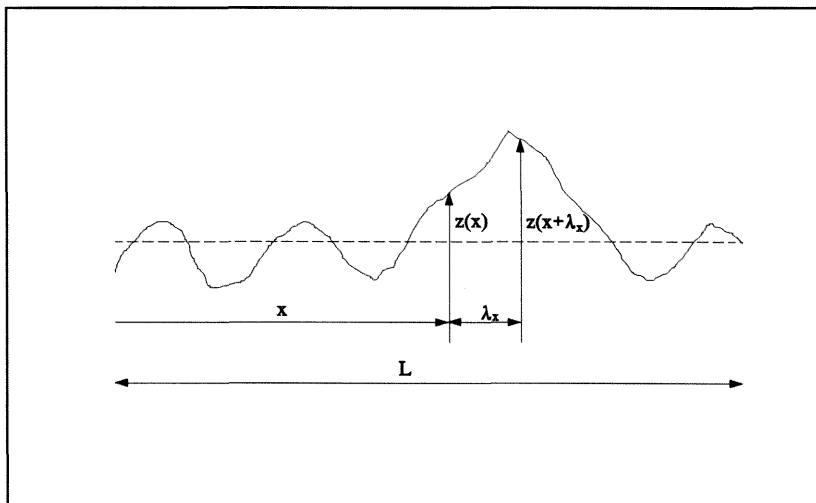


Figure 2.6 Construction of the autocorrelation function

The autocorrelation function provides a measure of the correlation between the heights of the surface at positions separated by a distance λ_x along the surface. The shape of the curve summarizes statistical information on the characteristic spacings, if any, of the surface features. Any regular undulation of the surface will show up as an oscillation of the same wavelength in the value of the autocorrelation function.

The surface texture represents a three-dimensional system. The height $z(x,y)$ of a rough surface may be considered as a two dimensional random variable. The height $z(x,y)$ is measured from the mean plane of the surface.

CHAPTER 2.

Assuming the surface to be homogenous (statistical properties are invariant with respect to a translation along the surface), the formalism introduced above is applied to the surface analysis. Thus, by the analogy with Equations [2.6] and [2.7] the autocorrelation function of a surface is defined as

$$R(\lambda_x, \lambda_y) = \lim_{L_x \rightarrow \infty} \lim_{L_y \rightarrow \infty} \frac{1}{L_x L_y} \int_0^{L_x} \int_0^{L_y} z(x+y)z(x+\lambda_x, y+\lambda_y) dx dy \quad (2.8)$$

or

$$R(\lambda_x, \lambda_y) = E\{z(x,y)z(x+\lambda_x, y+\lambda_y)\} \quad (2.9)$$

where $E\{ \}$ denotes an average value of $z(x,y)z(x+\lambda_x, y+\lambda_y)$ and λ_x, λ_y are the delay lengths in the x and y direction.

The autocorrelation function of a profile along a direction θ is related to the one of the surface by

$$R_\theta(\lambda_\theta) = R(\lambda_x, \lambda_y) \quad (2.10)$$

where

$$\begin{aligned} \lambda_x &= \lambda_\theta \cos\theta \\ \lambda_y &= \lambda_\theta \sin\theta \end{aligned} \quad (2.11)$$

Hence the autocorrelation functions of the x and y profiles are

CHAPTER 2.

$$\begin{aligned} R_x(\lambda_x) &= R(\lambda_x, 0) \\ R_y(\lambda_y) &= R(0, \lambda_y) \end{aligned} \tag{2.12}$$

For many real surfaces, the autocorrelation function decays steadily to zero as the delay lengthens, and may be approximated by an exponential function (Peklenik 1967/1968, Whitehouse and Archard 1970).

2.3.3.2 Power Spectral Density Function (PSDF)

The power spectral density function (PSD) of a surface is defined as the Fourier transform of the autocorrelation function. N th moment of PSD is defined as:

$$m_n = \int_{-\infty}^{\infty} f(k) k^n dk \tag{2.13}$$

m_0 , m_2 and m_4 are known as the zeroth, second and fourth spectral moments of a surface. They are equivalent to the mean square roughness, slope and second derivative of a surface in an arbitrary direction.

When the surface is anisotropic the roughness characteristics m_0 , m_2 and m_4 generalize to nine values as bispectral moments. These values are designated with double subscripts which sum to 0, 2, and 4, i.e. m_{00} , m_{11} ,

CHAPTER 2.

m_{02} , m_{20} , m_{13} , m_{22} , m_{31} , m_{04} and m_{40} , which can be obtained through the formula

$$\left. \frac{\partial^{p+q} R(\lambda_x, \lambda_y)}{\partial \lambda_x^p \partial \lambda_y^q} \right|_{\substack{\lambda_x=0 \\ \lambda_y=0}} = i^{p+q} m_{pq} \quad (2.14)$$

where $i = \sqrt{-1}$

2.4 Topography of Engineering Surfaces

2.4.1 Typical Average Roughness

Engineering surfaces may range from a rough casting to that produced by machine lapping. Figure 2.7 lists typical ranges of R_a values for engineering surfaces finished by various processes (SAE Seal Committee ed. 1984). The actual values achieved depend on material and tooling details. The roughness of engineering surface are frequently specified only by average roughness (R_a) values.

CHAPTER 2.

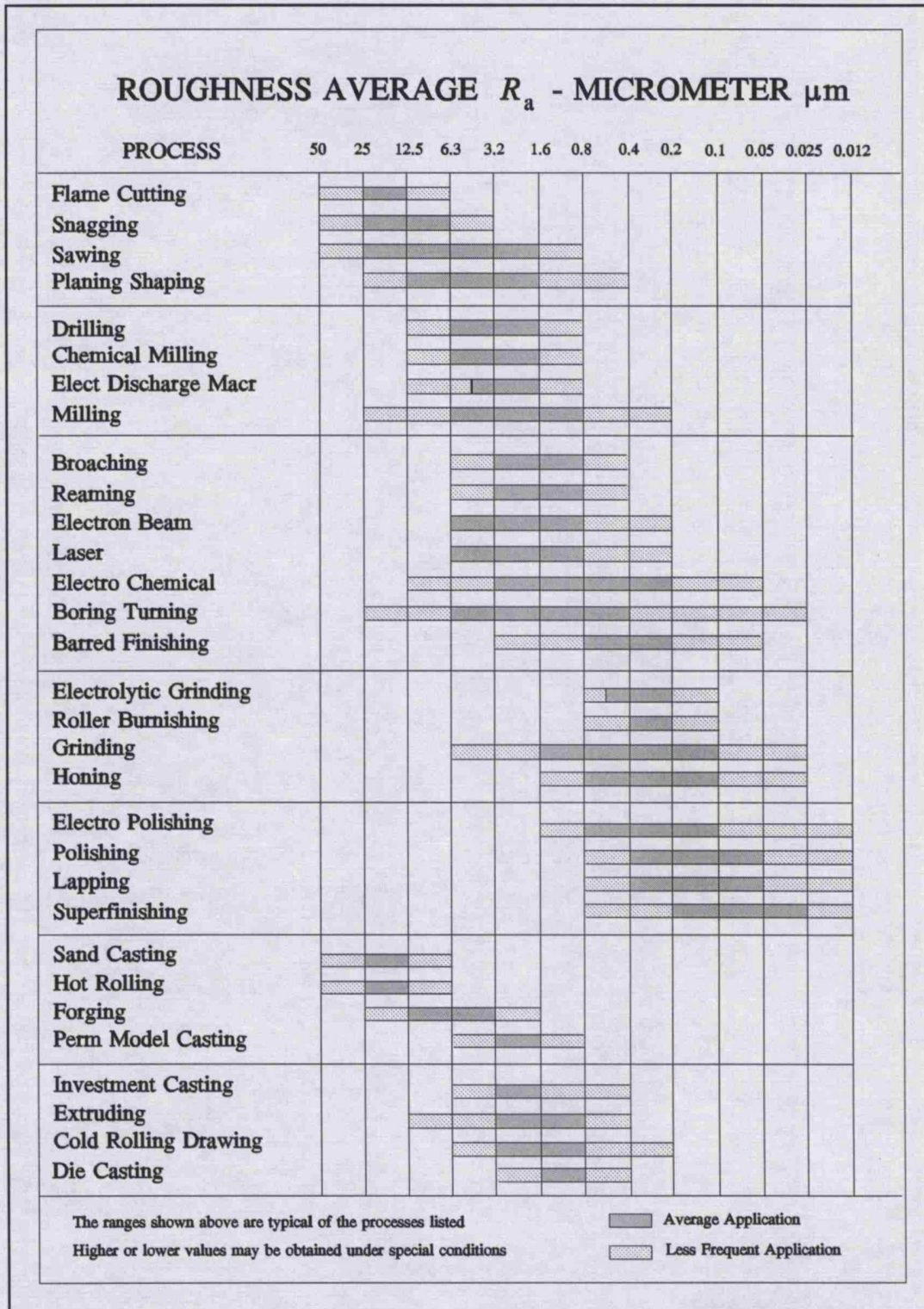


Figure 2.7 Surface roughness produced by common production methods

CHAPTER 2.

2.4.2 Isotropic and Anisotropic Surfaces

Surface characterization is not usually complete without considering the third dimension of the surface since many engineering surfaces have directional patterns. Directional surfaces might be generated for example by turning, milling or grinding etc.. In general, the finer grades of surface texture, those produced by abrasive processes such as lapping or honing, tend to be irregular and non-directional in character; surfaces produced by straight and cylindrical grinding tend to have irregularly spaced but directional texture; while the texture on surfaces produced by single point cutting tends to be both uniformly spaced and directional. These directional patterns are mostly in the longitudinal or transverse directions. Directional patterns of surfaces generated in various manufacturing processes are shown in Figure 2.8. Figure 2.8 a, b, and c exhibits surfaces with pronounced patterns. Figure 2.8 d shows less pronounced patterns, and Figure 2.8 e shows no directional patterns. These patterns may be observed on surfaces generated in shaping, milling, turning, grinding, spark erosion, electrochemical milling, etc. The directional properties of the surface roughness are most important in lubrication and seal practices because they would effect directly on the resistance to the fluid flow.

It is proposed that the roughness surface should be classified into two types:

- (1) isotropic surface;
- (2) anisotropic surface.

CHAPTER 2.

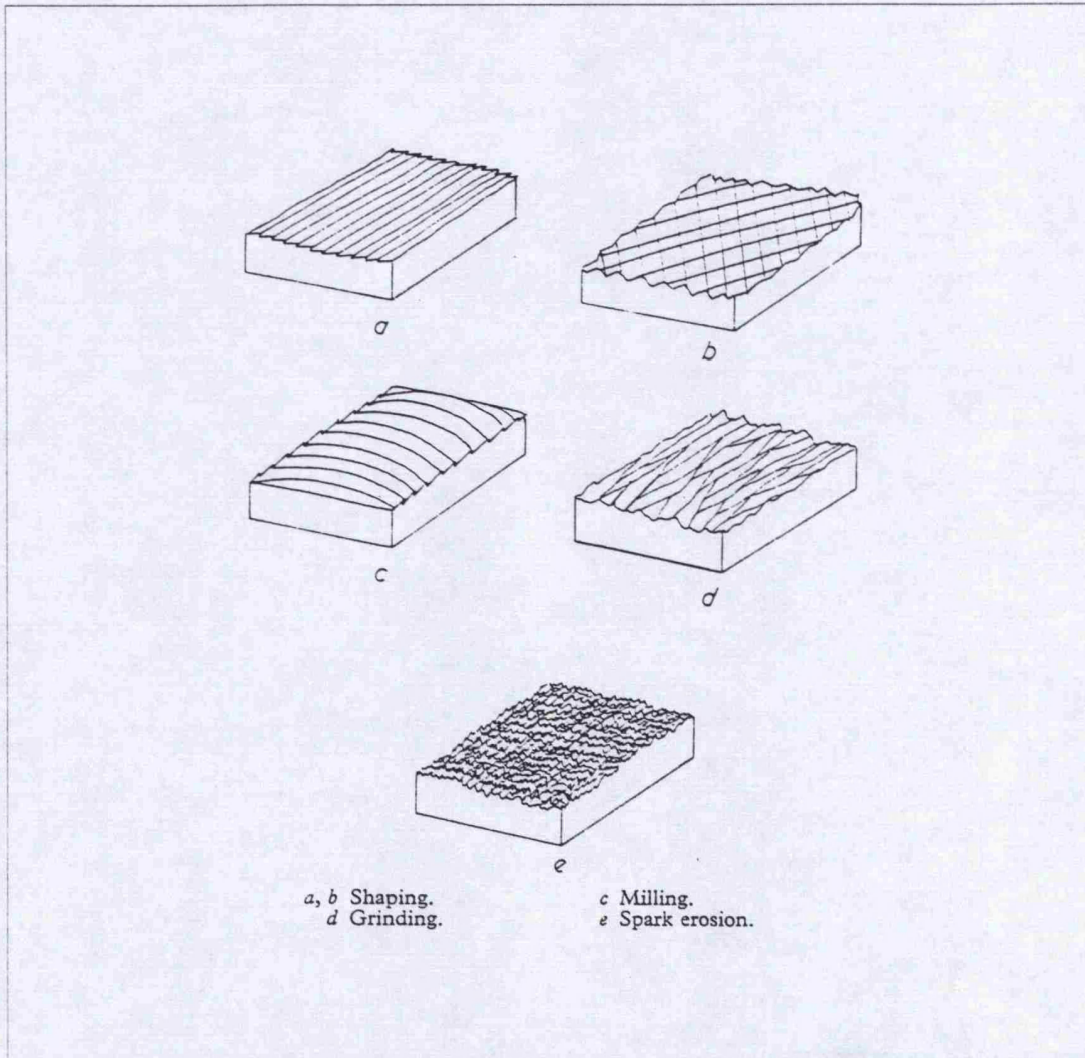


Figure 2.8 Directional pattern of surfaces generated in various manufacturing processes

For an isotropic surface roughness, there are no preferred orientations, i.e., statistical properties are constant along any direction; while an anisotropic surface roughness, there are directional patterns, i.e. statistical properties are not constant along any direction. The parameter γ of surface anisotropy, which shows the degree of anisotropy of a rough surface, will be introduced in Chapter 3.

CHAPTER 2.

2.4 Summary

In practice, all surfaces are rough to some degree and it is important to appreciate the nature of this roughness and its effect on contact problems in order to be able to analyze practical situations. Many surfaces have roughness of a random nature which must be analyzed by statistical methods. Most of the statistical parameters of a rough surface can be derived from two statistical functions: the probability density function and the autocorrelation function. The probability density function describes the distribution of surface heights, and the root-mean-square R_q or σ is a measure of the deviation of the surface from the mean plane; the autocorrelation function gives information on the shapes or spacings of the surface irregularities, and the correlation length measures the rate of the change of the roughness along the surface.

The finish of engineering surfaces can be obtained by various processes. Many engineering surfaces have directional patterns resulting from different manufacturing processes. These directional patterns are mostly in the longitudinal or transverse directions. It is proposed that the roughness of surfaces should be classified into two types:

- (1) isotropic surface;
- (2) anisotropic surface.

Therefore, surface characterization is not usually complete without considering the third dimension of the surface. The parameter γ of surface anisotropy, which shows the degree of anisotropy of a rough surface, will be

CHAPTER 2.

introduced in Chapter 3.

CHAPTER 3.

Random Rough Surfaces Numerical Simulation

3.1 Introduction

The geometric structure of rough surfaces influences a multitude of physical phenomena which are relevant to many engineering problems such as friction, wear, lubrication, sealing and contact resistance etc.. It is considered that numerical simulation has been an important tool for analysing the effects of surface roughness on these problems. Such a study would require quantitative information in three dimensions, which can either be measured from a rough surface or generated numerically, to be in digital form.

Archard, Hunt and Onions (1975) used the digital form of the profilometer readings of a profile for simulation of the contact of rough surfaces. Although accurate measurement of a profile is relatively simple using a stylus profilometer, the disadvantage of profile analysis is that only a section of the surface is examined. It is possible to integrate a large number

CHAPTER 3.

of closely spaced parallel profiles into a three-dimensional map of the surface, but this again is much more complex. Surface measurements are done by taking a number of parallel profile measurements which requires an accurate relocation technique and an additional software requirement to align the profiles numerically. The availability of powerful micro computers has led to the development of surface measurement. One such fully automated three-dimensional mapping system, which uses a Talysurf stylus instrument to record a matrix of surface heights from flat to curved surfaces, has been devised by Webster, West and Sayles (1986). The technique can provide not only a good visual image of topographical detail but also quantitative information that can be used directly for assessment and analysis.

However, randomly generating a rough surface by numerical simulation is much simpler than measuring and offers certain advantages. Such simulations can substitute surface measurement by artificially creating surfaces so that all the hardware requirements for surface measurement is eliminated. It also eliminates the need to filter out the unwanted wavelengths from a measured surface. Furthermore any parametric study involving roughness requires a surface with known statistical properties, and it is more convenient to generate them numerically rather than to measure a mechanically produced rough surface. Therefore, they also facilitate the simulation of surface-related random phenomena which may be difficult to control experimentally.

Although the numerical simulation of random rough surfaces is so important, the subject has received very little attention compared with the measurement of rough surfaces in the published literature so far. The only

CHAPTER 3.

exception is Lai and Cheng's work (1985), which describes the computer simulation of rough surfaces having Gaussian height distribution and bilinear autocorrelation function. The bilinear autocorrelation is only an approximation to the exponential autocorrelation which is typical in many applications. By introducing an autocorrelation function matrix, the simulation algorithm can, in principle, be extended to deal with the general form autocorrelation function. The derivation of the numerical simulation model of random rough surfaces having Gaussian height distribution and general form autocorrelation function is therefore the subject of the following sections of this chapter.

3.2 Numerical Simulation Algorithm

An essential requirement for the numerical simulation of rough surfaces is the ability numerically to generate rough surfaces which have statistical properties similar to a real surface. From the analytical methods of surface characterisation in Chapter 2., we can know that most of the statistical properties of a rough surface can be derived from a knowledge of two statistical functions: the probability density function and the autocorrelation function. Therefore, a good simulation algorithm should be able to generate surfaces having predetermined probability density functions and autocorrelation functions.

Since a digital form of surface roughness is sought, it is more convenient to use an index notation. Let z_{ij} denote the roughness amplitude at $x_i = i \Delta x$, $y_j = j \Delta y$, where Δx and Δy are the sampling intervals in the

CHAPTER 3.

x and y direction, i.e. two perpendicular directions along the surface mean plane. Thus a rough surface can be described by a set of correlated random number z_{ij} , representing the height of the surface at the position (x_i, y_j) along the surface. The set of correlated random numbers may be expressed in matrix form thus:

$$[z_{ij}] = \begin{pmatrix} z_{11} & z_{12} & \dots & z_{1N_y} \\ z_{21} & z_{22} & \dots & z_{2N_y} \\ \vdots & \vdots & \vdots & \vdots \\ z_{N_x1} & z_{N_x2} & \dots & z_{N_xN_y} \end{pmatrix} \quad (3.1)$$

where N_x and N_y are the total number of sampling points in x and y direction.

3.2.1 Input Matrix of Random Numbers

Using random number generators, it is possible to generate an matrix $[\eta_{ij}]$ whose components are a set of uncorrelated random numbers. The matrix $[\eta_{ij}]$ is defined as the input matrix in this chapter. The desired probability density of the roughness heights is obtained by controlling the probability density of the uncorrelated random numbers in the input matrix. For a Gaussian distribution of roughness heights it suffices to generate the input matrix with a Gaussian density function. The components in the input matrix are independent identically distribution Gaussian random numbers with zero

CHAPTER 3.

mean and unit standard deviation.

3.2.2 Linear Transformation on Input Matrix

To generate surfaces with a given autocorrelation function, linear transformations on the input matrices of random numbers are utilized.

Based on the characteristic that linear transformations on independent Gaussian random variables results in Gaussian variables (Davenport 1970), a set of correlated random numbers, representing the roughness height, can be obtained by performing the linear transformation on these numbers in the input matrix:

$$Z_{ij} = \sum_{k=1}^{n_x} \sum_{l=1}^{n_y} a_{kl} \eta_{i+k, j+l} \quad \begin{array}{l} i = 1, 2, \dots, N_x \\ j = 1, 2, \dots, N_y \end{array} \quad (3.2)$$

where a_{kl} are the linear transformation coefficients to be determined so as to give the desired autocorrelation function. Thus the autocorrelation function of the generated surface depends on the set of linear transformation coefficients. In the following section, we will discuss how these coefficients are determined so as to give the desired autocorrelation function.

CHAPTER 3.

3.2.2.1 Autocorrelation Matrix

Similarly, the autocorrelation function may be expressed by using an index notation. Thus R_{pq} is defined as

$$R_{pq} = R(p\Delta x, q\Delta y) = E(z_{ij}, z_{i+p, j+q}) \quad (3.3)$$

As the arguments of the autocorrelation function increases, R decreases to a small value, which is assumed here to be zero, so that a finite order autocorrelation matrix is obtained. Let n_x and n_y be two integers such that R_{pq} is zero if $p \geq n_x$ or $q \geq n_y$. This yields an $n_x \times n_y$ autocorrelation matrix.

$$[R_{pq}] = \begin{pmatrix} R(0,0) & R(0,\Delta y) & \dots & R(0,q\Delta y) \\ R(\Delta x,0) & R(\Delta x,\Delta y) & \dots & R(\Delta x,q\Delta y) \\ \vdots & \vdots & \vdots & \vdots \\ R(p\Delta x,0) & R(p\Delta x,\Delta y) & \dots & R(p\Delta x,q\Delta y) \end{pmatrix} \quad (3.4)$$

3.2.2.2 Linear Transformation Coefficients

Since the components in input matrix $[\eta_{ij}]$ are independent and have unit variance, the following relation can be obtained:

$$E(\eta_{ij}\eta_{kl}) = \begin{cases} 1 & \text{if } i = k, j = l \\ 0 & \text{if } i \neq k, j \neq l \end{cases} \quad (3.5)$$

CHAPTER 3.

Using this relation along with the definition of R_{pq} in Equation (3.3), then the following relation can be obtained:

$$R_{pq} = \sum_{k=1}^{n_x-p} \sum_{l=1}^{n_y-q} a_{kl} a_{k+p, l+q} \quad \begin{array}{l} p = 0, 1, \dots, n_x-1 \\ q = 0, 1, \dots, n_y-1 \end{array} \quad (3.6)$$

Equations (3.6) represent $n_x \times m_y$ simultaneous non-linear equations for the determination of the coefficients a_{kl} . They can be solved by an iterative technique. Here the Newton method is adopted (Rektorys 1969), the set of non-linear equations (3.6) is solved iteratively using the following relation.

$$a^{v+1} = a^v - [J^v]^{-1} f(a^v) \quad v = 0, 1, \dots \quad (3.7)$$

where:

$$\left\{ \begin{array}{l} a = \{a_{11}, a_{12}, \dots, a_{1n_y}, a_{21}, \dots, a_{n_x n_y}\} \\ f = \{f_{00}, f_{01}, \dots, f_{0, n_y-1}, f_{10}, \dots, f_{n_x-1, n_y-1}\} \\ f_{pq} = \sum_{k=1}^{n_x-p} \sum_{l=1}^{n_y-q} a_{kl} a_{k+p, l+q} - R_{pq} \end{array} \right. \quad (3.8)$$

and J is the Jacobian matrix having the components

CHAPTER 3.

$$J_{rs}^v = \frac{\partial f_{pq}}{\partial a_{ij}^v} = a_{i+p, j+q}^v + a_{i-p, j-q}^v \quad (3.9)$$

where:

$$\begin{cases} r = pn_y + q + 1 \\ s = (i-1)n_y + j \end{cases} \quad (3.10)$$

An initial approximation to the coefficient vector may be obtained by the formulae:

$$a_{ij}^0 = sc_{ij} \quad (3.11)$$

where:

$$\begin{cases} c_{ij} = \frac{R_{i-1, j-1}}{(n_x - i + 1)(n_y - j + 1)} \\ s^2 = \frac{R_{00}}{\sum_{i=1}^{n_x} \sum_{j=1}^{n_y} c_{ij}^2} \end{cases} \quad (3.12)$$

CHAPTER 3.

3.3 Numerical Simulation Parameters

3.3.1 Correlation Length

When the autocorrelation function is close to unity, two points on the surface profile at λ_x or λ_y distance apart are strongly interdependent. However, when the autocorrelation function attains values close to zero, two points on the surface profile at λ_x or λ_y distance apart are weakly correlated and therefore essentially independent.

The decay parameters λ_x^* and λ_y^* , for which the autocorrelation function becomes zero, are called the correlation lengths. One can define the correlation length of a profile. Hence the correlation lengths of the x and y profiles are

$$\begin{aligned}\lambda_x^* &= n_x \Delta x \\ \lambda_y^* &= n_y \Delta y\end{aligned}\tag{3.13}$$

The correlation lengths λ_x^* and λ_y^* , at which the autocorrelation functions of the x and y profiles reduce to 10% of their values at origin, have been defined as the correlation lengths of the x and y profiles by Peklenik (1967/1968) as being sufficiently small that two points on the surface may be regarded as being independent. The definition of the correlation length is somewhat arbitrary, therefore this definition will be referred to as the 0.10 correlation length shown as in Figure 3.1.

CHAPTER 3.

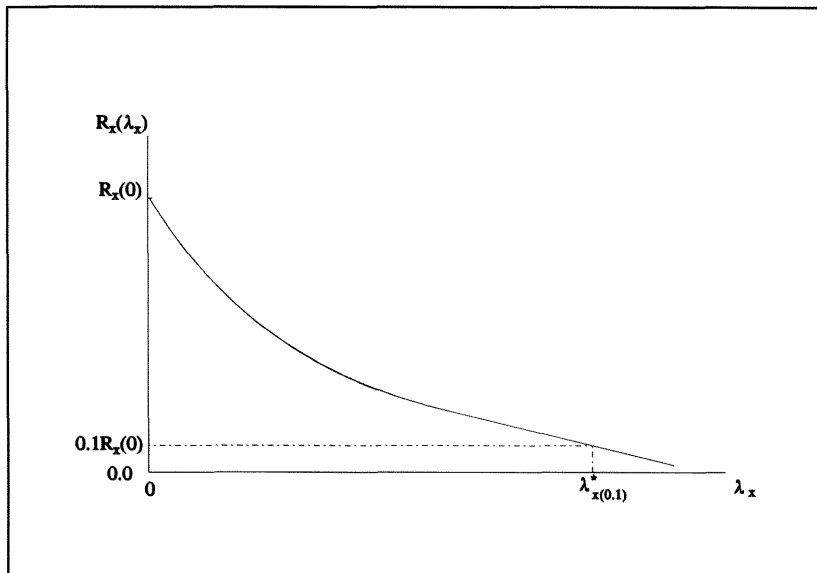


Figure 3.1 Correlation length λ_x^* Criteria

The 0.10 correlation length of a profile along the θ direction is given by

$$\lambda_\theta^* = \frac{\lambda_x^* \lambda_y^*}{\{ (\lambda_x^* \sin\theta)^2 + (\lambda_y^* \cos\theta)^2 \}^{1/2}} \quad (3.14)$$

3.3.2 Sampling Interval

A large sampling interval will miss out many small peaks; on the other

CHAPTER 3.

hand a sampling interval which is too small will include the measurements of many peaks which are far too small to affect the deformation of the surface. It has been shown by Whitehouse and Archard (1970) that many statistical parameters of measured profile depend on the sampling interval. The dependence of the statistical properties on the sampling interval could also be seen from the following example. The square of the principal mean slopes σ'_x which is equal to m_{20} , can be calculated from Equation (2.14) by numerical differentiation (noting the symmetry of R about the origin):

$$\begin{aligned}
 (\sigma'_x)^2 = m_{20} &= -\frac{\partial^2 R}{\partial \lambda_x^2} \Bigg|_{\substack{\lambda_x=0 \\ \lambda_y=0}} = -\frac{R_{10} - 2R_{00} + R_{-10}}{\Delta x^2} \\
 &= \frac{2}{\Delta x^2}(R_{00} - R_{10})
 \end{aligned}
 \tag{3.15}$$

In the numerical simulation procedure, the sampling interval is determined by choosing the n_x and n_y values. Choosing large n_x and n_y reveals the fine structure of the roughness since this means that the sampling interval is chosen as a small fraction of the correlation length. Choosing the sampling interval to be equal to one-tenth of the correlation length reveals short wavelength fine structure of the roughness and indicates the separation at which points on the profile are statistically dependent on each other; while choosing it to be equal to the correlation length reveals the main structure of the roughness and it is the length most appropriate for the measurement of those geometrical properties of a profile which will determine the surface deformation (Whitehouse and Archard 1970). Therefore, n_x , n_y , Δx and Δy should be chosen carefully so as to generate the desired roughness structure.

CHAPTER 3.

The number of calculations required for generating a rough surface increases significantly with increasing n_x and n_y .

3.3.3 Surface Anisotropy

To study surface roughness with directional properties, we will use a surface anisotropy parameter γ defined by Peklenik (1976/1968). The anisotropic properties of the rough surface can be seen from the polar coordinate representation of λ_θ^* as suggested by Peklenik. For the assumed autocorrelation function this representation forms an ellipse with an ellipticity ratio:

$$\gamma = \frac{\lambda_x^*}{\lambda_y^*} \quad (3.16)$$

This ellipse can also be considered as the locus of all points whose heights have the same correlation with the height of a point located at the centre of the ellipse. Therefore asperities should have roughly elliptical shapes with the given ellipticity ratio. The parameter γ , which is the ratio of the x and y correlation lengths, shows the degree of anisotropy of a rough surface. A value of $\gamma = 1$ corresponds to an isotropic surface, while $\gamma \neq 1$ corresponds to an anisotropic surface and the limiting cases $\gamma = \infty$ and $\gamma = 0$ correspond to one-dimensional transverse or longitudinal ridges.

The surface anisotropy is most important in lubrication and seal

CHAPTER 3.

practices because it would affect directly the resistance to fluid flow. The sensitivity of the fluid flow on γ in the partial lubrication or seal regime can be explained by a simple visual experiment, where the direction of the fluid flow is defined as the y direction. For a general three dimensional surface, contact areas can be modeled as ellipses with the mean ellipticity ratio being equal to γ . Figure 3.2 shows typical contact area configuration for three different ranges of the ellipticity parameter γ .

CHAPTER 3.

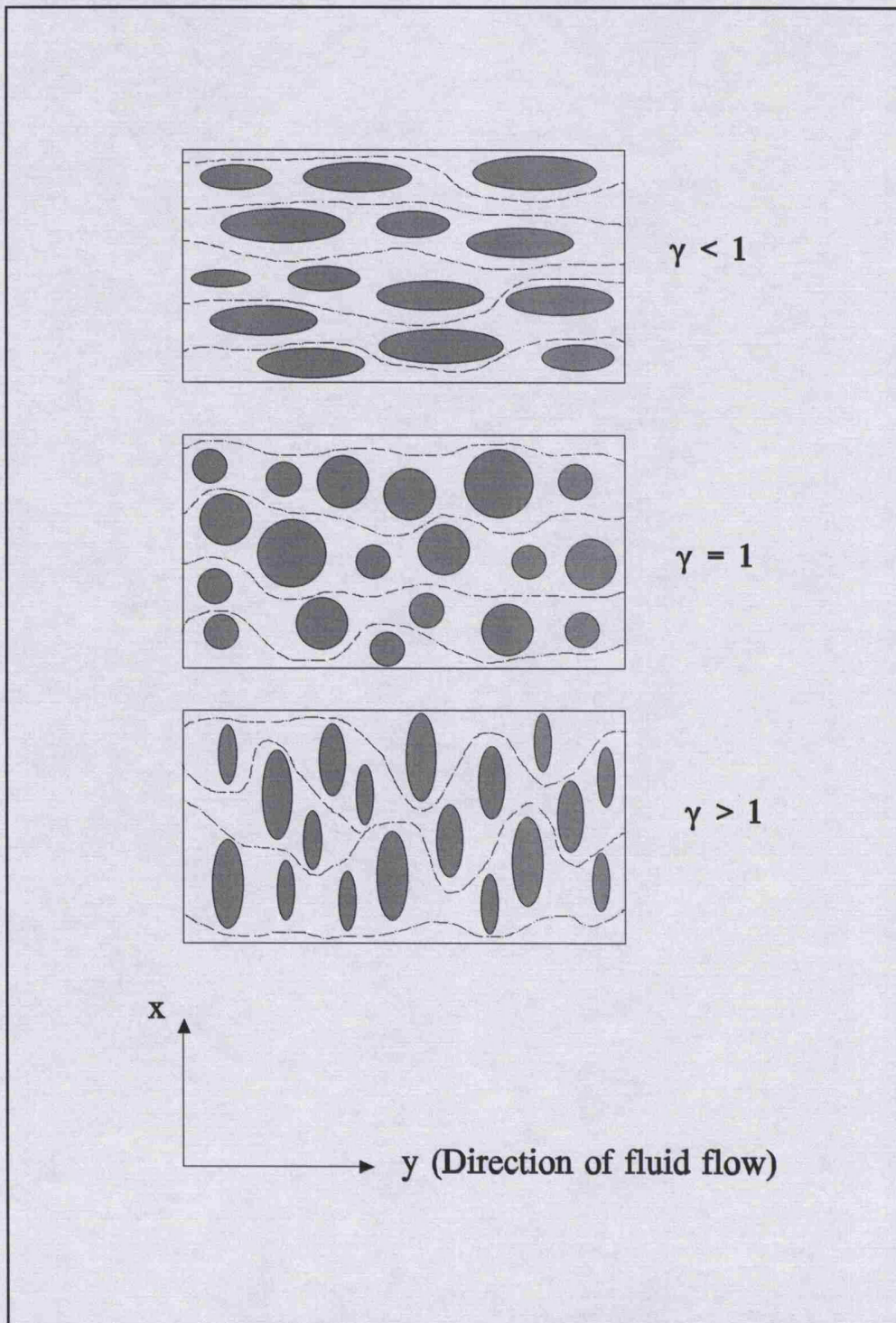


Figure 3.2 Typical contact areas for longitudinally oriented ($\gamma < 1$), isotropic ($\gamma = 1$) and transversely oriented ($\gamma > 1$)

CHAPTER 3.

3.4 Computer Program Structure

A computer program called NSRRS in FORTRAN has been completed by the author for generating numerically random rough surfaces.

A rough surface having predetermined probability density function (Gaussian distribution) and autocorrelation function can be simulated numerically as follows:

Step 1: Set up initial values

Values N_x , N_y , n_x , n_y , Δx and Δy should be chosen carefully so as to generate an area of reasonable size and the desired roughness structure. These values along with σ are input. Note that the number of calculations required for roughness generation increases significantly with increasing n_x and n_y .

Step 2. Generate input matrix

Using a random number generator, the input matrix with Gaussian distribution is generated. In NSRRS, the random number is generated by random number generator called RAN3 (William 1992). For a given RMS height, there are an infinite number of input matrices that can be generated by varying the seed values of the random number generator.

Step 3. Generate autocorrelation matrix

CHAPTER 3.

Based on a given autocorrelation function along with the chosen n_x and n_y values, the autocorrelation matrix $[R_{pq}]$ is generated by using Equation (3.3).

Step 4. Calculate linear transformation coefficients

By solving a system of non-linear equation (3.6) using Newton's iterative method, the linear transformation coefficients a_{ki} are determined.

Step 5. Linear transformation

The roughness heights are then obtained by performing a linear transformation on the input matrix by using Equation (3.2).

Figure 3.3 is a flow chart representing the main features of the numerical simulation program for generating random rough surfaces with the predetermined statistical properties.

CHAPTER 3.

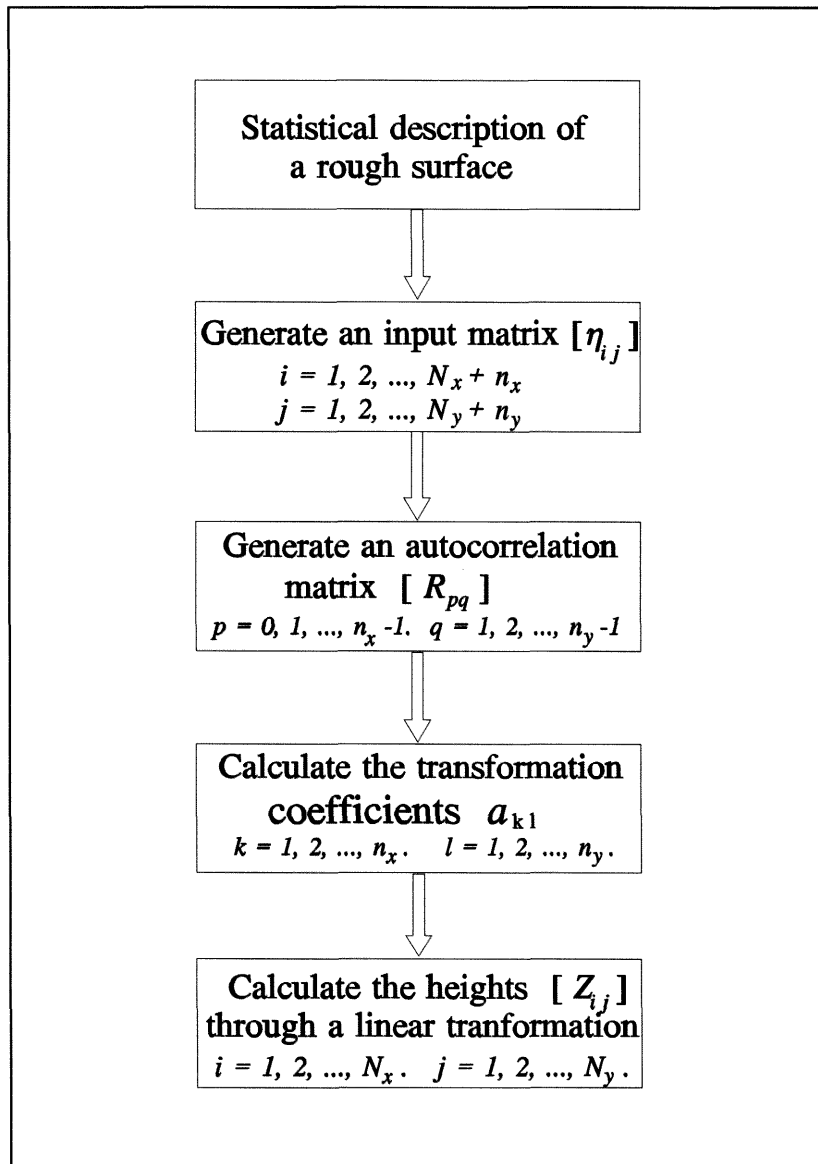


Figure 3.3 Flow chart for numerical simulation of a random rough surface

CHAPTER 3.

3.5 Numerical Examples

3.5.1 Generated Rough Surfaces

To illustrate the numerical simulation procedure, rough surfaces having a Gaussian height distribution and an exponential autocorrelation function are generated, which are considered in this thesis. The exponential function is found to fit the autocorrelation function of many random surfaces (Thomas 1982). The exponential function has been used by many authors such as Peklenik (1967/1968) and Whitehouse and Archard (1970) in the modelling the autocorrelation function of a profile. This model can be extended to the autocorrelation function of anisotropic rough surfaces by assuming that all the profiles on the surface have an exponential autocorrelation function with a decay constant depending on the orientation of the profile. A possible autocorrelation function for such a surface is

$$R(\lambda_x, \lambda_y) = \sigma^2 \exp \left\{ -2.3 \left[\left(\frac{\lambda_x}{\lambda_x^*} \right)^2 + \left(\frac{\lambda_y}{\lambda_y^*} \right)^2 \right]^{1/2} \right\} \quad (3.17)$$

The autocorrelation function of a profile along the θ direction is then:

$$R_\theta(\lambda_\theta) = \sigma^2 \exp \left\{ -2.3 \left(\frac{\lambda_\theta}{\lambda_\theta^*} \right) \right\} \quad (3.18)$$

In order to obtain a finite order autocorrelation function matrix, the

CHAPTER 3.

exponential autocorrelation function is assumed to drop to zero after the 0.10 correlation length. Hence the digital form of the autocorrelation function is:

$$R_{pq} = \sigma^2 \exp\left\{-2.3\left|\left(\frac{p}{n_x}\right)^2 + \left(\frac{q}{n_y}\right)^2\right|^{1/2}\right\} \quad (3.19)$$

$$R_{pq} = 0 \quad \text{if } p \geq n_x \text{ or } q \geq n_y$$

Two examples of surfaces generated using this simulation technique are given in Figure 3.4. In simulation, the sampling interval in x and y direction is chosen as the same, i.e. $\Delta x = \Delta y$.

As can be seen from Figure 3.5 and 3.6, where profiles, i.e. 2D slices, through the surfaces are shown, the roles of *RMS* height and correlation length in determining the surface forms are apparent. The *RMS* height controls the deviation of the surface from the mean plane and the correlation length controls the rate of the change of roughness along the surface. For each set of these two parameters there are an infinite number of possible surface forms in theory. Using the numerical simulation technique, many surface forms can be generated by varying the seed value in random number generator. Three examples of which are given in Figure 3.7; here, choosing $\sigma = 1$ because this will produce normalized roughness amplitudes. To obtain roughness with a given *RMS* value, it suffices to multiply the roughness amplitudes by the desired *RMS* value.

A set of isotropic rough surfaces having Gaussian statistics and the same statistical parameters ($\sigma = 1 \mu\text{m}$ and $\lambda_x^* = \lambda_y^* = 20 \mu\text{m}$), but different

CHAPTER 3.

values of simulation parameters n_x and n_y are generated, which means that different sampling intervals are chosen in numerical simulation. Figure 3.8 shows typical profiles taken from the set of the generated rough surfaces. Because the generated rough surfaces are a set of isotropic surfaces, the parameter γ of surface anisotropy is equal to 1, i.e. $n_x = n_y$. To reveal the different structure of the roughness, the sampling intervals are chosen to be equal to the correlation length, i.e. $n_x = n_y = 1$ in Figure 3.8 (a); to be equal to the half of the correlation length, i.e. $n_x = n_y = 2$ in Figure 3.8 (b); to be equal to the one-tenth of the correlation length, i.e. $n_x = n_y = 10$ in Figure 3.8 (c). As can be seen from Figure 3.8, a large sampling interval can reveal the main structure of the roughness and will miss out many small peaks, while a small one will reveal more fine structure of the roughness.

Figure 3.4 (b) represents a generated anisotropic rough surface with Gaussian statistics. The anisotropic parameter γ is chosen to be 2 and the statistical parameters are $\sigma = 1 \mu\text{m}$ and $\lambda_x^* = 40 \mu\text{m}$, $\lambda_y^* = 20 \mu\text{m}$. Figure 3.9 shows typical x and y profiles taken from the generated surface in Figure 3.4 (b). The x profiles are smooth and have longer asperity dimensions than the y profiles, owing to the higher correlation length of the y profiles. The anisotropy of the roughness can be seen from longer dimension of the asperities in x direction.

CHAPTER 3.

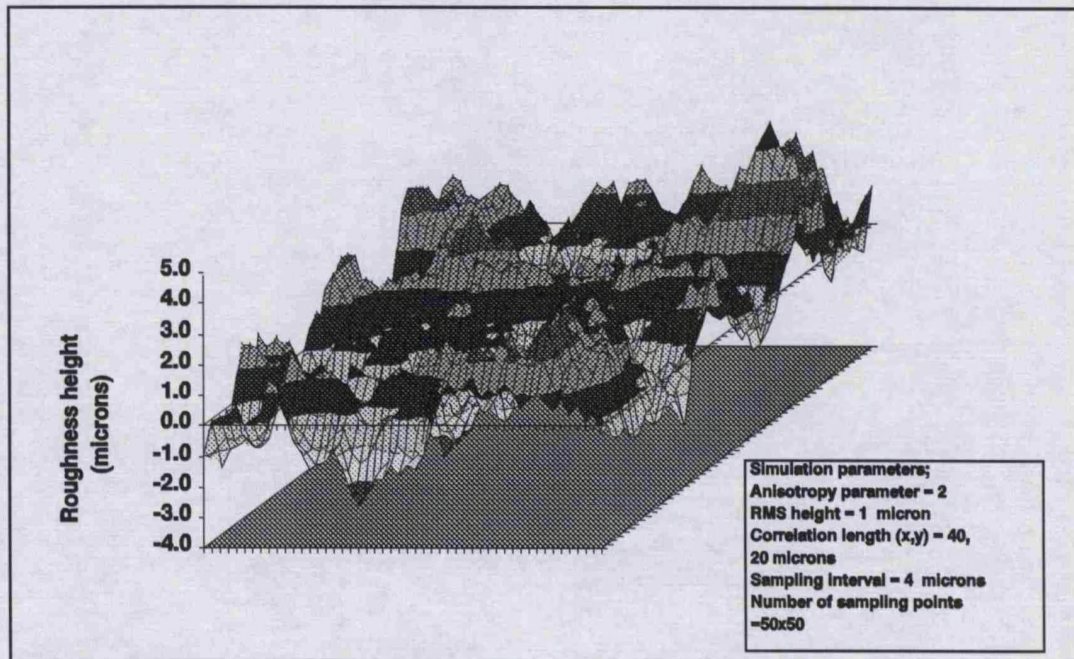
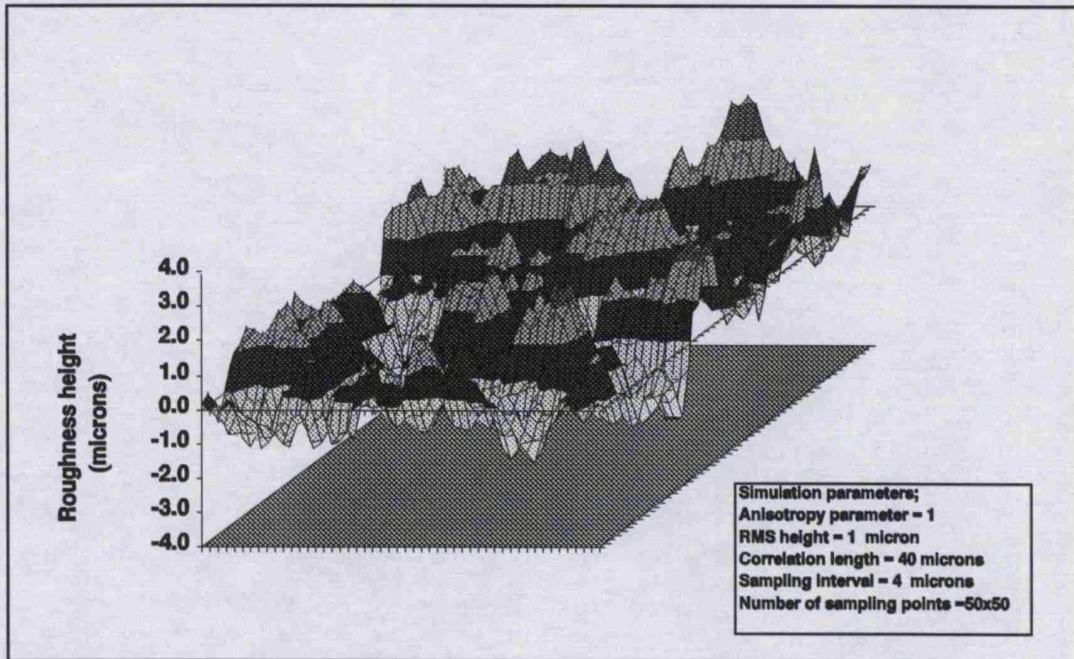


Figure 3.4 Generated rough surfaces with Gaussian statistics

CHAPTER 3.

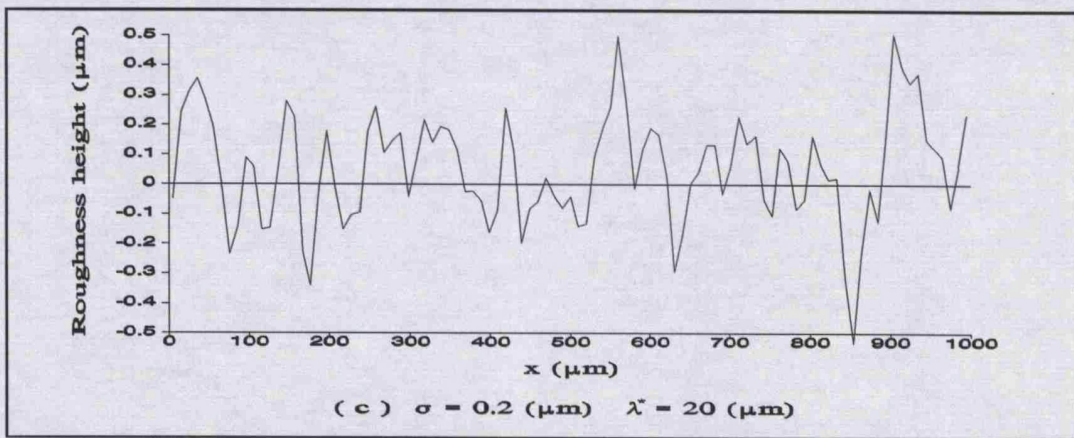
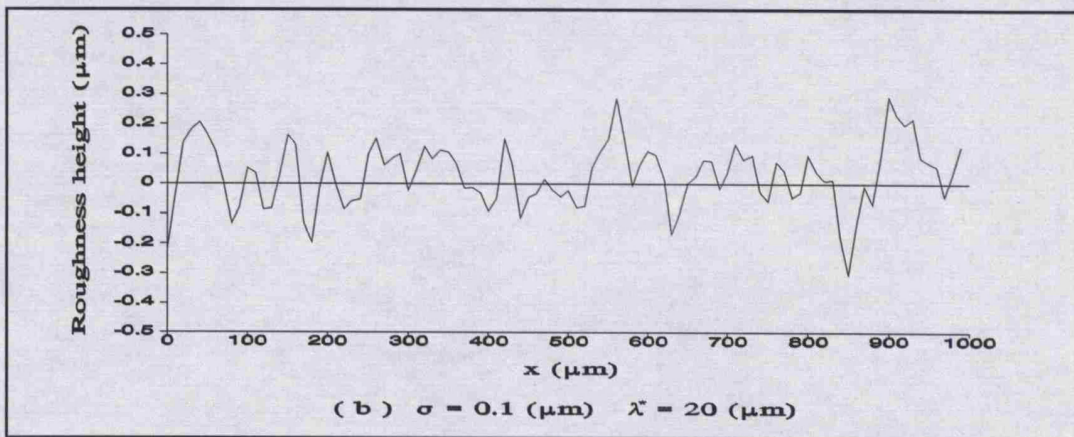
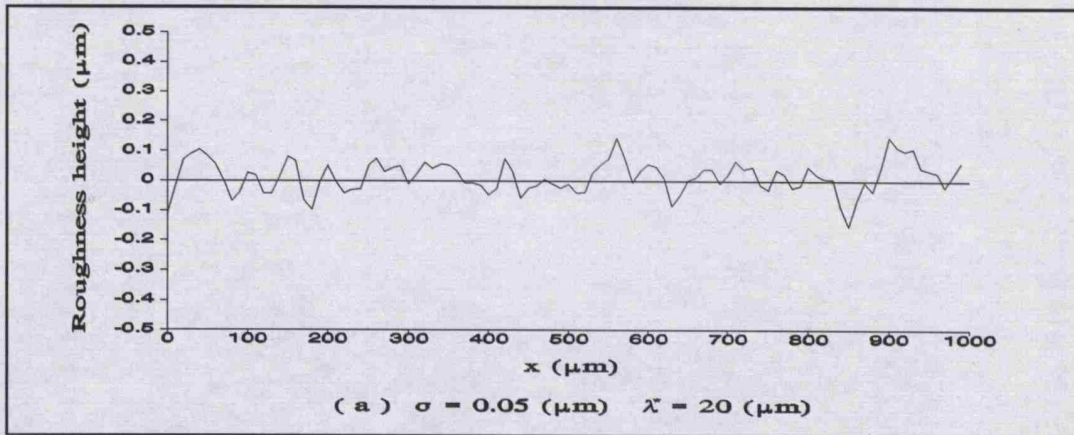


Figure 3.5 Profiles of generated isotropic rough surfaces with Gaussian statistics, but different RMS height σ

CHAPTER 3.

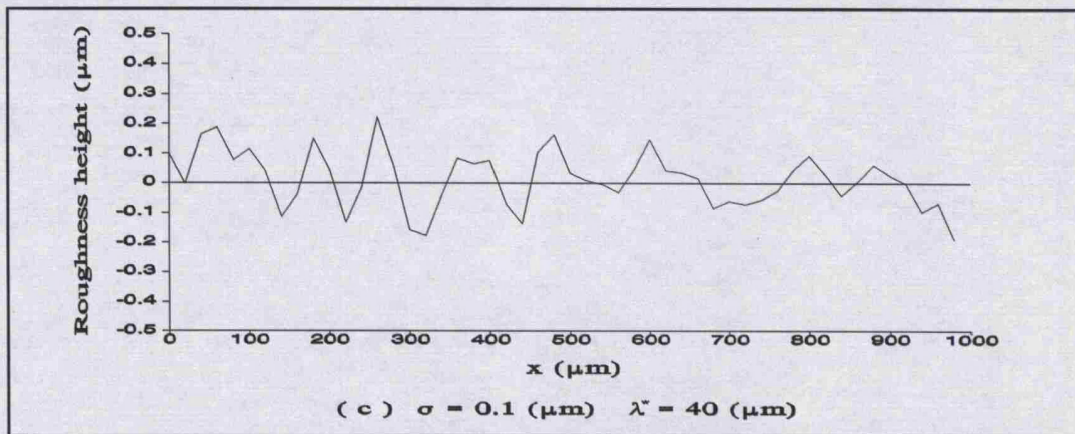
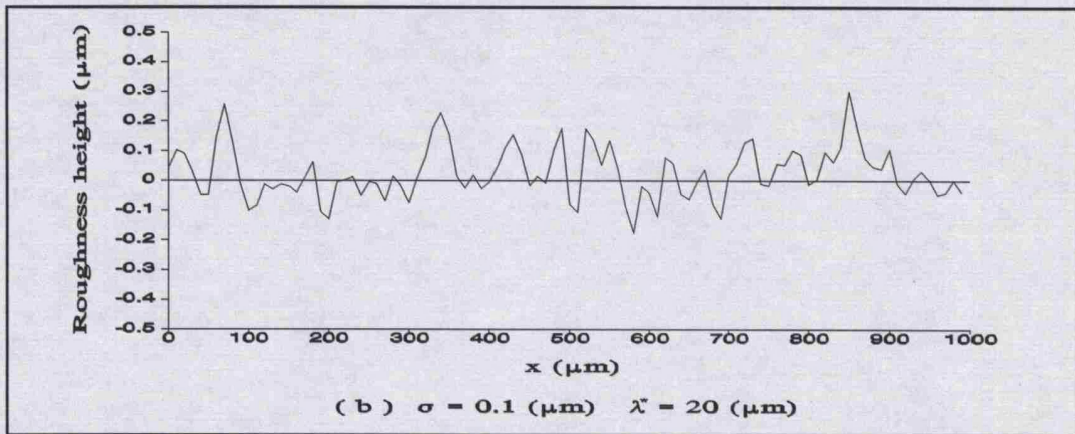
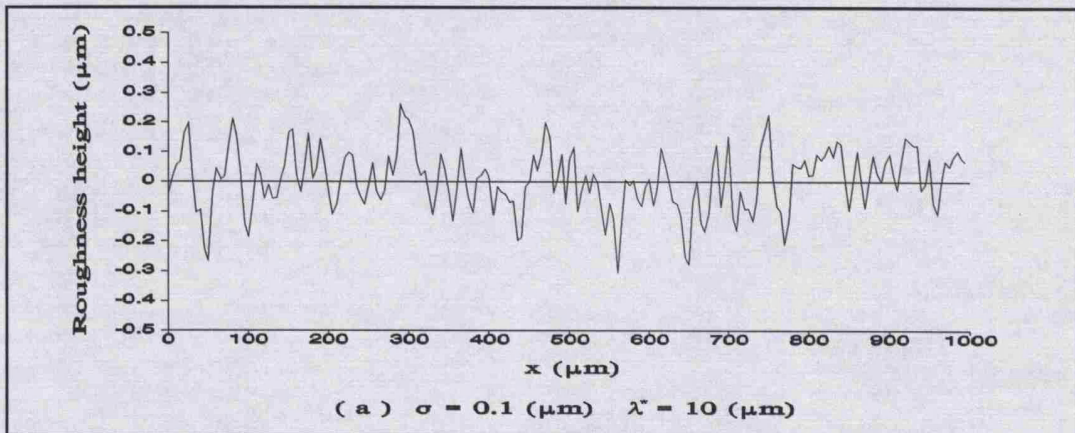


Figure 3.6 Profile of generated isotropic rough surfaces with Gaussian statistics, but different correlation length λ^*

CHAPTER 3.

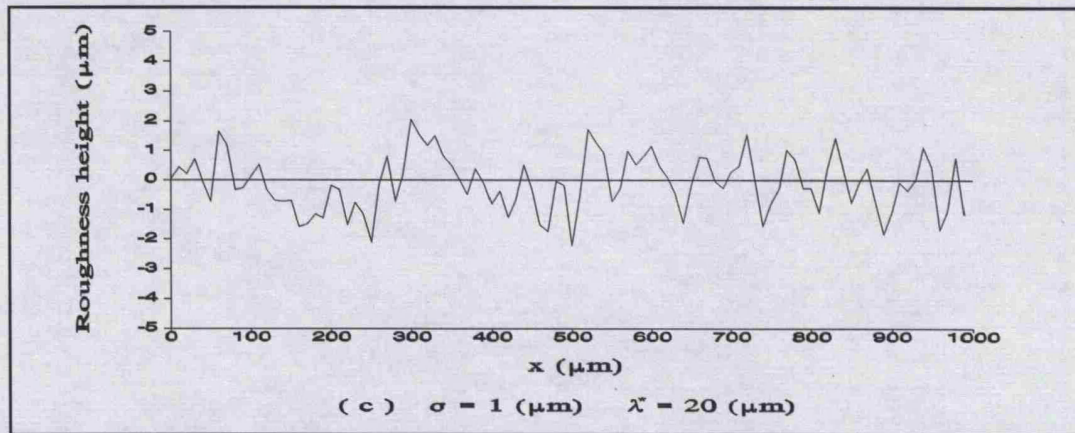
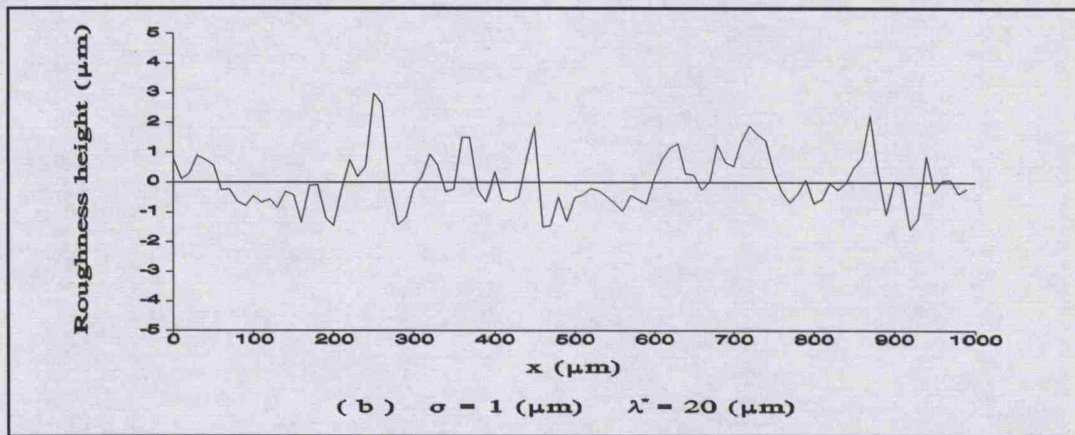
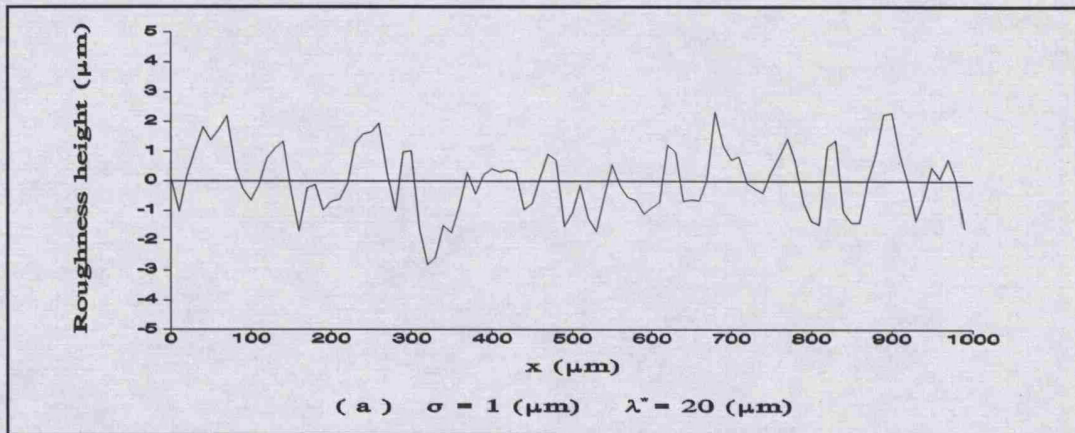


Figure 3.7 Profiles of generated rough surfaces with Gaussian statistics and same statistical parameters but different surface forms

CHAPTER 3.

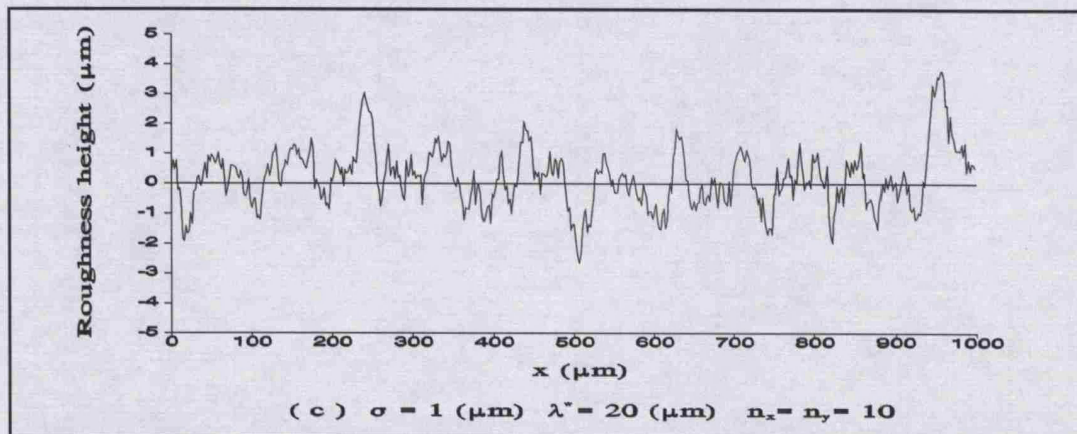
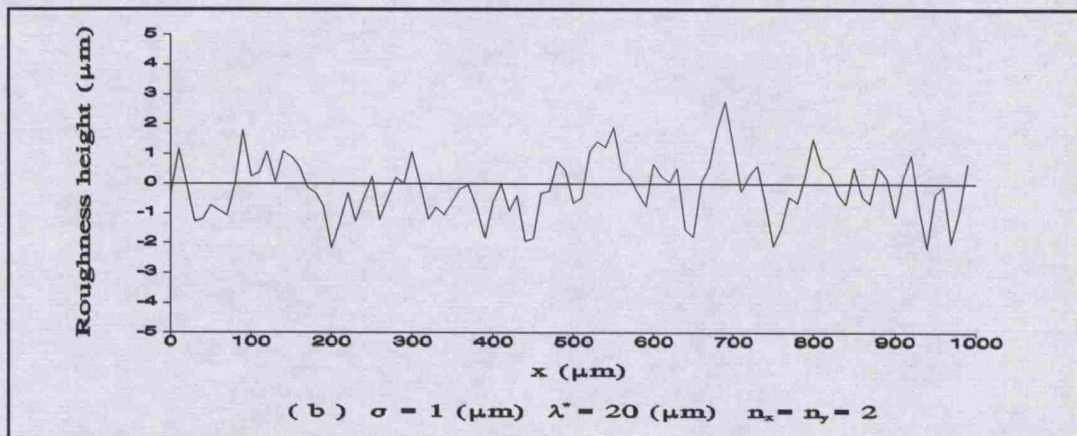
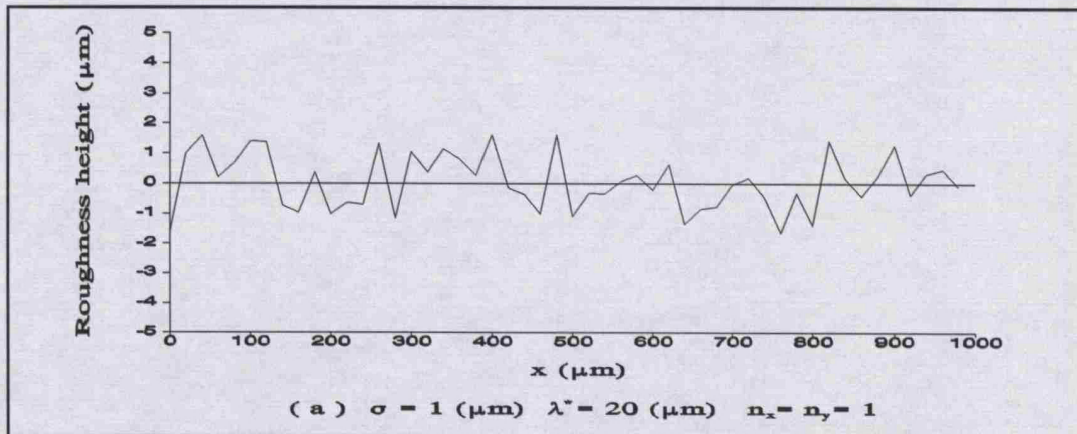


Figure 3.8 Profiles of generated surfaces with Gaussian statistics and same statistical parameters but different values of simulation parameter

CHAPTER 3.

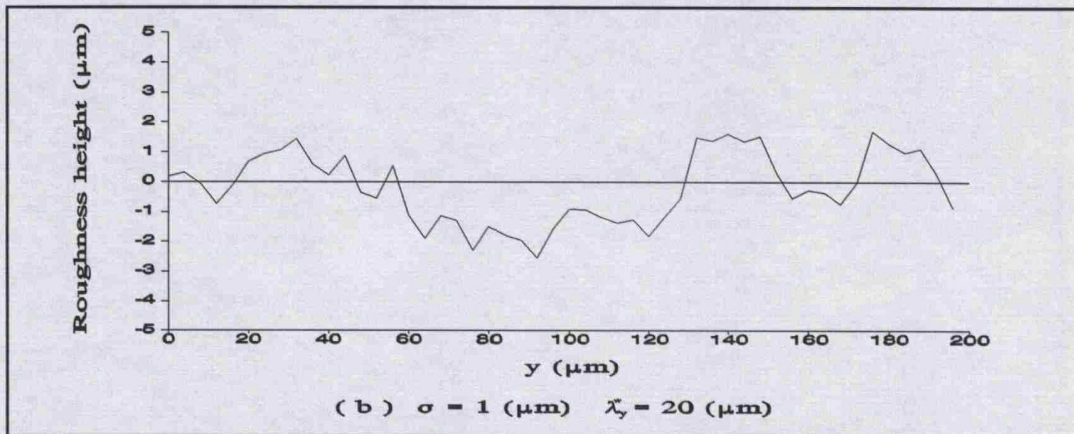
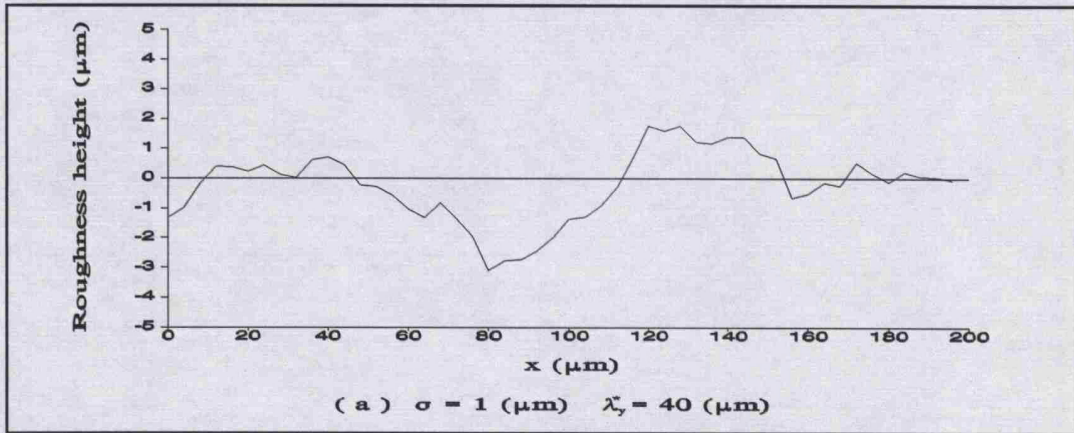


Figure 3.9 Typical x and y directional profiles of the generated surface in Figure 3.4(b)

CHAPTER 3.

3.5.2 Comparison of Numerical Simulation and Theoretical Results

Since generated rough surfaces are random and are known to have given Gaussian probability distribution and exponential autocorrelation function, it is necessary to check statistically the numerical simulation. A series of such statistical checks for generated rough surfaces have been done. Figure 3.10 shows comparisons of the probability density function of the generated rough surfaces in Figure 3.4 (a) and (b) by numerical simulation with that of a Gaussian distribution. The results show that they produce the close agreement between the theory and simulation.

CHAPTER 3.

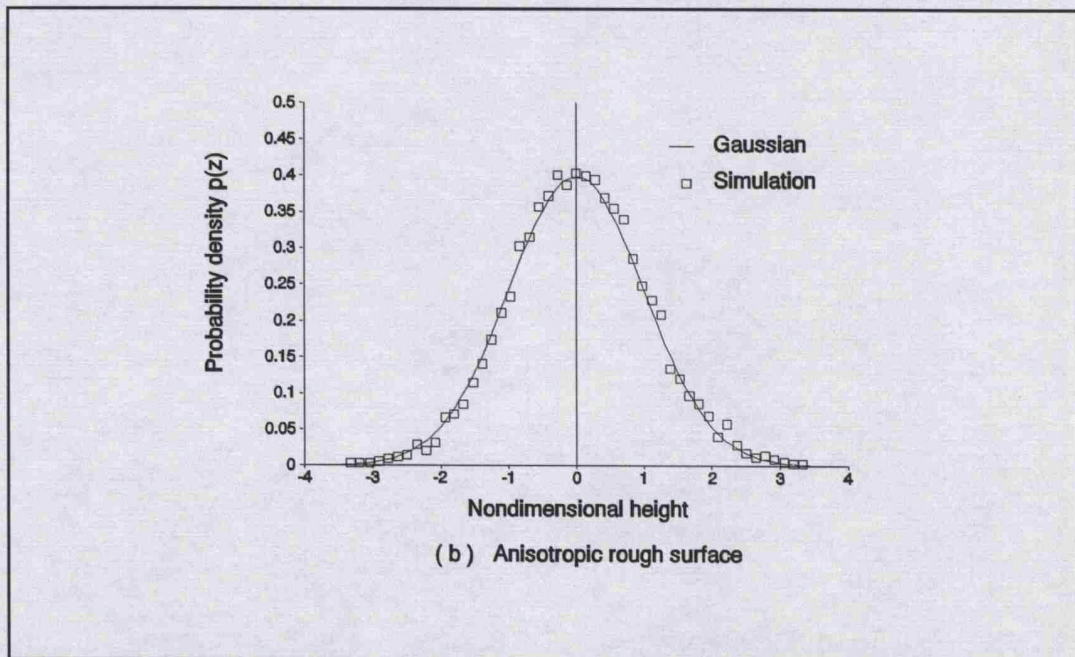
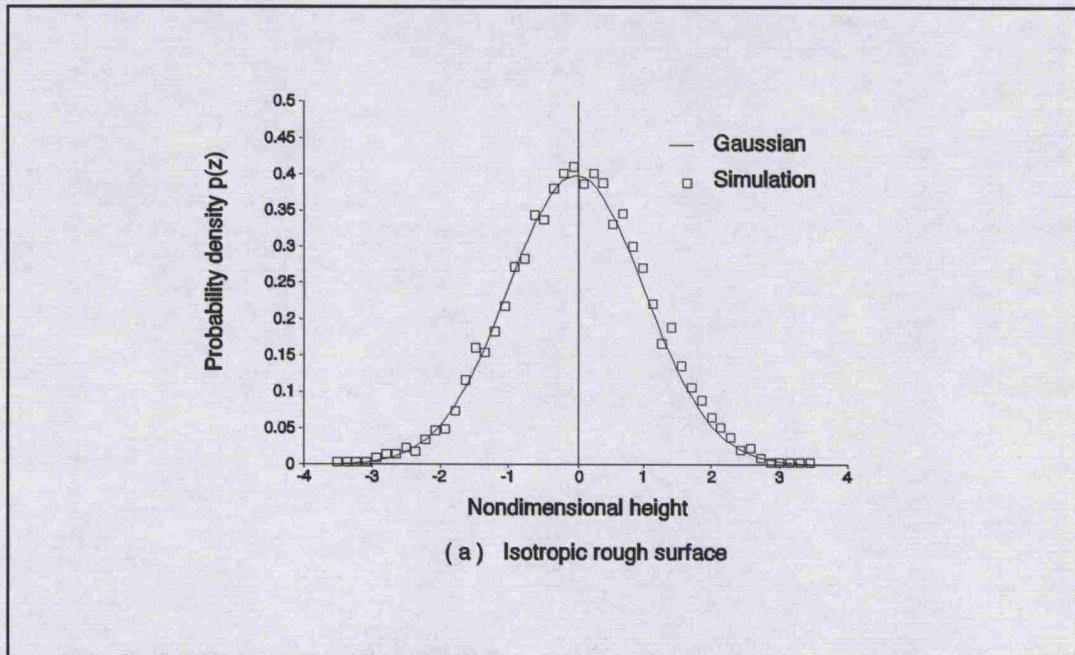


Figure 3.10 Comparison of probability density functions with respect to nondimensional height (z/σ)

CHAPTER 3.

To compare the ACF of the generated surface with the expected ACF, the x and y profile ACFs of the generated surface are calculated (Peklenik 1967/1968), it is:

$$R_{p0} = E(Z_{ij}Z_{i+p,j}) = \frac{1}{(N_x-p)N_y} \sum_{i=1}^{N_x-p} \sum_{j=1}^{N_y} Z_{ij} Z_{i+p,j} \quad (3.20)$$
$$R_{0q} = E(z_{ij}z_{i,j+q}) = \frac{1}{N_x(N_y-q)} \sum_{i=1}^{N_x} \sum_{j=1}^{N_y-q} Z_{ij} Z_{i,j+q}$$

The theoretical value of the autocorrelation function which has the form given in Equation 3.17 can be calculated by Equation (3.19). For the generated rough surfaces shown as in Figure 3.4 (a) and (b), the ACF values of the expected and the generated surface are given in Table 3.1 and Table 3.2.

Figure 3.11 and Figure 3.12 show the x and y profile ACFs of the generated rough surfaces in Figure 3.4 (a) and (b) which agree well with the desired ACFs. Since the ACF is fundamentally a random function, we cannot expect the ACF of every generated surface to be identical. Good agreement between the expected and observed ACFs, however, depends critically on how well the random number generator generates a set of mutually independent identically distribution Gaussian random numbers $[\eta_{ij}]$.

The close agreement between the theory and simulation validates the use of this procedure to numerically simulate a random rough surface having predetermined probability density functions and autocorrelation functions

CHAPTER 3.

Table 3.1 ACF values of the expected and the generated surface in Figure 3.4(a)

x profile ACFs												
	p = 0	p = 1	p = 2	p = 3	p = 4	p = 5	p = 6	p = 7	p = 8	p = 9	p = 10	p = 11
R_{p0} (expected)	1.000000	0.794534	0.631284	0.501576	0.398519	0.316637	0.251579	0.199888	0.158817	0.126186	0.100000	0.000000
R_{p0} (simulated)	1.005065	0.779231	0.617834	0.523068	0.385769	0.336983	0.246166	0.187292	0.161074	0.122356	0.090085	0.034200
y profile ACFs												
	q = 0	q = 1	q = 2	q = 3	q = 4	q = 5	q = 6	q = 7	q = 8	q = 9	q = 10	q = 11
R_{q0} (expected)	1.000000	0.794534	0.631284	0.501576	0.398519	0.316637	0.251579	0.199888	0.158817	0.126186	0.100000	0.000000
R_{q0} (simulated)	0.985754	0.776038	0.662465	0.515340	0.401323	0.308655	0.261231	0.187668	0.150765	0.131676	0.084731	0.020044

CHAPTER 3.

Table 3.2 ACF values of the expected and the generated surface in Figure 3.4(b)

x profile ACFs												
	p = 0	p = 1	p = 2	p = 3	p = 4	p = 5	p = 6	p = 7	p = 8	p = 9	p = 10	p = 11
R_{p0} (expected)	1.000000	0.794534	0.631284	0.501576	0.398519	0.316637	0.251579	0.199888	0.158817	0.126186	0.100000	0.000000
R_{p0} (simulated)	0.989765	0.8135183	0.649678	0.481339	0.389740	0.3146785	0.260475	0.1911408	0.1621543	0.124159	0.089272	0.015141
y profile ACFs												
	q = 0	q = 1	q = 2	q = 3	q = 4	q = 5	q = 6					
R_{q0} (expected)	1.000000	0.631284	0.398519	0.251579	0.158817	0.100000	0.000000					
R_{q0} (simulated)	0.998701	0.662285	0.410259	0.247788	0.162295	0.0852762	0.0310871					

CHAPTER 3.

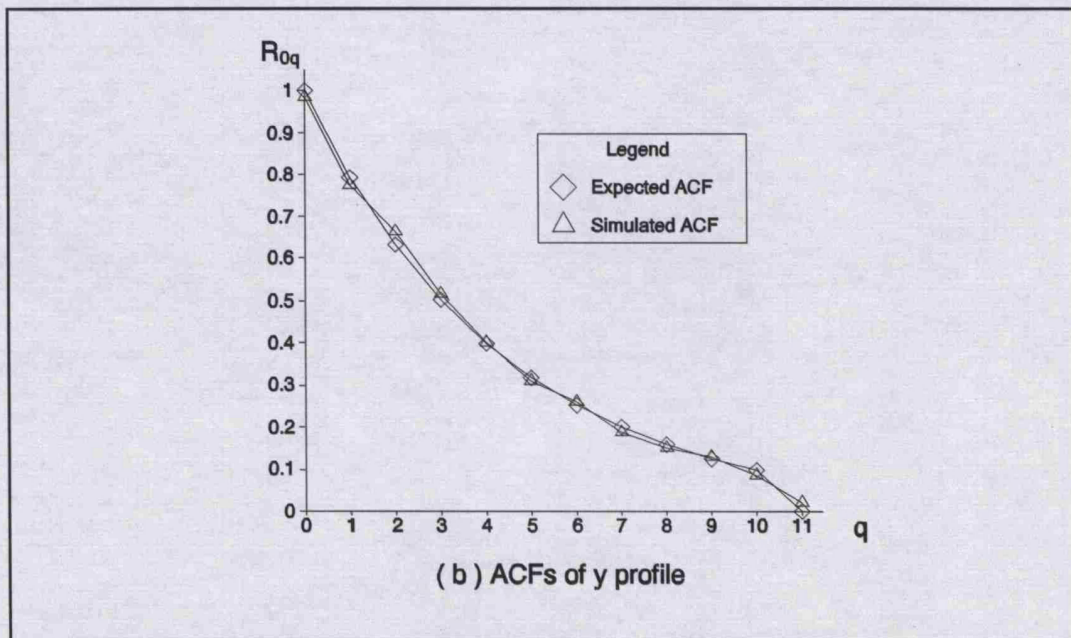
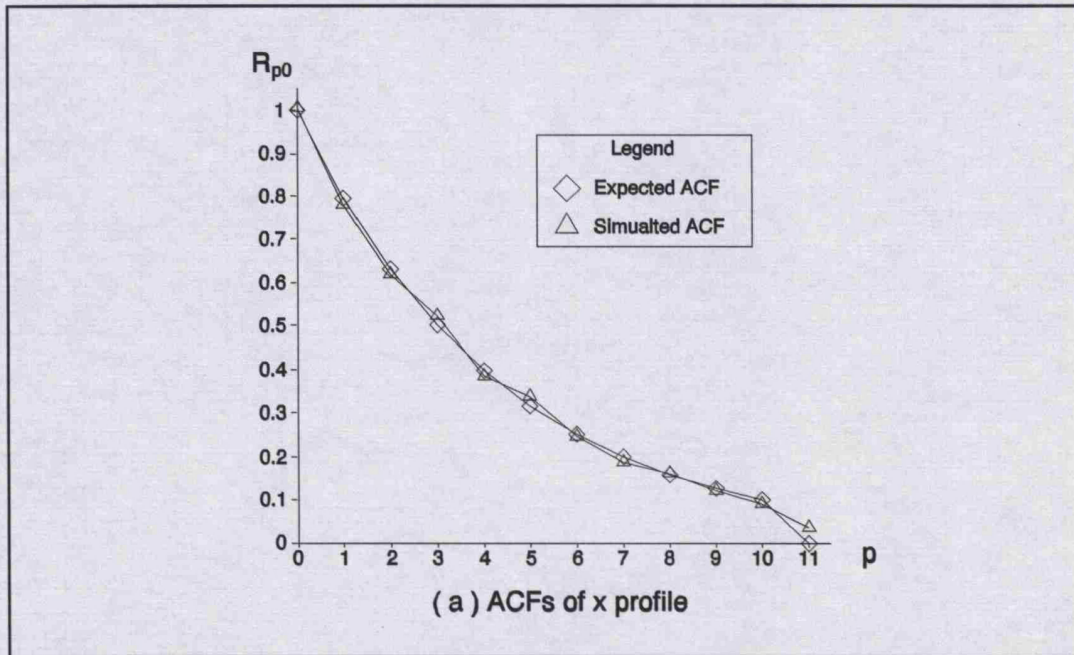


Figure 3.11 x and y profile ACFs of the generated surface in Figure 3.4

(a)

CHAPTER 3.

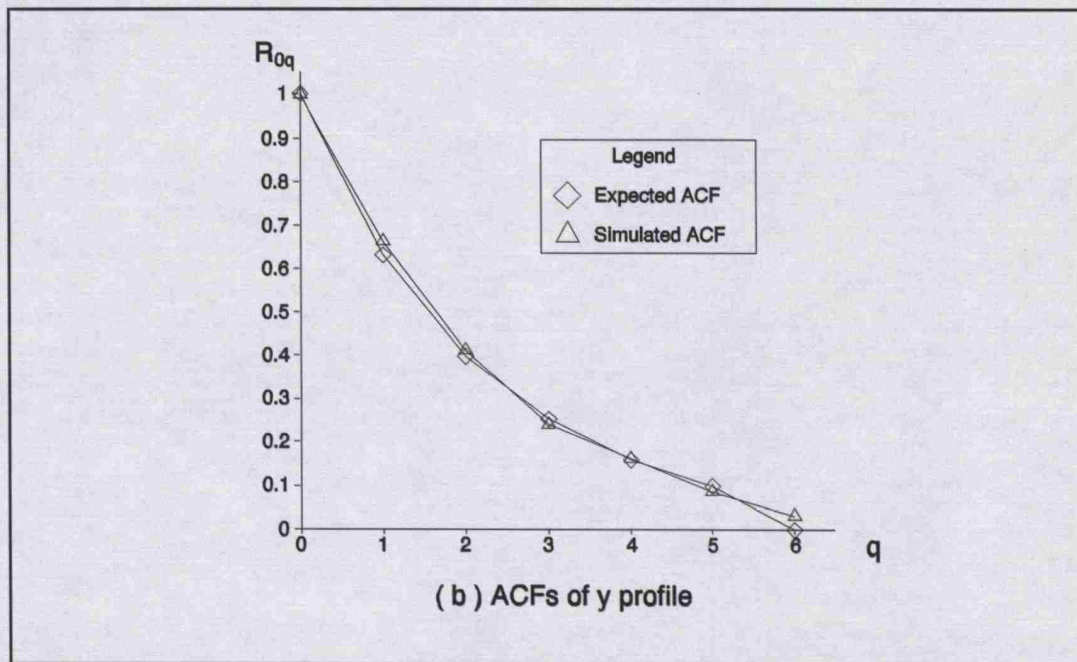
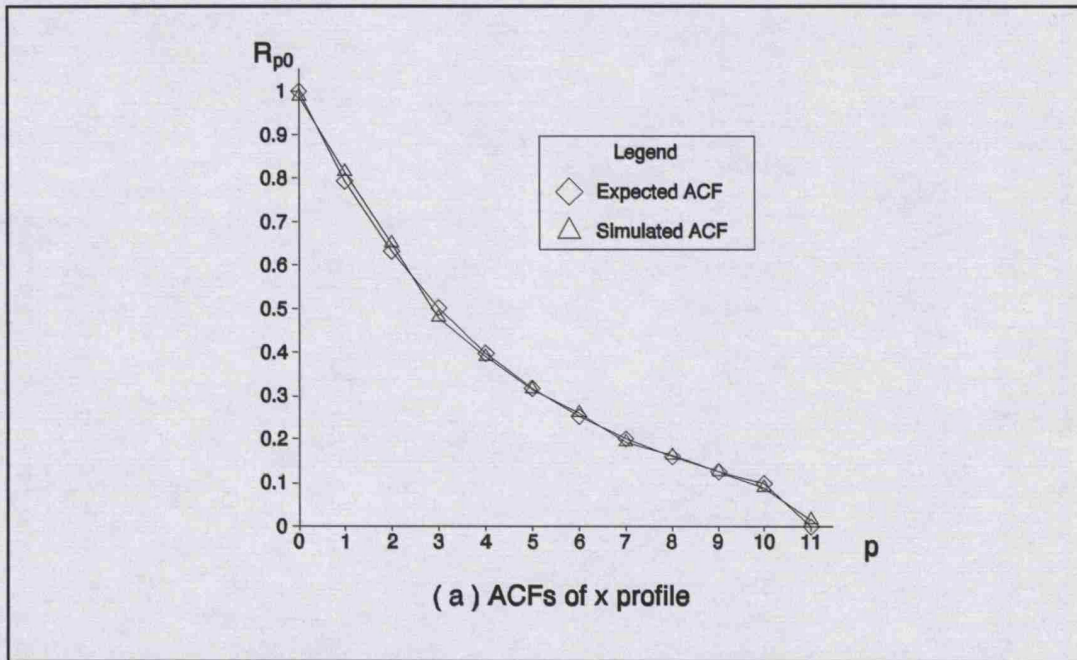


Figure 3.12 x and y profile ACFs of the generated surface in Figure 3.4

(b)

CHAPTER 3.

3.6 Conclusion

With complex problems involving random inputs, numerical simulation is a promising tool for analysing roughness-related phenomena in tribology, fluid sealing etc. An essential requirement for such simulation studies is the ability numerically to generate rough surfaces which have statistical properties similar to real surfaces. Most of the statistical properties of a rough surface can be derived from a knowledge of two statistical functions, the probability density and the autocorrelation function (ACF). Hence a good algorithm should be able to generate surfaces having prescribed probability density functions and ACFs.

An algorithm which can satisfy such demand has been devised and the computer program corresponding to the algorithm has developed in Fortran. In simulation, first, an input matrix, whose components are independent identically distributed random numbers, is generated using random number generators. The desired probability density of the roughness heights is obtained by controlling the probability density of the random numbers in the input matrix. For a Gaussian distribution of roughness heights it suffices to generate the input matrix with a Gaussian density function. To generate surfaces with a given ACF, linear transformations on random matrices are utilized on the input matrix, where these coefficients of the transformation matrix have to be determined by solving a system of non-linear equations formulated based on the autocorrelation matrix. Thus a set of correlated random numbers representing the height of the rough surface is obtained.

CHAPTER 3.

The numerical simulation technique has been verified through a series of comparisons. The close agreement between the theory and simulation validates the use of this procedure to numerically simulation a random surfaces.

Numerical simulations of rough surfaces not only substitute surface measurements by artificially creating surfaces, but they also facilitate the simulation of surface-related random phenomena.

CHAPTER 4.

Contact of Rough Surfaces

4.1 Introduction

The study of the contact of deformable bodies has historically been divided between two approaches, reflecting the interests of the general engineer or designer and the tribologist. The first assumed that the bodies are smooth and can be adequately described by their nominal geometry. This approach yields information on the overall level of stress and deformation. The second admits that engineering surfaces are comprised of a multitude of peaks and valleys which determine the true nature of the contact.

The first significant elastic contact analysis was produced by Hertz (1896), who solved the problem of three-dimensional non-conformal contact of elastic solids. This classic work has stood the test of time and over the past 100 years (Johnson, 1982) has provided the basic of much of our understanding of contact mechanics.

The contact between rough surfaces has strong influence on the

CHAPTER 4.

phenomena of friction, wear, lubrication and sealing, as well as conduction of heat and electricity. It has led to the development of various contact models of rough surfaces so that these studies have been independent of one another. According to the approach used in this study, the contact model of rough surfaces may be divided into two different types: the stochastic contact model and the numerical contact model (Webster and Sayles 1986).

4.2 Contact Models of Rough Surfaces

4.2.1 Stochastic Contact Model

Several stochastic models for the mechanical behaviour of contacting rough surfaces, i.e. the relation between load and mean separation and real contact area, have been developed. Some of these models are better suited for lightly loaded contacts with large separations where the surface asperities deform elastically, while other models are more suitable for high loads and small separations corresponding to plastic deformation of the surface asperities.

Greenwood and Williamson (hereafter referred to as GW) (1966) developed the earliest analysis model accounting for the random nature of surface roughness. In their model, the rough surface is presumed to be covered with local high spots or asperities whose summits are all spherical in shape. All the summits are presumed to have the same radius, but the summit heights are randomly variable. Based on the experimental observation, they

CHAPTER 4.

found that the height distributions of many manufactured surface profiles are close to Gaussian or normal probability law. Moreover, the peak height distribution is also Gaussian. Based on the assumption that the contacting asperities deform elastically according to Hertz theory, they studied the contact of an elastic rough surface having the Gaussian height distribution and a rigid smooth plane. The model was defined by three parameters; the standard deviation of the summit height distribution; the radius of the curvature of the summits; and the density of summits per unit area. The relationship between real contact area and load is found to be approximately linear.

The basic GW model has been extended further to include such as aspects as curved surfaces by Greenwood and Tripp (1967) and two rough surfaces with misaligned asperities (Greenwood and Tripp 1971). The GW model is called as the asperity-based model. This asperity-based model provided information on modes of deformation with the restriction of using idealised asperity shapes. In a more general paper Greenwood (1967) discussed the relative merits of contact theories based on asperity models and profile measurements. Each approach has advantages over the other. Profilometric theories, using the bearing area curve to define the contact area as a function of separation, provide information on load-compliance laws and can deal with both surfaces being rough, but this is achieved at the cost of using simple contact stress laws.

To some extent a marriage between profilometric and asperity based theories was achieved by Whitehouse and Archard (hereafter referred to as WA) (1970). They presented a more rigorous analysis of a random surfaces.

CHAPTER 4.

The simplification in the GW model of using a constant radius of curvature was removed in WA model. They regarded the surface profiles as random signals represented by a height distribution and an autocorrelation function. They assumed that the surface height distribution is Gaussian and that surface profiles have an exponential autocorrelation function, and derived the peak height distribution and asperity curvature distribution. The model could be completely represented by parameters; the standard deviation of height distribution, and the exponent of the exponential autocorrelation function. Based on their model, they obtained an approximately linear real contact area-load relationship, and mean contact pressure higher than that obtained by Greenwood and Williamson. Following Whitehouse and Archard, Onions and Archard (1973) discussed the contact of random surfaces, and their derived results were compared with the earlier work of Greenwood and Williamson.

Bush, Gibson and Thomas (hereafter referred to as BGT) (1975) used the Nayak microgeometry assumptions in the random process model to develop an elastic contact model for isotropic surface that treated asperities as elliptical paraboloids with random principle axis orientation and aspect ration, i.e., the microcontacts appear. Random process theory, following the work of Longuet-Higgins (1957a, 1957b) and Nayak (1971), was used to the deduce the density of extremes by jointing the distribution of summit heights and the distribution of the mean curvatures. At large separations, their model achieved an exact proportionality between load and area. The analysis was extended in Bush, Gibson and Thomas (1979) to cover strongly anisotropic rough surfaces. Except for the constant of proportionality involving extra terms requiring elliptical integrals, the results were similar to the isotropic surface.

CHAPTER 4.

However more comprehensive comparisons of stochastic models mentioned above for the contact of rough surfaces are contained in McCool (1986).

Both experimental and theoretical studies of plastic rough surface contact have been reported by Williamson and Hunt (1972), Pullen and Williamson (1973), Uppal, Probert, and Thomas (1973), Childs (1973, 1977). These have centred around investigating the resistance of asperities to crushing under high loads.

The first contact model including the condition of elastic-plastic deformation was presented by Chang, Etsion and Bogy (hereafter referred to as CEB model) (1986). The CEB model is based on volume conservation of an asperity control volume during plastic deformation with the basic assumptions of the GW asperity-based model. The CEB elastic-plastic model not only produced a close agreement with GW elastic model in their prediction of contact area for the condition of elastic deformation but also used in cases where the separation of contacting surfaces is critical, such as in sealing or magnetic recording.

Stochastic contact models for the analysis of the contact of rough surfaces, such as the models mentioned above, are numerous. They have been refined from the simple asperity to the complex random process models and from the condition of elastic or plastic deformation to that of elastic-plastic deformation, over many years.

These stochastic contact models have a number of shortcomings:

CHAPTER 4.

- (1) They require a number of assumption regarding the probability distribution of asperity heights, slope, curvatures etc.;
- (2) They require the use of the simple asperity shapes;
- (3) They are limited to discrete contact "spots" which are often assumed to deform independently of one another;
- (4) They do not predict the deformed shape of the surfaces, particular for the areas not in contact.
- (5) Knowledge is required about the size of asperities that are important to the problem.

These models are of great importance to the understanding of the average properties of the contact of rough surfaces; However the nature of the statistical contact model limits their ability to calculate the real pressure distribution and the deformed shape. This information might be very important in simulation analysis of leakage.

4.2.2 Numerical Contact Model

Analytical methods for elastic contact analysis have continued to be the subject of attention during the past decade. Analytical solutions to elastic contact problems require a simple assumption for the undeformed shape of the

CHAPTER 4.

surfaces. For instance, in the case of Hertz (1986) it was assumed that the surfaces could be approximated by second degree polynomials near the contact region. The advent of computers, and in particular the subsequent development of the numerical methods in stress analysis, has to some extent relaxed this restriction on the class of contact problems that can be solved. Therefore, researchers have attempted to analyze a more sophisticated range of body shapes by employing numerical techniques.

The general approach to solving contact problems numerically is to divide the contacting surfaces into a number of discrete elements. Over each element an assumption is made about the local distribution of pressure, often a constant or a linear variation being used. From the shape of the element, and the assumed elemental pressure distribution, it is possible to use half space theory to derive expressions for the displacements anywhere on the surface. The total displacement at a given point is merely the sum of the displacements due to all the elemental pressures. This leads to a set of linear simultaneous equations that relate displacements to pressures. The numerical solution can be obtained by different methods.

Many advances have been made in the development of numerical methods for the analysis of contact problems over many years. The numerical methods for the analysis of general elastic bodies in contact, in principle, can be extended further to deal with the analysis of rough surfaces in contact. The contact behaviour of deformable bodies considering the effect of roughness is usually studied in two different ways. The first assumed that the bodies are smooth, the numerical elastic contact model is produced by the general

CHAPTER 4.

numerical approach to solving contact problems; the second considers the contact effects of surface roughness and topography.

First, it is necessary to define two-dimensional numerical contact model and three-dimensional numerical contact models. Normally two-dimensional contact models are developed based on the assumption of plane strain and used directly data representing a surface profile; while three-dimensional contact models are developed based on a full three-dimensional stress analysis and used directly data representing a topographical surface.

Webster and Sayles (1986) developed a two-dimensional numerical contact model based on the Boussinesq force-displacement relationship for an elastic half-space to solve the elastic contact of two-dimensional real rough surfaces. The significant numerical model presented by Webster and Sayles showed a link between the numerical analysis in which smooth boundaries are assumed and the statistical treatments adopted for the contact of analysis of rough surfaces. The model was constructed in the following way: first, a basic model of numerical elastic contact was produced by assuming that the bodies are smooth; then the basic model was modified by taking account of the effects of roughness on the contact. The model used data directly recorded from a stylus measuring instrument and could yield important results about the real pressure distribution and the deformed shape of surface profiles.

Lee and Cheng (1992) developed the first two-dimensional elastic-perfectly-plastic contact model of rough surfaces based on the Flamant solution (Flamant 1892). This model is principally based on elastic contact

CHAPTER 4.

but a simple model of plasticity has been incorporated so that the contact condition of elastic deformations can be made realistic. The plastic deformation on the high asperity peaks were taken into account by setting a ceiling on their pressures at the material hardness value. Once an element pressure determined by the elastic contact model has reached this ceiling value, the element would be allowed to deform without any further increase in pressure so that the element pressure is set to equal to the ceiling value. The extra load would automatically be redistributed to neighbouring elements. Although the proposed method is not accurate for plastic contact it reproduced the main features of a mixed elastic-perfectly-plastic contact. The real area of contact predicted by the present model increases linearly with contact pressure when the load is very low, but as the pressure becomes greater it deviates from linearity. The relationship of load-areas predicted by the model was compared with that of Onions and Archard's work. The result showed that the model should give much larger real contact area for all loads as compared to Onions and Archard's model.

The disadvantage of two-dimensional profile analysis is that only a section of the surface is examined. However, many engineering problems such as friction, wear, lubrication, sealing and contact resistance etc. would require quantitative information in three dimensions. It has led to the development of three-dimensional numerical contact models of rough surfaces.

Xian and Zheng (1991) provided a numerical model for the elastic contact of three-dimensional rough surfaces on the basis of the Boussinesq solution for a normal point load. The concept of "intersection asperities" was

CHAPTER 4.

introduced to be the numerical calculation element, and hence the contact problems of real rough surfaces could be simplified into a non-Hertzian contact problem of an intersection asperity. This leads to the explicit calculation of all the contact area for individual rough surfaces. The mutual of neighbouring intersection asperities was ignored, so that the three-dimensional contact model is only useful in cases where the real contact area is relatively small. The present model was applied to predict the relationship of load-v-area. It had been shown that the real contact area was proportional to the load for relatively smooth surfaces ($R_a \leq 0.7 \mu\text{m}$), which coincides with the conclusions of the GW and WA models; however, the relationship between the real contact area and the load is nonlinear for relatively rough surfaces ($R_a \geq 1.9 \mu\text{m}$).

The choice of numerical solution technique to solve elastic contact problems is important, as it will determine the accuracy of solutions and the time required for solution. The method adopted by Webster and Sayles (1986), Lee and Cheng (1992) and Xian and Zheng (1991) is called the Matrix Inversion Method (Johnson 1985), in which boundary conditions are satisfied exactly at specified "matching points". The method is straightforward and simple for numerical solution. However, for many contacts problems requiring numerical analysis it is not easy to determine to the contact area at the outset. Therefore, an initial estimate must be made. If this estimate is too large some values of p_i obtained will be tensile, whereas if too small an area was postulated there will be interpenetration of the surfaces exterior to the contact. It will therefore be necessary to check the solution for both of these violations. If tensile traction occurs then non-contact should be assumed at

CHAPTER 4.

those pressure elements and if interpenetration occurs exterior to the assumed contact then additional pressure elements and contact points will be required in these areas. If the formulation is altered in this way it is possible to resolve the equations and repeat the test for consistency. In most cases iteration in this manner will yield a fully consistent solution after several cycles.

One of the observations made by Webster and Salyes (1986) had been the increase in run time with small values of surface roughness. This is probably due to the increased contact area and a "decoupling" effect as contacting points become more close to one another thus more iterations are required to achieve a solution. And for some cases, there is difficulty in the convergence of solutions. Another conclusion made by Hartnett (1980) had been that the resulting system of linear equations would be extremely ill-conditioned as the number of elements increases, thus computer rounding off greatly distorts the results and limits this approach to unacceptably coarse discretizations of the contact region. Clearly it might be advantages to use an alternative method of solution.

A powerful alternative method of numerical solution is called the variational method based on variational principles (Johnson 1985), in which the values of the traction elements are chosen to minimise an appropriate energy function. The variational method will be adopted for the cases of frictionless contact of rough surfaces with the advantage that no iteration is involved for cases of frictionless contact where only the normal pressure needs to be determined, thus the distortion of solution may be eliminated. The full

CHAPTER 4.

explanation to this approach is given in Sections 5.4.1 and 6.3.3. In Chapter 5 and Chapter 6, two-dimensional and three-dimensional numerical model for the elastic contact of rough surfaces will be developed based on the numerical solution technique of variational method.

4.3 Contact Geometry

In the frictionless contact of elastic solids, the contact stresses depend only upon the relative profile of their two surfaces, i.e upon the shape of the gap between them before loading; the contact system may then be replaced, without loss of generality, by a flat, rigid surface in contact with a body having an effective modulus E' and an equivalent roughness (or composite roughness) defined by $z_1(x,y)+z_2(x,y)$ which results in same undeformed gap between the surfaces (Lee and Cheng 1992). The equivalent Young's modulus E' is given by:

$$\frac{1}{E'} = \frac{1 - \nu_1^2}{E_1} + \frac{1 - \nu_2^2}{E_2} \quad (4.1)$$

where E_1, E_2 is Young's modulus and ν_1, ν_2 is Poisson's ratio for bodies 1 and 2 respectively.

In the following analysis, we will consider the contact of a rigid flat plane with a deformed surface of equivalent roughness as shown in Figure 4.1, which has been used in the contact analysis of rough surfaces by Greenwood

CHAPTER 4.

and Tripp (1971) amongst others. The original undeformed mean plane of the rough surface is assumed to be the reference plane from which other points are measured. $z(x,y)$ is the surface roughness (positive upward) and d is the distance between the reference plane and the rigid plane, called the normal mean separation. The threshold normal separation d_c is defined by

$$d_c = \max\{ z(x,y) \} \quad (4.2)$$

When a current separation d is great than d_c , there is no contact for two surfaces. For a given value δ defined as the approach between the reference plane and the rigid plane, the current normal separation d is numerically equal to $d_c - \delta$.

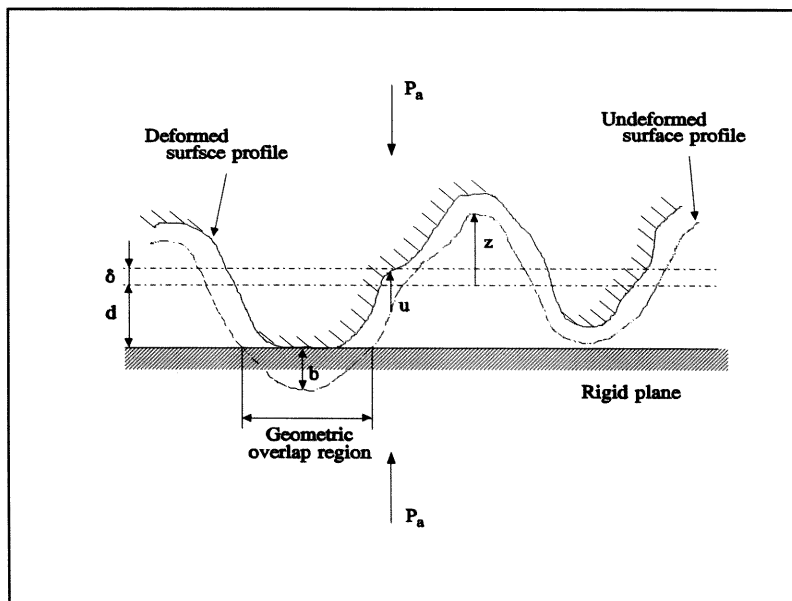


Figure 4.1 Configuration of elastic rough surface contact

CHAPTER 4.

4.3.1 Modified Original Surface Profile

The contact of rough surfaces are classified into two cases by Lai and Cheng (1985). They are:

- (1) Contact between an elastic rough punch and a rigid plane;
- (2) Contact between an elastic rough half-space and a rigid, smooth infinitely wide plane.

Since two rough surfaces in contact has been combined to form an equivalent or composite rough surface against a rigid plane, for Cases 1, this presents physically the contact between two rough punches. For Cases 2, this presents physically a mathematical equivalent of two infinitely wide half-space in contact. Because the digitized surface roughness is finite, the roughness is assumed to exist only within a square of the same finite area as rough punch as Cases 1. and smooth everywhere else. The numerical contact models developed by Webster and Sayles (1982), Liang and Linqing (1992) only can be used to the Case 1.

It may be more reasonable to consider the contact of static sealed joints as Case 2. When a "bowing" technique has been adopted (Lee and Cheng 1992), the contact analysis for Case 1 can be extended to deal with the Case 2 and the formulation for Case 2 is very similar to the formulation for Case 1. The only difference is that a uniform pressure is applied everywhere on the half-space except for the finite width rough punch in contact with the rigid

CHAPTER 4.

plane; the magnitude of this uniform pressure is set equal to the average contact pressure. In this way the average pressure over the entire half-space is constant. The application of this uniform pressure simulates the contact between two infinitely wide bodies. Figure 4.2 illustrates the physics of this approach. The top illustration of Figure 4.2 shows the uniform pressure being applied on a smooth half space over its entire area. The shape of its deformed surface is perfectly flat since this pressure, like the hydrostatic pressure, causes no relative deformation. If the pressure within the strip region is removed, the surface deforms as shown at the bottom of Figure 4.2. If a rigid plane strip is now pushed up against this deformed surface until it becomes perfectly flat, the contact pressure is again uniform everywhere. When the smooth half space with a rough strip is considered, the rough surface profile is superimposed on the same deformation $\delta_0(x,y)$. If the rigid plane is pushed up against this composite profile until it is at about the same height level as the smooth surface, the average asperity contact pressure should be very close to the surrounding uniform pressure. This is the physical basis for the approach used in Case 2 by Lee and Cheng (1992).

Thus for Case 2, the surface profile $z'(x,y)$ is defined as the original rough surface profile $z(x,y)$ superimposed on $[-\delta_0(x,y)]$, i.e.

$$z'(x,y) = z(x,y) - \delta_0(x,y) \quad (4.3)$$

where $\delta_0(x,y)$ is the displacement due to a uniform pressure

In the following sections, the general formulations for the contact problems will be derived from the contact case 1, while for contact case 2

CHAPTER 4.

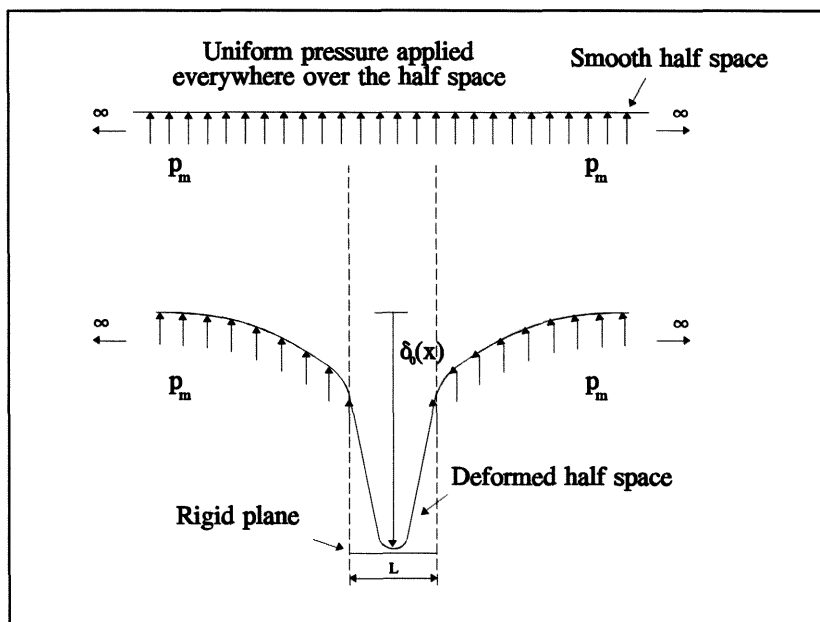


Figure 4.2 Deformation due to removal of the pressure in the rigid plane region

where a uniform pressure is applied everywhere on the half-space except for the contact simulation segment length L , the formulations derived from the Case 1 are still valid, providing the original surface profile is replaced by the modified surface profile defined by Equation (4.3).

4.3.2 Gap between Two Surfaces

The normal distance between two surfaces is called the gap. Before contact, i.e. the undeformed state, the gap geometry denoted $b(x,y)$ is known

CHAPTER 4.

and is defined by their surface geometries:

$$b(x,y) = d + z(x,y) \quad (4.4)$$

When the undeformed asperity of the surface $z(x,y)$ intersects the rigid plane, i.e. $z(x,y) > d_c$, we call the intersecting part the "intersection asperity". This gap $b(x,y)$ is negative where the bodies intersect. For an intersection asperity of real rough surfaces, there may be one or more enclosed boundaries, where the projection of the outside boundary on the $x - y$ plane is called the 'interpenetration curve', which was earlier defined by Singh and Paul (1974). The region inside the interpenetration curve is called the interpenetration region or geometric overlap region.

Due to a applied load, material points in a body undergo rigid-body translation and elastic deformation. The gap geometry in deformed states, denoted $g(x,y)$ can be given by:

$$g(x,y) = d + z(x,y) + u(x,y) \quad (4.5)$$

where $u(x,y)$ is elastic displacements of rough surface.

For points on the surface of the body, it can be shown from geometric consideration that:

$$\begin{aligned} g(x,y) &> 0 && \text{where two bodies have no contact} \\ g(x,y) &= 0 && \text{where two bodies have contact} \end{aligned} \quad (4.6)$$

The gap geometry in a deformed state is an important result for fluid

CHAPTER 4.

sealing problems. When two rough surfaces are in contact the gap between surfaces provides a path through which fluid flow may take place so that the leakage occurs.

4.3.3 Deformed Surface Shape

If the displacement of any point on the surface can be calculated, the deformed surface function $z_i^*(x,y)$ is known and equals numerically $z_i(x,y) - u_i(x,y)$ ($i = 1,2$). For frictionless contact ignoring the relative horizontal displacements for the case $E_1 \neq E_2$, the vertical displacement on the surface of each body can then related by (Webster and Sayles 1986):

$$u_1(x,y) \frac{E_1}{(1-\nu_1^2)} = u_2(x,y) \frac{E_2}{(1-\nu_2^2)} \quad (4.7)$$

The total displacement of any point on two surfaces, say $u = u_1 + u_2$, can be found and it will be discussed later. Substituting u into Equation (4.7), for the general case where $E_1 \neq E_2$ and $\nu_1 \neq \nu_2$, the displacement on the surface of each body is related to the total displacement by:

CHAPTER 4.

$$u_1(x,y) = \frac{u(x,y)}{1 + \frac{E_1(1-\nu_2^2)}{E_2(1-\nu_1^2)}} \quad (4.8)$$

and

$$u_2(x,y) = \frac{u(x,y)}{1 + \frac{E_2(1-\nu_1^2)}{E_1(1-\nu_2^2)}}$$

For the special case where $E_1 = E_2$ and $\nu_1 = \nu_2$, gives:

$$u(x,y) = u_2(x,y) = \frac{1}{2} u(x,y) \quad (4.9)$$

4.4 Boundary Condition of Contact

4.4.1 Displacement Boundary Condition

From the Equation (4.6), we can get the rules governing displacement of these points on the surfaces, the expression is:

CHAPTER 4.

$$\begin{aligned}d + z(x,y) + u(x,y) &> 0 && \text{outside } \Omega_c \\d + z(x,y) + u(x,y) &= 0 && \text{inside } \Omega_c\end{aligned}\tag{4.10}$$

where Ω_c is the region of contact. Equation (4.10) gives the boundary condition of the surface displacement.

4.4.2 Pressure Boundary Condition

First, we impose two restrictions on forces:

- (1) Pressure values must remain positive within the region of contact and diminish to zero outside this zone;
- (2) The integrated pressure distribution over the contact area is equal to the applied load.

Stated mathematically, these restrictions become:

$$\begin{aligned}p(x,y) &> 0 && \text{inside } \Omega_c \\p(x,y) &= 0 && \text{outside } \Omega_c\end{aligned}\tag{4.11}$$

$$P_a = \int_{\Omega_c} p(x,y) \, dx dy\tag{4.12}$$

CHAPTER 4.

where P_a is the applied load and $p(x,y)$ is the pressure of surface contact.

This first requirement precludes the possibility of tensile stresses occurring normal to the bodies because the two bodies cannot exert tension upon one another as a result of contact. For most engineering rough surfaces, the slope of asperities is sufficiently small such that we can make the assumption: the tangential planes are approximately parallel to the average plane of the surface, so all forces act in the vertical direction (Singh and Paul 1974). Then according to the equilibrium requirement, we get the second restriction.

Equation (4.11) gives the boundary condition of contact pressure. Combining Equation (4.10) and (4.11) gives the boundary condition of rough surfaces contact. It is:

$$\begin{aligned} d + z(x,y) + u(x,y) > 0 & \quad p(x,y) > 0 \\ d + z(x,y) + u(x,y) = 0 & \quad p(x,y) = 0 \end{aligned} \quad (4.13)$$

4.5 Deformation of Rough Surface Contact

Conventionally, rough surface contact is divided into the elastic, plastic or mixed regime by the plasticity index originally introduced by Greenwood and Williamson (1966). The plasticity index is defined as

CHAPTER 4.

$$\Psi = \frac{E'}{H} \left(\frac{\sigma_s}{\beta} \right)^{1/2} \quad (4.14)$$

where H is the indentation hardness of the rough surface (a measure of the plastic flow stress of the asperities); σ_s is the standard deviation of the distribution of asperity heights and β is the curvature radius of summits. The quantity $(\sigma_s/\beta)^{1/2}$ is approximately equal to the average slope of the asperities.

They related this plasticity index ψ to the load at which 2% of all asperities will have passed the elastic limit and be yielding plastically. It is found that this load is very sensitive to the numerical value of the plasticity index; for $\psi < 0.6$ no practical load would be large enough to cause plastic flow, while for $\psi > 1$ plastic flow will occur at the lightest load. In the intermediated region the transition is load-dependent.

Ogilvy (1992) derived a conventional plasticity index ψ_c based on the plasticity index ψ . This plasticity index defined in Equation (4.14) was rewritten as:

$$\Psi = \frac{E'}{H} (\sigma \kappa)^{1/2} \quad (4.15)$$

where κ is the curvature of the isotropic asperities, assumed the same for all asperities. In practice, κ varies from asperity to asperity, so that it is necessary to define ψ in an average sense, and then to interpret ψ as measure of the average likelihood that any asperity is plastically yielding. For

CHAPTER 4.

surfaces with Gaussian statistics, Ogilvy (1991) showed that the mean curvature $\langle \kappa \rangle$ is equal to $2\sqrt{3}\sigma/\lambda_0^2$ for all points on the surface, where λ_0 is the correlation length defined by Ogilvy (1991) and λ_0 is related to λ^* by $\lambda_0 = \lambda^*/2.3$. However, the value of κ that should appear in Equation (4.15) is the value appropriate to the contacting asperities, this generally being larger than the value of κ for all points on the surface. Making use of the results obtained by Greenwood (1984), which shows that κ varies from around 1.25 to 1.8 times the mean surface curvature, for peaks height from around σ to 4σ , gives the conventional plasticity index ψ_c by Ogilvy, it is:

$$\psi_c = (1.6-2.2) \frac{E'}{H} \left(\frac{\sigma}{\lambda_0} \right) \quad (4.16)$$

dependent on the range of heights of the peaks which are in contact. This conventional plasticity index ψ_c may be calculated for the surfaces used in this thesis, to determine the nature of rough surface in contact. In this thesis, the plasticity index ψ_c is calculated according to Equation (4.16) with the constant set to 2, to represent the approximate mean value of ψ_c .

As can be seen from the Equation (4.16), the plasticity index ψ_c contains two dimensionless groups. The first group is related to the mechanical properties of the contacting surfaces and the second group to the surface roughness. It is clear from Equation (4.16) that hard and/or smooth surfaces yield low values of the plasticity index, while soft and/or rough surfaces result in high values of ψ_c . The first case, where ψ_c is small, corresponds to a mostly elastic contact and the second case, where ψ_c is large, correlates to a mostly plastic contact of the mating rough surfaces.

CHAPTER 4.

In order to determine the deformation assumption for the static sealed joints, the values of plasticity index for typical seals should be evaluated. Thomas (1973) had calculated the values of plasticity index for typical static sealed joints by assuming the contact to be between two surfaces of mild steel, which is for a range of $\psi = 0.18 \sim 0.88$ where the surfaces used were Rubert roughness gauges of a nominal surface roughness of $0.2 \mu\text{m}$. These values used for the material constants corresponding to the contact between two surfaces of mild steel by Thomas are tabulated in Table 4.1.

Table 4.1 Material properties of typical static sealed joints

Material	Young's modula E' (GPa)	Poisson's ratio v	Yield stress Y (GPa)
mild steel	100	0.3	~ 1

In static sealed joints practice, more wide range of surface roughness used is $\sigma = 0.1 \mu\text{m} \sim 0.5 \mu\text{m}$ (Flitney, Nau and Hisakado 1984). The correlation lengths of rough surfaces produced by a variety of lapping and grinding processes are for a range of $\lambda^* = 20 \mu\text{m} \sim 50 \mu\text{m}$ (Thomas 1973). According the assumptions of surface roughness and the contact to be between two surface of mild steel, the plasticity index for typical sealed joints has been evaluated and are listed in Table 4.2.

CHAPTER 4.

Table 4.2 Values of the plasticity index ψ_c for typical sealed joints

Plasticity index ψ_c		
Correlation length λ^* (μm)	RMS height $\sigma = 0.1$ (μm)	RMS height $\sigma = 0.5$ (μm)
$\lambda^* = 20$	0.2365	1.182
$\lambda^* = 30$	0.1576	0.7883
$\lambda^* = 40$	0.1183	0.5913
$\lambda^* = 50$	0.0946	0.4730

For the values of plasticity index listed in Table 4.2, the deformation mode of rough surface contact is neither purely elastic or fully plastic, but mixed elastic-plastic. However, in view of the overall range for plasticity index, making the general assumption that static sealed joints will deform elastically is reasonable, although it is not strictly true for all cases.

The elastic-plastic contact model will predict larger real contact area than the purely elastic contact model (Lee and Cheng 1992 and Ogilvy 1992). Furthermore, the purely elastic contact model to be used in the leakage analysis of sealed joints is on the safe side for design, since it predicts less intimate surface contact and hence greater leakage, than for plastic deformations.

CHAPTER 5.

Two-dimensional Numerical Model for the Elastic Contact of Rough Surfaces

5.1 Introduction

The numerical contact model of rough surfaces is an important tool for simulation analysis of leakage because it can provide information about the real contact situation at the interface of sealed joints. In this chapter, the numerical relationship between contact pressure and surface displacement for two-dimensional elastic frictionless contact will be derived based on the corrected Timoshenko's solution for vertical surface displacements due to an arbitrary pressure distribution. The numerical solution technique based on variational principles will be adopted to develop two-dimensional numerical contact of rough surfaces with the advantage that no iteration is involved for cases of frictionless contact. Using the variational method, the contact problem become a quadratic programming problem. To make sure that there is no difficulty in the convergence of solution, the quadratic programming routine will selected carefully. A computer program will be completed for

CHAPTER 5.

two-dimensional elastic frictionless contact of rough surfaces.

5.2 Statement of Contact Problem

5.2.1 Constrains and Assumptions

In this section, the constrains and assumptions used to develop a two-dimensional numerical contact model are presented:

- (1) The contact between two bodies is linear elastic;
- (2) The contact conditions allow the use of half space solutions;
- (3) The bodies are in a state of plane strain;
- (4) The elastic contact area is completely contained within the geometric overlap region, as shown in Figure 4.1;
- (5) Relative horizontal strains and displacements are ignored, i.e. frictionless contact;
- (6) The contact between two bodies satisfies the boundary condition defined by Equation (4.13).

CHAPTER 5.

5.2.2 Distributed normal tractions

In general, a contact surface transmits normal pressure and tangential traction due to friction. To solve the contact problem, we need to relate a boundary displacement $u(x)$ to a normal pressure $p(x)$ and a tangential traction $q(x)$. For cases of frictionless contact where only normal pressure needs to be determined (i.e. $q(x) = 0$), the relationship is given by Johnson (1985):

$$u(x) = \frac{2(1-\nu^2)}{\pi E} \int_{\Omega_n} p(x') \ln|x-x'| dx' \quad (5.1)$$

where Ω_n is the contact region.

If a general form for the pressure distribution $p(x')$ is assumed, the solution of Equation (5.1) would yield the contact pressures and displacements. If we now consider surface topography we know that the smooth contact region is in fact made up of any number of arbitrarily shaped contact spots. For this more general case Equation (5.1) is still valid, providing we can define $p(x')$. However we cannot make any simple assumption about the variation of $p(x')$ with x' , except that over much of the apparent smooth contact region $p(x')$ will be zero.

The problem can be approached in the following way: since the non-contacting regions make no contribution to the vertical displacements at any point, we divide the integral expressions in Equation (5.1) into the sum of a

CHAPTER 5.

number of integrals within the contact region , thus:

$$u(x) = \frac{2(1-\nu^2)}{\pi E} \sum_{i=1}^{M'} \int_{\Omega_{n_i}} p(x') \ln|x-x'| dx' \quad (5.2)$$

where M' is the number of contact spots.

An analytical solution requires the form of $p(x')$ for each contact-spot, thus a numerical solution was adopted with the advantage that the contact pressures and the displacements could be solved simultaneously, without the need for simplifying assumptions.

5.3 Numerical Solution

The first step in the numerical solution is to divide the contact boundary into an appropriate number M of elements. A form of pressure distribution is assumed for each element which in the simplest example might be uniform pressure or even a concentrated force at the element centre. Usually the distribution is chosen so that its magnitude can be described by a single parameter p_j for each element although higher order discretization are possible. There are thus M unknowns p_j to be determined in the solution of the problem. An equal number of contact points j are then chosen at which the normal displacement is to be matched. Usually these are taken to be the centre of each pressure element. Influence coefficients C_{ij} are then calculated which give the difference in normal displacement of the two

CHAPTER 5.

contacting surfaces at point i arising from a pressure element of unit magnitude at element j . The difference in displacement at i due to the M pressure elements, can then be expressed as

$$u_i = \sum_{j=1}^M C_{ij} P_j \quad (5.3)$$

where M is the total number of elements.

The full explanation to this numerical method is given in the following sections.

5.3.1 Types of Pressure Elements

A number of possibilities can be suggested and several different choices were considered by Mostofi and Gohar (1984). The same basic information is required for any element, namely the influence coefficient C_{ij} in Equation (5.3) which gives the normal displacements due to application of a normal pressure.

The simplest approach which might be adopted is to use a concentrated force at the centre of each element as shown in Figure 5.1 (a). This method produces an immediate difficulty in that the displacements are singular at the point of application of each load. This prohibits the use of these points for displacement matching. A better approach would be to employ traction which

CHAPTER 5.

are uniform over each element as shown in Figure 5.1 (b). This method of dividing the contact area into elements of uniform pressure has been used in the analysis of rough contact by Webster and Sayles (1986) amongst others and is equally applicable to smooth contacts. The infinite displacements inherent in the point force method are now avoided but there are, of course, discontinuities in stress at the boundaries of the elements where a step change in traction occurs.

A more sophisticated solution would be one that was continuous in traction between adjacent elements. Such a solution may be constructed with little complexity by using overlapping triangular traction elements as first suggested by Bentall and Johnson (1967). Figure 5.1 (c) shows an array of overlapping triangular traction elements. It will be immediately seen that the use of elements results in a piecewise linear approximation to the surface traction and is thus free from the discontinuities associated with the piecewise step methods. This method, which a distribution of traction in two-dimensional contact may be built up by the superposition of overlapping triangular traction elements, has been successfully used to solve frictional contact problems by Bentall and Johnson (1967) and Azarkhin (1988) amongst others. The same traction elements are used by Kalker (1971) in a variational solution technique.

Although the accuracy achieved by using overlapping triangular traction elements instead of the uniform traction elements would increase, this does not justify the added complications to the calculation of the contact problems of rough surfaces (Webster and Sayles 1986). Therefore, the element of uniform

CHAPTER 5.

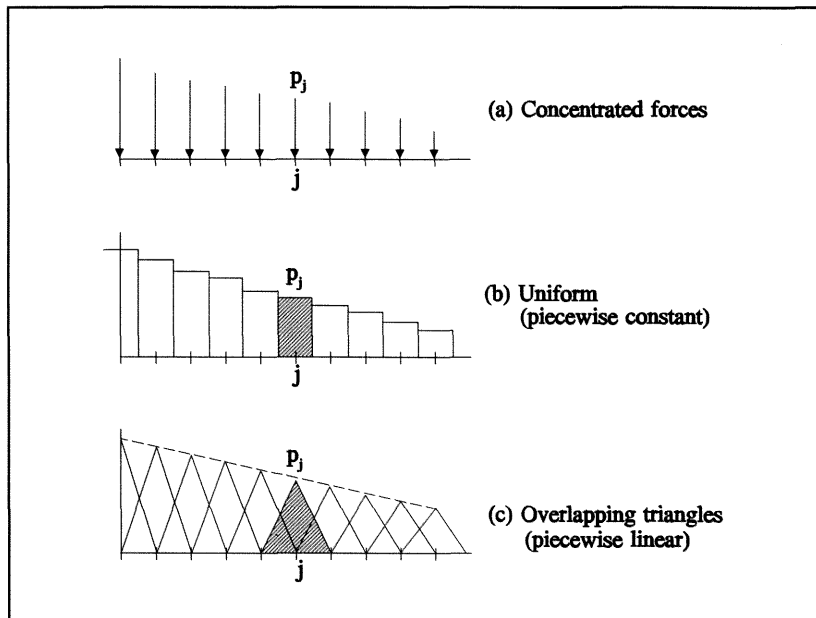


Figure 5.1 Possible traction elements for use in two-dimensional contact problems

pressure is chosen to use in the following analysis.

5.3.2 Contact Pressure Element Equations

Using Equation (5.1) the expressions for the vertical displacements of a surface due to an applied uniform pressure over an elemental length of the surface profile shown as in Figure 5.2 can be derived:

CHAPTER 5.

$$u(x) = \frac{(1-\nu^2)}{\pi E} p \left\{ (x+a) \ln \left(\frac{x+a}{a} \right)^2 - (x-a) \ln \left(\frac{x-a}{a} \right)^2 \right\} + \text{const} \quad (5.4)$$

for $u(x)$ not within the element, i.e. for a point outside the loaded region ($|x| > a$) and

$$u(x) = \frac{(1-\nu^2)}{\pi E} p \left\{ (a+x) \ln \left(\frac{a+x}{a} \right)^2 + (a-x) \ln \left(\frac{a-x}{a} \right)^2 \right\} + \text{const} \quad (5.5)$$

for $u(x)$ within the element, i.e. for a point within the loaded region ($|x| \leq a$).

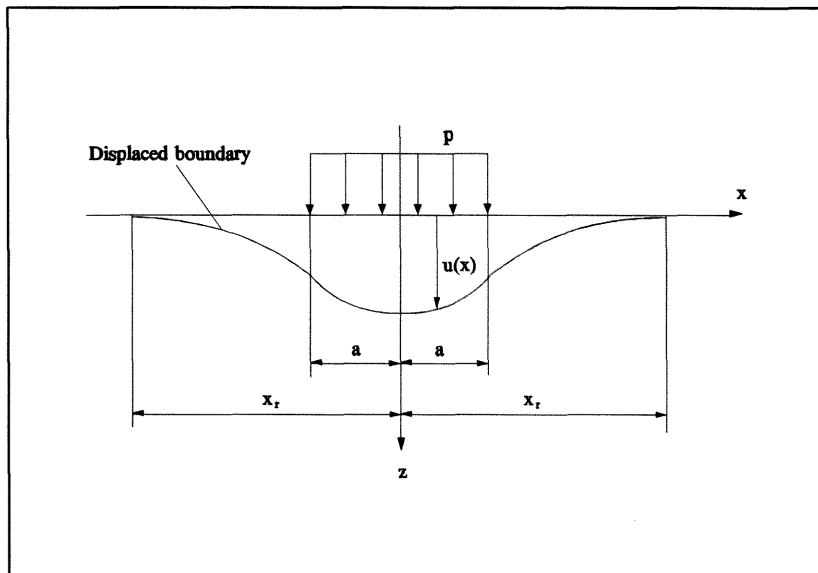


Figure 5.2 Vertical displacement on the surface due to uniform normal pressure element

The constant in Equation (5.4) and (5.5) is fixed by the datums chosen

CHAPTER 5.

for normal displacements. The distance x_r , at which zero vertical displacement is assumed, was taken by Lee and Cheng (1992) as $10L$, where L is the contact simulation segment length. Essentially all displacement are measured with respect to this point in space.

For numerical solution, expressing all distances in terms of the elemental ΔL . Substituting for $x = m\Delta L$ and $a = \Delta L/2$ in equation (5.4) and (5.5), we may derive the following expressions:

$$u(m) = \frac{2(1-\nu^2)\Delta L}{\pi E} p \left[\left(m + \frac{1}{2}\right) \ln\left(m + \frac{1}{2}\right) - \left(m - \frac{1}{2}\right) \ln\left(m - \frac{1}{2}\right) \right] + \text{const} \quad (5.6)$$

for the displacement $u(x)$ at values of x that correspond to the centres of the remaining surface profile pressure elements and

$$u(0) = \frac{2(1-\nu^2)\Delta L}{\pi E} p \left[\ln\frac{1}{2} \right] + \text{const} \quad (5.7)$$

for the mid point of the element over which the uniform pressure is applied.

5.3.3 Formulation of Numerical Solution

For the case of the contact of two elastic bodies, the elasticity of

CHAPTER 5.

another body can be taken into account by replacing $(1-\nu^2)/E$ by $1/E'$, where E' is the equivalent Young's modulus. From Equation (5.6) the displacement at point i due to a uniform applied pressure over element j is:

$$u_{ij} = \frac{2\Delta L}{\pi E'} p_j \left[\left(m + \frac{1}{2}\right) \ln\left(m + \frac{1}{2}\right) - \left(m - \frac{1}{2}\right) \ln\left(m - \frac{1}{2}\right) \right] + \text{const} \quad (5.8)$$

where $i \neq j$ (i.e. outside the loaded region); Similarly for case $i = j$ (i.e. within the loaded region) we use Equation (5.7):

$$u_{ii} = \frac{2\Delta L}{\pi E'} p_j \left[\ln \frac{1}{2} \right] + \text{const} \quad (5.9)$$

where:

$$m = |i - j| \quad (5.10)$$

We can now find the total vertical displacement due to all the element pressure p_j by the following expression:

$$u_i = \sum_{j=1}^M u_{ij} \quad (5.11)$$

where M is the total number of elements in contact simulation.

Since we are using linear elastic theory, each term u_{ij} , is proportional

CHAPTER 5.

to the elemental pressures p_j , hence we can express u_y as the displacement due to a unit uniform elemental pressure times the real elemental pressure, giving us the following expression for the total displacement at point i :

$$u_i = \sum_{j=1}^M C_{ij} p_j \quad (5.12)$$

where the terms C_{ij} are normally referred to as the influence coefficients and can be calculated by:

$$C_{ij} = \frac{2\Delta L}{\pi E'} \left[\left(m - \frac{1}{2}\right) \ln\left(m - \frac{1}{2}\right) - \left(m + \frac{1}{2}\right) \ln\left(m + \frac{1}{2}\right) \right] + \text{const}$$

$$C_{ij} = \frac{2\Delta L}{\pi E'} \left[\ln \frac{1}{2} \right] + \text{const} \quad (5.13)$$

Considering displacements for all points, Equation (5.12) represents a set of M simultaneous equations which may be expressed in matrix form thus:

$$\begin{pmatrix} u_1 \\ u_2 \\ \vdots \\ u_M \end{pmatrix} = \begin{pmatrix} C_{11} & C_{12} & \dots & C_{1M} \\ C_{21} & C_{22} & \dots & C_{2M} \\ \vdots & \vdots & \vdots & \vdots \\ C_{M1} & C_{M2} & \dots & C_{MM} \end{pmatrix} \begin{pmatrix} p_1 \\ p_2 \\ \vdots \\ p_M \end{pmatrix} \quad (5.14)$$

The matrix of influence coefficients is square and symmetric (as $m = |i - j|$),

CHAPTER 5.

therefore $C_{ij} = C_{ji}$), the terms can be calculated by Equation (5.13).

5.4 Numerical Solution Techniques

In order to solve elastic contact problem by the numerical method described above it is also important to choose an effective numerical solution technique, which will determine the accuracy of solutions and the time consumption of solution procedure.

5.4.1 Variational Methods

A powerful method of numerical solution for the contact problems is the variational method based on variational principles, in which the values of the traction elements are chosen to minimise an appropriate energy function (Johnson 1985). Variational methods have been applied to non-Hertzian contact problems by Kalker (1990) amongst others for two reasons:

- (1) to establish conditions which determine the shape and size of the contact area and the contact stresses uniquely;
- (2) to enable well-developed techniques of optimisation such as quadratic programming to be used in numerical solutions.

When the variational methods are applied for the cases of frictionless contact where only the normal pressure needs to be determined, no iteration is involved (Kalker 1990).

CHAPTER 5.

Fichera (1964) and Duvaut & Lions (1972) have investigated general principles which govern the existence and uniqueness of solution to contact problems. For two bodies having continuous profiles, pressed into contact by an overall displacement δ , Duvaut & Lions show that the true contact area and surface displacements are those which minimise the total strain energy U_E (with δ kept constant), provided that there is no interpenetration, i.e. provided:

$$u_1(x,y) + u_2(x,y) + h(x,y) - \delta \geq 0 \quad (5.18)$$

everywhere. Where $h(x, y)$ is the distance between the two surfaces before deformation, δ is the approach of two bodies.

For numerical solution of contact problems it is more convenient to work in terms of unknown tractions rather than displacements. Kalker (1977, 1978) has therefore proposed an alternative principle in which the true contact area and distribution of surface traction are those which minimise the total complementary energy V^* , subject to the constraint that the contact pressure p is everywhere positive. Now the total complementary energy can be written:

$$V^* = U_E^* + \int_{\Omega_n} p(x,y) \{h(x,y) - \delta\} dS \quad (5.19)$$

where Ω_n is the surface on which p acts and U_E^* is the internal complementary energy of the two stressed bodies. For linear elastic materials the complementary energy U_E^* is numerically equal to the elastic strain energy U_E , which can be expressed in terms of the surface tractions and

CHAPTER 5.

displacements by

$$U_E^* = U_E = \frac{1}{2} \int_{\Omega_n} p(x,y) \{u_1(x,y) + u_2(x,y)\} dS$$

i.e. (5.20)

$$U_E^* = \frac{1}{2} \int_{\Omega_n} p(x,y) u(x,y) dS$$

Substituting Equation (5.20) into Equation (5.19) gives

$$V^* = \int_{\Omega_n} \left\{ p(x,y) [h(x,y) - \delta] + \frac{1}{2} p(x,y) u(x,y) \right\} dS$$
(5.21)

The solution can be found by minimizing V^* , subject to $p(x,y) > 0$, that is:

$$\text{Min! } V^* = \int_{\Omega_n} \left\{ p(x,y) [h(x,y) - \delta] + \frac{1}{2} p(x,y) u(x,y) \right\} dS$$
(5.22)

Subject to: $p(x,y) > 0$

CHAPTER 5.

5.4.2 Quadratic Programming Formulation

To obtain a numerical solution the prospective contact area Ω_n in Equation (5.22) is subdivided into a mesh on which elements of pressure act. The $[h(x, y) - \delta]$ is numerically equal to the gap $b(x, y)$ defined in Equation (4.4). $b(x, y)$ is taken as constant over each element.

Using Equation (5.17), in which displacement u and pressure p is related, we can get the numerical expression as follows:

$$\text{Min! } V^* = \sum_{i=1}^M A_{ei} p_i b_i + \frac{1}{2} \sum_{i=1}^M \sum_{j=1}^M A_{ei} C_{ij} p_i p_j \quad (5.23)$$

Subject to: $p_j > 0$

where A_{ei} is constant depending upon the form and size of the pressure element. For a uniform pressure element, the value of A_{ei} is equal to the surface area of the element, i.e. $A_{ei} = \Delta L \times \Delta L$.

Using the complementary energy, the contact problem is formulated as minimizing this energy under the inequality constraint that the pressure must everywhere be greater than zero. It then follows that the penetration is just zero inside the contact, while outside the contact the pressure is zero and no penetration occurs. This leads to a quadratic programming problem with pressure on the rectangle as unknowns, which can be found by using a standard quadratic programming routine.

CHAPTER 5.

E04NAF routine is designed by Gill, Murray and Wright (1983) to solve the quadratic programming (QP) program - the minimization of a quadratic function subject to a set of linear constraints on the variables. E04NAF allows the user to provide the indices of the constraints that are believed to be exactly satisfied at the solution. This facility, known as a warm start, can lead to significant saving in computational effort when solving a sequence of related problems. Therefore, the routine is chosen to develop the numerical contact model.

5.4.3 Reduction of Equation Order

In order to numerically model the contact of the rough surfaces, a large number of elements are required. If a surface profile is discretised into 2000 elements, for example, this requires a set of 2000 simultaneous equations and an array space for 2000×2000 components of the influence coefficient matrix in Equation (5.17). Because the computer memory is limited, this would restrict the total number of elements, which may produce unacceptably coarse discretizations of the contact region for some cases.

However, some treatment must be adopted to reduce the problem. The fact that the contact of rough surfaces occurs only at the tip of the asperities can be used to advantage. Thus we may divide the total elements M into two parts: the contact elements, say M' , and non-contact elements $M'' = M - M'$. Since for random rough surfaces the contact region can occur in a random manner it is necessary to use an extra storage array, say $I(i)$ (

CHAPTER 5.

$i = 1, 2, \dots, M'$) and $J(j)$ ($j = 1, 2, \dots, M''$), to record the position of contacting and non-contacting elements separately. According to the matrix properties, the Equation (5.17) can be rewritten as follows:

$$\begin{pmatrix} u_{I(1)} \\ \vdots \\ u_{I(M')} \\ u_{J(1)} \\ \vdots \\ u_{J(M'')} \end{pmatrix} = \begin{pmatrix} C_{I(1)I(1)} & \cdots & C_{I(1)I(M')} & C_{I(1)J(1)} & \cdots & C_{I(1)J(M'')} \\ \vdots & \vdots & \vdots & \vdots & \vdots & \vdots \\ C_{I(M')I(1)} & \cdots & C_{I(M')I(M')} & C_{I(M')J(1)} & \cdots & C_{I(M')J(M'')} \\ C_{J(1)I(1)} & \cdots & C_{J(1)I(M')} & C_{J(1)J(1)} & \cdots & C_{J(1)J(M'')} \\ \vdots & \vdots & \vdots & \vdots & \vdots & \vdots \\ C_{J(M'')I(1)} & \cdots & C_{J(M'')I(M')} & C_{J(M'')J(1)} & \cdots & C_{J(M'')J(M'')} \end{pmatrix} \begin{pmatrix} P_{I(1)} \\ \vdots \\ P_{I(M')} \\ P_{J(1)} \\ \vdots \\ P_{J(M'')} \end{pmatrix} \quad (5.24)$$

Here $p_{I(i)}$ ($i = 1, 2, \dots, M'$) are the element pressures at contact points. Since the element pressures in non-contact regions are zero, i.e. $p_{J(j)} = 0$ ($j = 1, 2, \dots, M''$), they make no contribution to the vertical displacements at any points. Thus the Equation (5.17) can be split into two set of simultaneous equations as follows:

$$\begin{pmatrix} u_{I(1)} \\ u_{I(2)} \\ \vdots \\ u_{I(M')} \end{pmatrix} = \begin{pmatrix} C_{I(1)I(1)} & C_{I(1)I(2)} & \cdots & C_{I(1)I(M')} \\ C_{I(2)I(1)} & C_{I(2)I(2)} & \cdots & C_{I(2)I(M')} \\ \vdots & \vdots & \vdots & \vdots \\ C_{I(M')I(1)} & C_{I(M')I(2)} & \cdots & C_{I(M')I(M')} \end{pmatrix} \begin{pmatrix} P_{I(1)} \\ P_{I(2)} \\ \vdots \\ P_{I(M')} \end{pmatrix} \quad (5.25)$$

For the points within the contact region, and

CHAPTER 5.

$$\begin{pmatrix} u_{J(1)} \\ u_{J(2)} \\ \vdots \\ u_{J(M')} \end{pmatrix} = \begin{pmatrix} C_{J(1)I(1)} & C_{J(1)I(2)} & \dots & C_{J(1)I(M)} \\ C_{J(2)I(1)} & C_{J(2)I(2)} & \dots & C_{J(2)I(M)} \\ \vdots & \vdots & \vdots & \vdots \\ C_{J(M')I(1)} & C_{J(M')I(2)} & \dots & C_{J(M')I(M)} \end{pmatrix} \begin{pmatrix} P_{I(1)} \\ P_{I(2)} \\ \vdots \\ P_{I(M)} \end{pmatrix} \quad (5.26)$$

For the points outside the contact region.

In this manner two sets of relatively lower order system equations can be formed that are easily solved. Thus the surface displacements can be divided into two parts to be determined: first for the contact region using the Equation (5.25), then for the non-contact region using Equation (5.26). The matrix of influence coefficients in Equation (5.25) and Equation (5.26) is still calculated by using Equation (5.16), where the integer m representing the distance between two points becomes:

$$m = | I(i) - I(j) | \quad (5.27)$$

for the contacting points and

$$m = | J(i) - I(j) | \quad (5.28)$$

for the non-contacting points.

After the treatment described above, the total number of elements M in Equation (5.23) will be reduced to M' , where M' is the total number of elements having geometry overlap, i.e $b_i < 0$.

CHAPTER 5.

5.5 Algorithm and Computer Programm

For the contact case 1, i.e the contact between an elastic rough punch and a rigid plane, the complete solution for a given load and surface geometry is obtained as follows:

Step 1. Set up initial values

The first stage is setting up some constants. Values such as E_1 , E_2 , ν_1 , ν_2 , ΔL , M , the total applied normal load P_n and the approach step $\Delta \delta$ are input into the computer. The next is setting up surface geometry. Either read data from files of previously recorded surface profiles or generate the appropriate surface shapes.

Step 2. Calculate threshold separation

It is necessary to calculate the threshold separation d_c . When the current normal separation d_i is great than or equal to d_c , the contact will not occur.

Step 3. Decrease the normal separation

The upper body is given a rigid body vertical displacement $\Delta \delta$ toward the lower body, the normal separation d is decreased. The current normal separation d_i is calculated by $d_i = d_c - i\Delta \delta$ ($i = 1, 2, 3, \dots$). The contact has been detected for current normal separation d_i .

CHAPTER 5.

Step 4. Set up the index array

The gap values b_i is calculated by using Equation (4.4) to find the initial contact elements. The geometric overlap is detected at the points for the value of $b_i < 0$ ($i = 1, 2, \dots, M$). An index array $I(i)$ ($i = 1, 2, \dots, M'$) is used to store the positions corresponding to the geometric overlap points and another index array $J(i)$ ($i = 1, 2, \dots, M - M'$) is used to store the positions corresponding to non-contacting points, i.e. the points for the value of $b_i \geq 0$ ($i = 1, 2, \dots, M$).

Step 5. Calculate the linear terms of QP

The first section in Equation (5.23) is calculated and is stored as the linear terms of the Quadratic Programming problem (i.e QP), see Appendix A.

Step 6. Set up matrix of influence coefficient

The index array $I(i)$ ($i = 1, 2, \dots, M'$) is then used to calculate the values of m in Equation (5.27) and to calculate the corresponding components C_{ij} for the matrix of influence coefficients at contacting points.

Step 7. Calculate quadratic terms of QP

The second section in Equation (5.23) is calculated and is stored as the quadratic terms of the Quadratic Programming problem (i.e QP), see Appendix

CHAPTER 5.

A.

Step 8. Solve quadratic programming problem

The quadratic programming problem defined in Equation (5.23) is solved by using E04NAF - NAG Fortran Library Routine Document. E04NAF is a comprehensive routine for solving quadratic programming (QP) problem - the minimization of a quadratic function subject to a set of linear constraints on the variables.

Step 9. Check for force equilibrium

Using Equation (4.13), the total pressure carried by the contact is calculated by adding all the nonzero elemental pressures. The total load per unit width between the two bodies is calculated by multiplying by the elemental size ΔL . If the calculated load P_c is less than the required load P_a , the process is repeated from step 3.

Step 10. Output some results

For an applied load P_a and surface geometries, the contact pressure distribution, the real contact region and the real contact area, the gap geometries in deformed state etc. can be output as the calculated results.

The steps described above represent the algorithm of the present numerical contact model for the contact Case 1. As can be seen from the

CHAPTER 5.

algorithm, for a given normal separation, no iteration is involved to yield a fully consistent solution. The computer program based on the algorithm has been completed in FORTRAN and is named **2DNECM** by the author. Figure 5.3 is a flow chart representing the main features of the contact program **2DNECM** for two-dimensional numerical elastic contact.

With a few minor modifications to the original program above, the **2DNECM** has been extended to include the contact case 2, where an equivalent rough half-space is loaded against a rigid, infinitely wide plane. For contact case 2, first the average pressure p_m over the entire half-space is calculated according to the contact case 1, thus the modified surface profiles are determined by the using Equation (4.3), then the final solutions are obtained based on the modified surface profiles. For two-dimensional contact problems, the displacement $\delta_0(x)$ is given by Lee and Cheng (1992):

$$\delta_0(x) = \frac{2 p_m}{\pi E'} \left\{ \left(x_r + \frac{L}{2} \right) \ln \left(x_r + \frac{L}{2} \right) - \left(x_r - \frac{L}{2} \right) \ln \left(x_r - \frac{L}{2} \right) - \left(\frac{L}{2} - x \right) \ln \left(\frac{L}{2} - x \right) - \left(\frac{L}{2} + x \right) \ln \left(\frac{L}{2} + x \right) \right\} \quad (5.29)$$

where p_m is the average contact pressure.

CHAPTER 5.

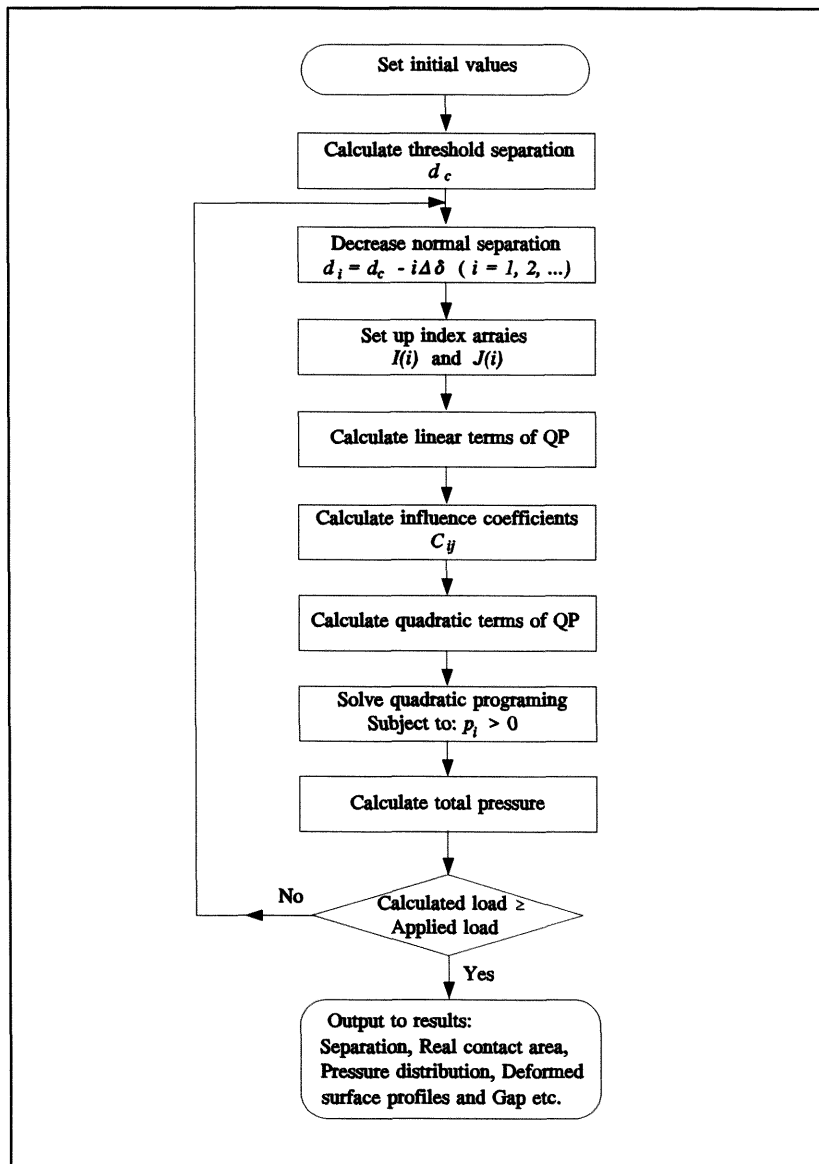


Figure 5.3 Computer program flow chart for two-dimensional numerical contact model

CHAPTER 5.

5.6 Numerical Examples

5.6.1 Contact of Two Elastic Smooth Cylindrical Bodies

A number of test load cases were used to build up confidence in the analysis techniques and assess the magnitude of any errors in the solution. The most convenient comparison is the contact between two elastic smooth cylindrical bodies. For this case there exists analytical expressions for the contact length $2r$, maximum contact pressure p_{max} and the distribution of surface contact pressure $p(x)$ (Johnson 1985):

$$r^2 = \frac{4P_a R}{\pi E'} \quad (5.30)$$

$$p_{max} = \frac{2P_a}{\pi r} = \left(\frac{P_a E'}{\pi R} \right)^{1/2} \quad (5.31)$$

$$p(x) = p_{max} \left\{ 1 - \left(\frac{x}{r} \right)^2 \right\}^{1/2} \quad (5.32)$$

where P_a is the load/unit length of the cylinder and $1/R$ is the equivalent curvature, calculating by $(1/R = 1/R_1 + 1/R_2)$.

Thus the theoretical Hertzian results are calculated so that a direct comparison with the numerical results could be made. Figure 5.4 shows the pressure distribution $p(x)$ plotted for one of the test runs. The plot showing

CHAPTER 5.

the pressure distribution $p(x)$ is normalised by the theoretical maximum pressure given by Equation (5.31). The theoretical pressure distribution given by Equation (5.32) has been plotted on the same axis. The values used in Figure 5.4 are:

$$E_1 = E_2 = 200 \text{ GPa}, \quad \nu_1 = \nu_2 = 0.3$$

$$R_1 = R_2 = 50 \text{ mm}, \quad P = 500 \text{ N/mm}$$

and the element size used for numerical calculations is $\Delta L = 10 \mu\text{m}$.

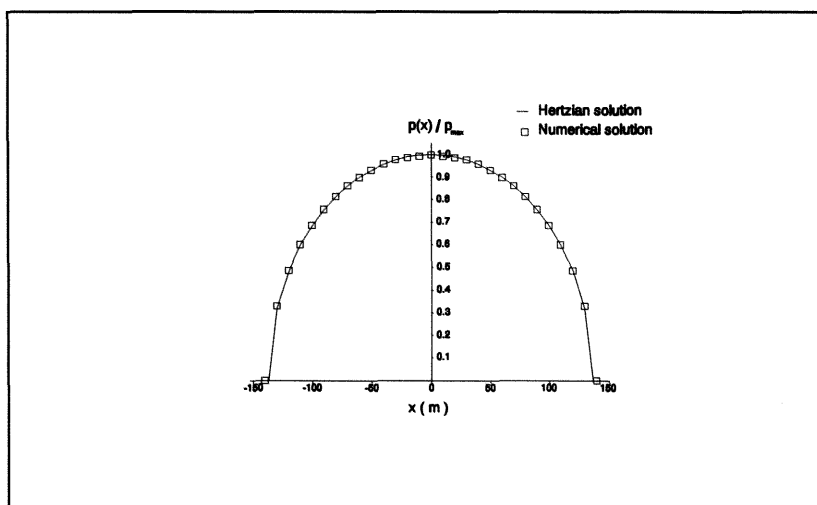


Figure 5.4 Comparison of pressure distribution for the contact of smooth cylinders

The influence of varying the pressure element size ΔL was also investigated. When the element sizes of $\Delta L = 2 \mu\text{m}$ is used for numerical calculations above, the two curves of the pressure distribution representing Hertzian solution and numerical solution are indistinguishable. The result of

CHAPTER 5.

this test, and many others, confirms that the numerical solution reproduces the analytical results to a high degree of accuracy. The numerical simulation solutions for the contact length $2r$, the calculated load P_c and the maximum pressure p_{max} were compared with Hertzian analytical solutions for the two different element sizes, given in Table 5.1.

Table 5.1 Comparisons between Hertzian and numerical solution

	Contact half length r (μm)	Maximum pressure p_{max} (N/mm^2)	Calculated Load P_c (N/mm)
Hertzian analytical solution	137.215	2319.78	500.000
Numerical solution $\Delta L = 2$ (μm)	138.000	2311.59	501.357
Numerical solution $\Delta L = 10$ (μm)	140.000	2276.43	520.501

The results show that with varying pressure element size the numerical solution did not change the overall result of the pressure distribution, however the solution for the contact length increases with increasing element size because of the edge errors of the contact boundary. The accuracy of the numerical solution may be improved by using a finer element size.

CHAPTER 5.

5.6.2 Contact of Rough Surfaces

A further test was attempted to check the ability of the analysis to deal with the contact of rough surfaces. A series of test cases were studied. Figure 5.5 and Figure 5.6 show the results for one of the test runs for the contact case 2. Longitudinal rigid rough surfaces having Gaussian statistics are generated by numerical simulation program NSRRS. For the cases, where two rough surfaces in contact have RMS roughness σ_1 and σ_2 respectively but same correlation length and same surface anisotropy, the equivalent rough surface can be generated simulated by using the equivalent roughness $\sigma = (\sigma_1^2 + \sigma_2^2)^{1/2}$. The equivalent rough surface used in contact analysis is generated numerically with the following conditions:

$$\sigma = 0.2 \text{ } \mu\text{m}, \quad \lambda_x^* = 20 \text{ } \mu\text{m}, \quad \lambda_y^* = \infty$$

$$N_x = 200, \quad \Delta x = 20 \text{ } \mu\text{m}.$$

These values used for the material constants correspond to the contact between two surfaces of mild steel, i.e

$$E' = 100 \text{ GPa}, \quad \nu = 0.3.$$

Figure 5.5 (a) and (b) show the undeformed surface profile and the deformed surface profile. As can be seen in Figure 5.5 (b), the gap geometry in the deformed state is determined by the deformed surface profile, which provides important information for the leakage analysis of static sealed joints. When the zero-leakage is required, all values of gap should be zero, which means that all flow paths should be blocked effectively, hence leakage cannot take place.

CHAPTER 5.

The distribution of the contact pressure has been plotted in Figure 5.5 (c). As can be seen from Figure 5.5 (c), local pressure can vary from asperity to asperity and the highest local pressure can be many times greater than the lowest. Of course, the possibility of plastic flow has been ignored and some of the asperities would reach a certain maximum pressure and collapse plastically as the applied load increases.

The relationship between the real contact area and the applied load is of great interest to the leakage analysis of static sealed joints. The program **2DNECM** can be used to yield the information. Two simulated results presenting the predicted variation of the true area of contact with applied load are presented in Figure 5.6, where the length is measured in the x direction and the contact length is the total length of the surface profile that is in contact. Thus if $(\text{load/unit length}) / (\text{contact length})$ is plotted, the result is equivalent to load/area. The simulated results show that the variation of real contact with load depends very much upon the characteristics of rough surfaces. The variation of contact length is found to be approximately linear, the variations away from this being attributed to the random nature in which new contacts can be formed.

CHAPTER 5.

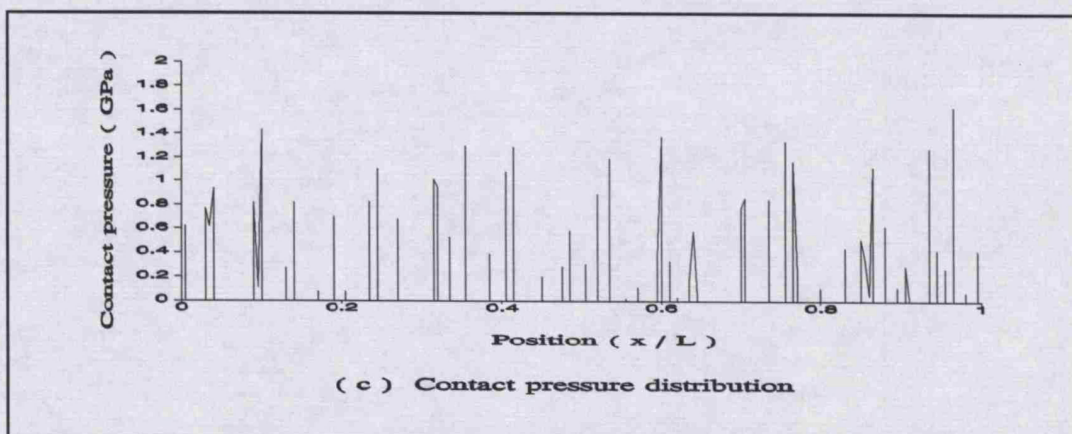
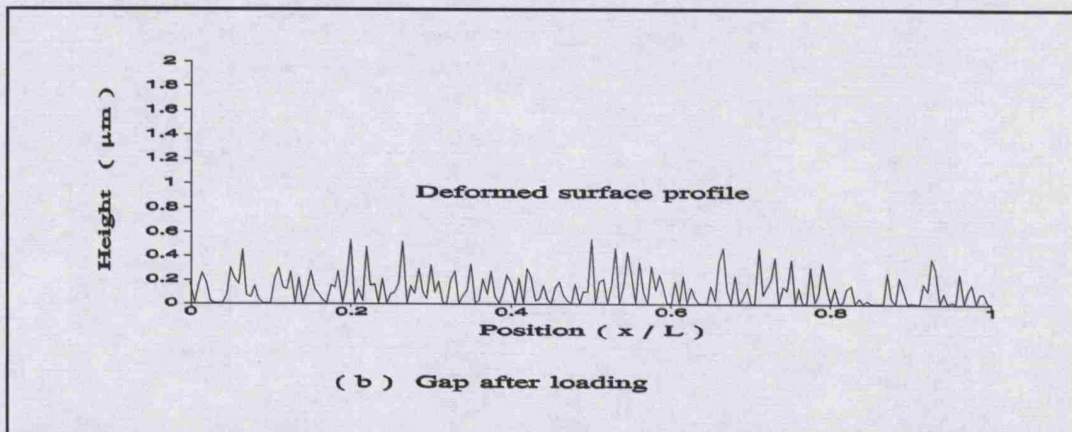
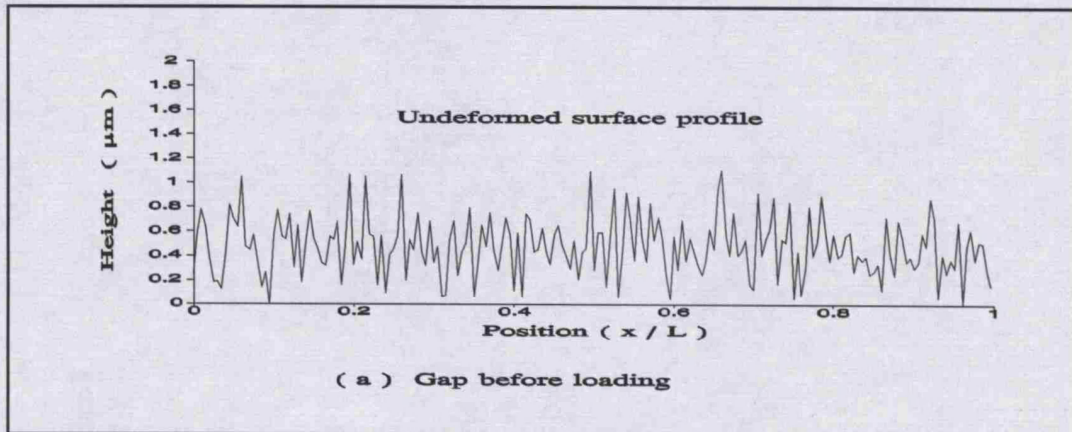


Figure 5.5 Simulated results for an equivalent rough surface loaded against a rigid plane

CHAPTER 5.

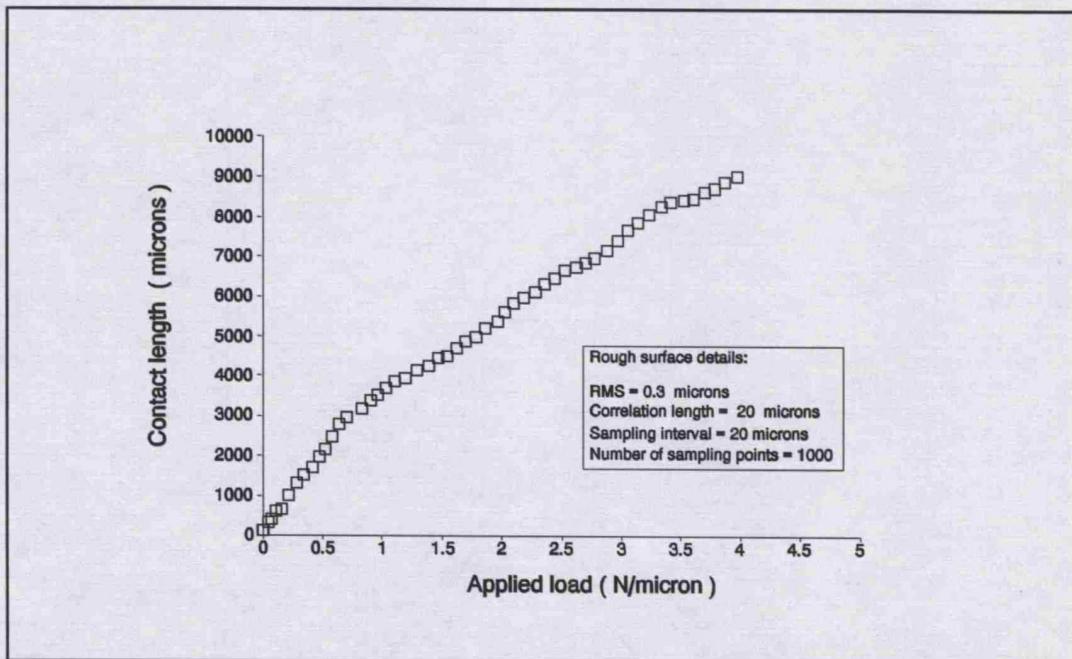
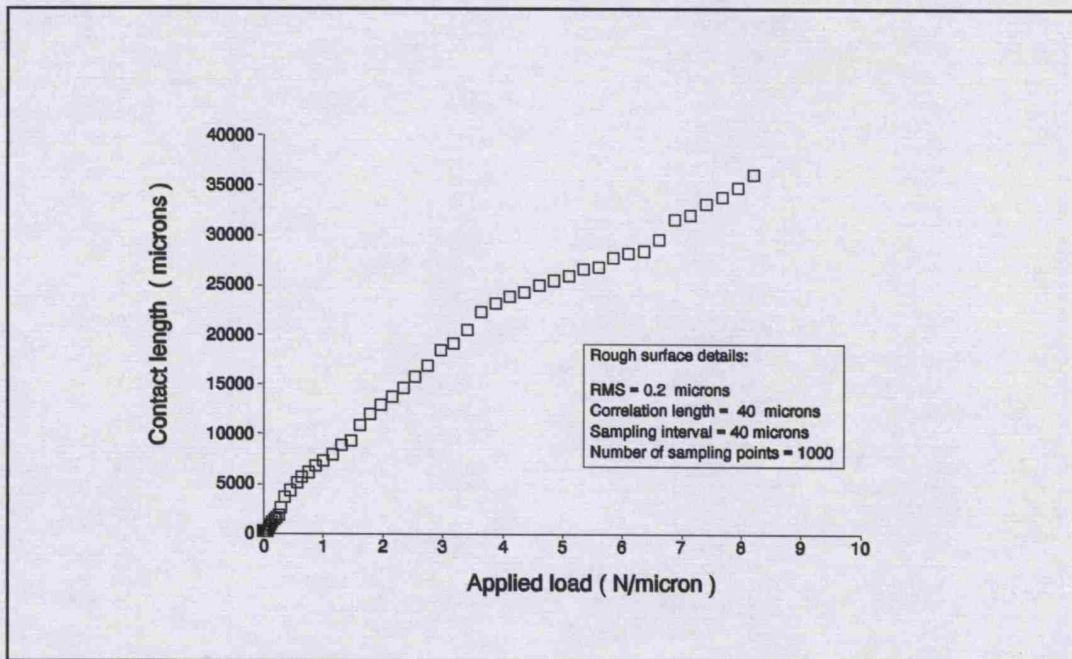


Figure 5.6 Predicted variation of contact length with applied load for two-dimensional contact of rough surfaces, showing the effect of rough surfaces

CHAPTER 5.

5.7 Comparison of Numerical and Stochastic Results

It is perhaps a worthwhile exercise to attempt a comparison between the contact results obtained by the present numerical model with an existing stochastic model. The use of a plane-strain contact model corresponds to the case of infinitely long asperities orthogonal to the profile (i.e. having an infinite degree of anisotropy). Bush, Gibson and Keogh (hereafter referred to as BGK) (1979) have studied the contact of strongly anisotropic rough surfaces, and therefore provide a suitable model for comparison. In their analysis they modelled the surface as parabolic ellipsoids having a Gaussian distribution of heights. They derived the following expressions for the variation of contact area A_c and normal load P_a :

$$\frac{P_a(s)}{A_c(s)} = \frac{\pi \xi (\gamma'^2 + k'^2)^{1/2}}{2^{2/3} k' K(k)} \quad (5.33)$$

where:

$$\xi = \frac{\sqrt{m_{02}}}{\sqrt{\pi}} E' \quad (5.34)$$

$$\gamma' = \left\{ \frac{(m_2)_{\min}}{(m_2)_{\max}} \right\}^{1/2} = \left(\frac{m_{20}}{m_{02}} \right)^{1/2} \quad (5.35)$$

CHAPTER 5.

$$k = \frac{0.4777 \gamma'}{1 - 1.3211 \gamma'} \quad (5.36)$$

$$k' = \sqrt{1 - k^2} \quad (5.37)$$

and $K(k)$ is the complete elliptical integral of the first kind given by

$$K(k) = \int_0^{\pi/2} \frac{d\phi}{(1 - k^2 \sin^2 \phi)^{1/2}} \quad (5.38)$$

The longitudinal ridge rough surfaces used in the comparison are generated numerically to have 1000 sampling points with $\Delta x = \lambda_x^*$. Unfortunately a direct comparison with these expression is not possible as the case for infinitely long asperities is indeterminate. To overcome this difficulty two values of γ have been assumed 0.1 and 0.01 in Equation (5.35), corresponding to two different degrees of anisotropy. To obtain a rough comparison value of m_2 , the second moment of the power spectral density function, was calculated by Appendix B. This value was then substituted for m_{02} in Equation (5.34).

Table 5.2 shows the results calculated from the above stochastic model together with the corresponding values calculated from the least squares line through the numerical results. The numerical results are consistently higher than the stochastic results calculated for $\gamma = 0.01$. However, in view of the many assumptions involved in both the random-process theory approach and

CHAPTER 5.

the numerical technique, the agreement is encouragingly good.

Table 5.2 Results comparing numerical and stochastic values of P_d/A_c

$P_d(s) / A_c (s) \quad (N / \mu m^2)$			
Parameters (μm)	BGK model		Numerical model
	$\gamma = 0.1$	$\gamma = 0.01$	$\gamma = 0$
$\sigma = 0.2, \lambda_x^* = 20$	3.877×10^{-4}	2.571×10^{-4}	3.293×10^{-4}
$\sigma = 0.3, \lambda_x^* = 20$	5.817×10^{-4}	3.858×10^{-4}	4.416×10^{-4}
$\sigma = 0.4, \lambda_x^* = 20$	7.754×10^{-4}	5.144×10^{-4}	6.832×10^{-4}
$\sigma = 0.2, \lambda_x^* = 30$	2.581×10^{-4}	1.711×10^{-4}	2.425×10^{-4}
$\sigma = 0.2, \lambda_x^* = 40$	1.934×10^{-4}	1.282×10^{-4}	2.021×10^{-4}

The effect of varying the sampling interval on the load-contact area relationship has also been investigated. The surfaces used in the comparison is first generated numerically to have 1000 sampling points with two sets of sampling interval size: $\Delta x = \lambda_x^*$ and $\Delta x = 1/2\lambda_x^*$. Table 5.3 gives the simulated results comparing the numerical and stochastic values of P_d/A_c showing the effect of changing the sampling interval. As can be seen from the results, the stochastic model predicts decreasing values of P_d/A_c as the sampling interval increases, which agrees with the trend observed from the numerical results. This means that the predicted area of real contact increases with increasing sampling interval. This is

CHAPTER 5.

caused by the lose of information on the small scale asperities. For a particular asperity contact at a large sampling interval, a large continuous contact is predicted; for a smaller sampling interval the equivalent region may well consist of a number of smaller asperity contacts, thus reducing the predicted contact area.

Table 5.3 Results comparing numerical and stochastic values of P_d/A_c showing the effect of sampling interval

Roughness parameters $\sigma = 0.3 \mu\text{m}$ $\lambda_x^* = 30 \mu\text{m}$	$F(s) / A_c (s) \quad (\text{N} / \mu\text{m}^2)$	
	BGK model $\gamma = 0.01$	Numerical model $\gamma = 0$
$\Delta L = \Delta x = \lambda_x^*$	3.375×10^{-4}	4.287×10^{-4}
$\Delta L = \Delta x = 1/2 \lambda_x^*$	5.552×10^{-4}	6.186×10^{-4}

The contact boundary condition defined by Equation (4.13) has been examined point by point for all of test cases, the results show that there is no distortion of solutions in the contact simulation of rough surfaces by using the numerical solution technique of the variational method.

The ability of the numerical model to analyze the contact of rough surface profiles is also confirmed. The model uses the actual digitized rough surface profiles produced by NSRRS and can yield important results about the gap geometry in the deformed state, which is an important

CHAPTER 5.

information for the leakage analysis of static sealed joints. The model is also capable of yielding results about the real pressure distribution and the real contact area, and predicting contact parameters such as the mean contact area and the mean contact pressure etc., where these will all vary with applied load, material properties and surface rough surfaces. Comparison with an existing stochastic contact model for highly anisotropic rough surfaces has been attempted. The results obtained from the stochastic and numerical models show an encouraging agreement considering the many differences between the two techniques.

CHAPTER 6.

Three-dimensional Numerical Model for the Elastic Contact of Rough Surfaces

6.1 Introduction

The two-dimensional numerical model presented in Chapter 5 can provide information about the contact situation at the interface of sealed joints with longitudinal roughness. However, for sealed joints having the general rough surface forms, a three-dimensional numerical model is needed to provide such quantitative information in three dimensions. In this chapter, a three-dimensional numerical model for the elastic contact of rough surfaces is developed on the basis of the Boussineq force-displacement relationship, which is widely used in a general numerical solution for elastic body contact problems by Hartnett (1980) amongst others. The contact characteristic of rough surfaces, in which contact can occur in a random manner, is considered by introducing two index matrices to record the position of contacting and

CHAPTER 6.

non-contacting points respectively. The numerical solution technique based on the variational principles, which has been widely used in the rolling contact problem by Kalker (1990), is also applied in the contact of rough surfaces.

6.2 Statement of Contact Problem

6.2.1 Constrains and Assumptions

Except for the assumption of plane strain, the constraints and assumptions used in the two-dimensional numerical contact model are still valid to develop a numerical contact mode for the frictionless, three-dimensional contact problems of elastic bodies, i.e:

- (1) The contact between two bodies is linear elastic;
- (2) The contact conditions allow the use of half space solutions;
- (3) The elastic contact area is completely contained within the geometric overlap region, as shown in Figure 4.1;
- (4) Relative horizontal strains and displacements are ignored, i.e frictionless contact.
- (5) The contact between two bodies satisfies the boundary condition defined by Equation (4.13).

CHAPTER 6.

6.2.2 Generalized Boussinesq Solution

To correlate the displacement field u with the contact pressure field p inside the contact region Ω_n , the contacting bodies are considered as elastic half-spaces, which has been shown to be an acceptable approximation (Singh and Paul 1974). For points on the frictionless surfaces of the bodies, u and p are related by integrating the Boussinesq solution for a normal point load, which leads to the following equation (Timoshenko 1951):

$$u_i(x,y) = \frac{(1-\nu_i^2)}{\pi E_i} \iint_{\Omega_n} \frac{p(x',y') dx' dy'}{\{(x-x')^2 + (y-y')^2\}^{1/2}} \quad (6.1)$$

$(i = 1, 2)$

Thus, the total displacement $u(x,y)$ of any point on the surfaces can be expressed by:

$$\begin{aligned} u(x,y) &= u_1(x,y) + u_2(x,y) \\ &= K_e \iint_{\Omega_n} \frac{p(x',y') dx' dy'}{\{(x-x')^2 + (y-y')^2\}^{1/2}} \end{aligned} \quad (6.2)$$

where the elastic parameter K_e is defined by

CHAPTER 6.

$$K_e = \frac{(1-\nu_1^2)}{\pi E_1} + \frac{(1-\nu_2^2)}{\pi E_2} \quad (6.3)$$

6.3 Numerical Method

The general numerical method for the solution of half-space contact problems has been illustrated by the two-dimensional contact model presented in Chapter 5. For three-dimensional contact problems, the procedure is very similar save that the contact area must be divided into elements of area over which a pressure function acts.

Similar types of traction element to those described in two-dimensional problems may be used in the solution of three-dimensional problems. The column of uniform traction in three-dimension is often to be preferred although a wide range of possible traction elements are available for use in the such numerical method. Uniform pressure elements have been employed in the analysis of smooth contact by Hartnett (1980) and de Mul et al. (1986). The contact of rough surfaces has also been analyzed with uniform pressure elements by Xian and Zheng (1991). The uniform pressure element will also be chosen to develop a three-dimensional numerical model of rough surface contact in this Chapter.

CHAPTER 6.

6.3.1 Contact Pressure Element Equation

The effect of a uniform pressure action a rectangular area $2a \times 2b$ has been analyzed in detail by Love (1929). The deflexion of a general point (x, y) on the surface is given by:

$$\begin{aligned} u(x, y) = \frac{(1-\nu^2)}{\pi E} p \left\{ (x+a) \ln \left[\frac{(y+b) + \{(y+b)^2 + (x+a)^2\}^{1/2}}{(y-b) + \{(y-b)^2 + (x+a)^2\}^{1/2}} \right] \right. \\ + (y+b) \ln \left[\frac{(x+a) + \{(y+b)^2 + (x+a)^2\}^{1/2}}{(x-a) + \{(y+b)^2 + (x-a)^2\}^{1/2}} \right] \\ + (x-a) \ln \left[\frac{(y-b) + \{(y-b)^2 + (x-a)^2\}^{1/2}}{(y+b) + \{(y+b)^2 + (x-a)^2\}^{1/2}} \right] \\ \left. + (y-b) \ln \left[\frac{(x-a) + \{(y-b)^2 + (x-a)^2\}^{1/2}}{(x+a) + \{(y-b)^2 + (x+a)^2\}^{1/2}} \right] \right\} \end{aligned} \quad (6.4)$$

By introducing an influence function $C(x, y)$ representing the deflection at point (x, y) because of a unit uniform pressure on the surface, the Equation (6.4) can be rewritten as:

$$u(x, y) = C(x, y) \times p \quad (6.5)$$

where:

CHAPTER 6.

$$\begin{aligned}
 C(x,y) = \frac{(1-\nu^2)}{\pi E} \left\{ (x+a) \ln \left[\frac{(y+b) + \{(y+b)^2 + (x+a)^2\}^{1/2}}{(y-b) + \{(y-b)^2 + (x+a)^2\}^{1/2}} \right] \right. \\
 + (y+b) \ln \left[\frac{(x+a) + \{(y+b)^2 + (x+a)^2\}^{1/2}}{(x-a) + \{(y+b)^2 + (x-a)^2\}^{1/2}} \right] \\
 + (x-a) \ln \left[\frac{(y-b) + \{(y-b)^2 + (x-a)^2\}^{1/2}}{(y+b) + \{(y+b)^2 + (x-a)^2\}^{1/2}} \right] \\
 \left. + (y-b) \ln \left[\frac{(x-a) + \{(y-b)^2 + (x-a)^2\}^{1/2}}{(x+a) + \{(y-b)^2 + (x+a)^2\}^{1/2}} \right] \right\} \quad (6.6)
 \end{aligned}$$

6.3.2 Formulation of Numerical Solution

To get the formulation of the numerical solution, the contact boundary is discretized into rectangular elements, as shown in Figure 6.1. Since the distribution pressure over each element is assumed to be constant with the use of the linear elastic theory, the total vertical displacement on the surface of the bodies due to all element pressures p_{kl} is given by:

$$\begin{aligned}
 u_{ij} = \sum_{k=1}^{M_x} \sum_{l=1}^{M_y} C_{ijkl} p_{kl} \quad i = 1, 2, \dots, M_x \\
 j = 1, 2, \dots, M_y \quad (6.7)
 \end{aligned}$$

where C_{ijkl} is defined as influence coefficient representing the deflection of element centre (i, j) because of a unit uniform pressure on element (k, l) .

CHAPTER 6.

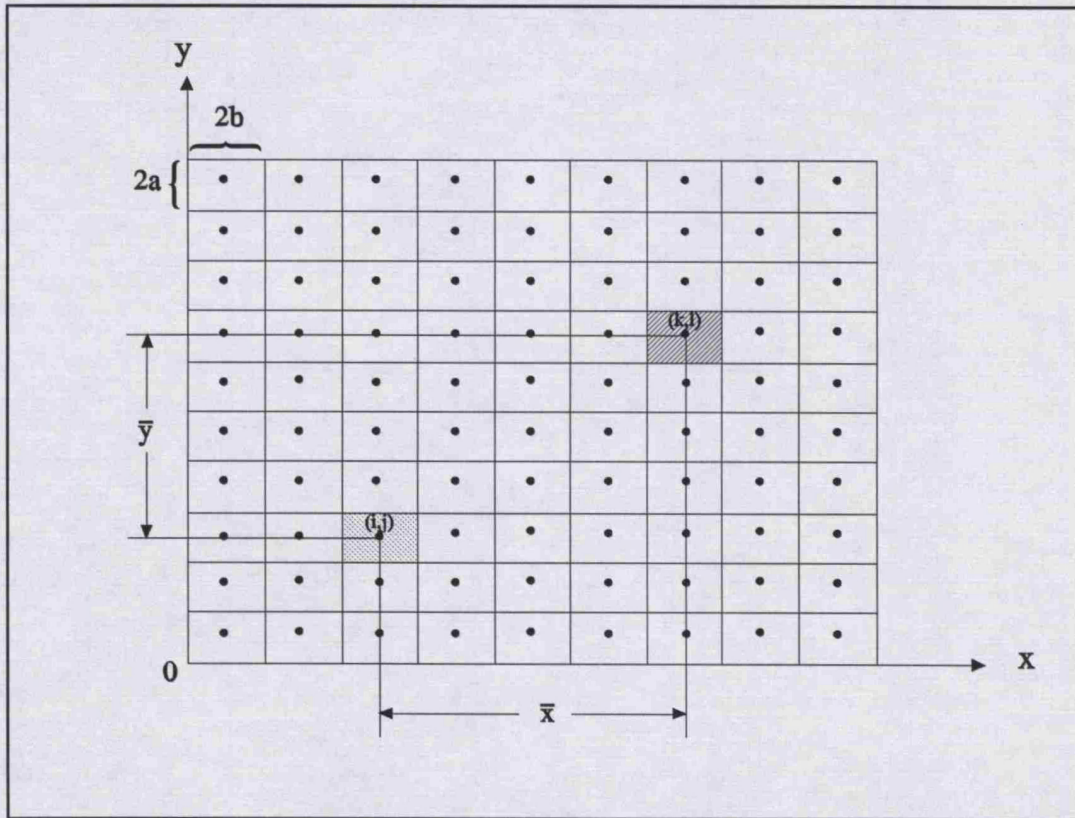


Figure 6.1 Discretization of the contact boundary

In order to determine the influence coefficients defined by Equation (6.6), for the case of the contact of two elastic bodies the elasticity of another body can be taken into account by replacing $(1-\nu^2)/\pi E$ by the elastic parameter K_e defined in Equation (6.3). Substituting the distance $x = \bar{x}$ and $y = \bar{y}$ in Equation (6.6), the influence coefficients $C_{ij\ kl}$ can be determined by:

CHAPTER 6.

$$\begin{aligned}
 C_{ij\ kl} = K_e \left\{ & (\bar{x}+a) \ln \left[\frac{(\bar{y}+b) + \{(\bar{y}+b)^2 + (\bar{x}+a)^2\}^{1/2}}{(\bar{y}-b) + \{(\bar{y}-b)^2 + (\bar{x}+a)^2\}^{1/2}} \right] \right. \\
 & + (\bar{y}+b) \ln \left[\frac{(\bar{x}+a) + \{(\bar{y}+b)^2 + (\bar{x}+a)^2\}^{1/2}}{(\bar{x}-a) + \{(\bar{y}+b)^2 + (\bar{x}-a)^2\}^{1/2}} \right] \\
 & + (\bar{x}-a) \ln \left[\frac{(\bar{y}-b) + \{(\bar{y}-b)^2 + (\bar{x}-a)^2\}^{1/2}}{(\bar{y}+b) + \{(\bar{y}+b)^2 + (\bar{x}-a)^2\}^{1/2}} \right] \\
 & \left. + (\bar{y}-b) \ln \left[\frac{(\bar{x}-a) + \{(\bar{y}-b)^2 + (\bar{x}-a)^2\}^{1/2}}{(\bar{x}+a) + \{(\bar{y}-b)^2 + (\bar{x}+a)^2\}^{1/2}} \right] \right\}
 \end{aligned} \tag{6.8}$$

Where (\bar{x}, \bar{y}) are the coordinate locations of the centre of element (k, l) with respect to the centre of element (i, j) , shown as in Figure 6.1.

Considering displacements for all points on the surfaces, Equation (6.7) represents a set of $(M_x \times M_y)^2$ simultaneous equations which may be expressed in matrix form thus:

$$(\mathbf{u}) = [\mathbf{C}] (\mathbf{p}) \tag{6.9}$$

where (\mathbf{u}) is the vector of surface displacements, $[\mathbf{C}]$ is the matrix of influence coefficients defined by Equation (6.8) and (\mathbf{p}) is the vector of contact pressures. The matrix of influence coefficients is square and symmetric (as $\bar{x} = |k - i|$ and $\bar{y} = |l - j|$, therefore $C_{ij\ kl} = C_{kl\ ij}$).

CHAPTER 6.

The set of linear simultaneous Equations (6.9) that relate displacements to pressures has the same formulation as in general smooth body contact problems. For the smooth body case, the values of (\bar{x}, \bar{y}) to be used to calculate the influence coefficient would show progressive variation, however for rough surface cases, this progressive variation is not valid because the contact of rough surfaces can occur in a random manner. Thus, the numerical solution of rough and smooth contact problems by using discretized traction elements has been seen to be conceptually straightforward, except for the special treatment adopted for the contact of rough surfaces.

The treatment adopted for the contact of rough surfaces that divides the surface displacements into two parts: the displacement of contact elements and the displacement of non-contact elements in two-dimensional numerical contact model, is still valid in three-dimensional numerical contact model, provided two index matrices $I(i,j)$ ($i = 1,2,\dots,M'_x$, $j = 1,2,\dots,M'_y$) and $J(i,j)$ ($i = 1,2,\dots,M_x-M'_x$, $j = 1,2,\dots,M_x-M'_y$) have been set to record the position of contacting elements and non-contacting elements respectively.

From the analysis above, we can also see that the numerical procedure of the contact problems in three-dimensional case by using discretized traction elements is very similar to in two-dimension case. However, the need to work in terms of relative displacements in two-dimensional case is removed since no arbitrary constant is present in expressions for the displacement due to pressure acting over an area of a three-dimensional half-space.

CHAPTER 6.

6.3.3 Quadratic Programming Formulation

Substituting Equation (6.9) correlating the displacement u and the pressure p for the contacting elements into Equation (5.22), the numerical formulation of the solution can be given by:

$$\text{Min! } V^* = \sum_{i=1}^{M'_x} \sum_{j=1}^{M'_y} A_{ei} p_{ij} b_{ij} + \frac{1}{2} \sum_{i=1}^{M'_x} \sum_{j=1}^{M'_y} \sum_{k=1}^{M'_x} \sum_{l=1}^{M'_y} A_{ei} C_{ijkl} p_{ij} p_{kl}$$

Subject to: $p_{ij} > 0$

(6.10)

where A_{ei} is constant depending upon the form and size of the pressure element. For a uniform pressure element having a shape of rectangle, the value of A_{ei} is equal to the surface area of the element, i.e. $A_{ei} = 2a \times 2b$.

Through solving the quadratic programming problem defined by Equation (6.10), the displacement and size of elements in contact and the contact pressure will be determined uniquely. Then the displacements for the non-contacting elements can also be determined by using Equation (6.9), where the values of (\bar{x}, \bar{y}) to be used to calculate the influence coefficient C_{ijkl} is the distance between the contacting and non-contacting elements.

With a few minor modifications, the algorithm and computer program developed in two-dimensional numerical contact model has been applied to three-dimensional numerical contact model, called as **3DNECM**. For three-

CHAPTER 6.

dimensional contact problems, the displacement $\delta_0(x,y)$ is given by:

$$\delta_0(x,y) = K_e \iint_{\Omega_N} \frac{p_m dx' dy'}{\{(x-x')^2 + (y-y')^2\}^{1/2}} \quad (6.11)$$

6.4 Numerical Examples

6.4.1 Contact of Two Elastic Smooth Spheres

To verify the computer program and confirm the accuracy of the present model, the contact of two elastic smooth spheres has been studied. The numerical results are compared with analytical Hertzian solution for the following conditions:

$$E_1 = E_2 = 200 \text{ GPa}, \quad \nu_1 = \nu_2 = 0.3$$

$$R_1 = R_2 = 65 \text{ mm}, \quad \delta = 0.01 \text{ mm}$$

Two element sizes used for numerical calculations are $A_e = 0.01 \times 0.01$ (mm^2) and $A_e = 0.05 \times 0.05$ (mm^2).

The analytical expressions for the contact size r (the radius of contact circle), the compression δ and the pressure distribution are (Johnson 1985):

$$r = \left(\frac{3P_a R}{4E'} \right)^{1/3} \quad (6.12)$$

CHAPTER 6.

$$\delta = \frac{r^2}{R} = \left(\frac{9P_a^2}{16RE^2} \right)^{1/3} \quad (6.13)$$

$$p_{\max} = \frac{3P_a}{2\pi r^2} = \left(\frac{6P_a E^{1/2}}{\pi^3 R^2} \right)^{1/3} \quad (6.14)$$

$$p(x) = p_{\max} \left\{ 1 - \left(\frac{x}{r} \right)^2 \right\}^{1/2} \quad (6.15)$$

The real contact area ratios of numerical results and Hertzian solution are calculated:

$$(A_{\mathcal{J}_1}) / (A_{\mathcal{J}_{HZ}}) = 1.012295 \quad (A_{\mathcal{J}_2}) / (A_{\mathcal{J}_{HZ}}) = 1.057193$$

where $(A_{\mathcal{J}_{HZ}})$ is the real contact area from Hertzian solution, $(A_{\mathcal{J}_1})$, $(A_{\mathcal{J}_2})$ are real contact area from numerical solution for element pressure size $A_e = 0.01 \times 0.01$ (mm²) and $A_e = 0.05 \times 0.05$ (mm²) respectively.

The pressure distribution from the numerical solution for $A_e = 0.01 \times 0.01$ (mm²) is plotted in Figure 6.2. Figure 6.3 shows the comparison of pressure distribution, where the pressure distribution $p(x)$ is normalised by the theoretical maximum pressure given by Equation (6.14). From the comparison, it is evident that the numerical model yields fairly accurate pressure distribution in the region where the pressure gradient is small. The accuracy can be improved by using a finer grid size. The real contact ratios of numerical results and Hertzian solution also shows that the numerical contact model used to calculated real contact area gives reasonable results.

CHAPTER 6.

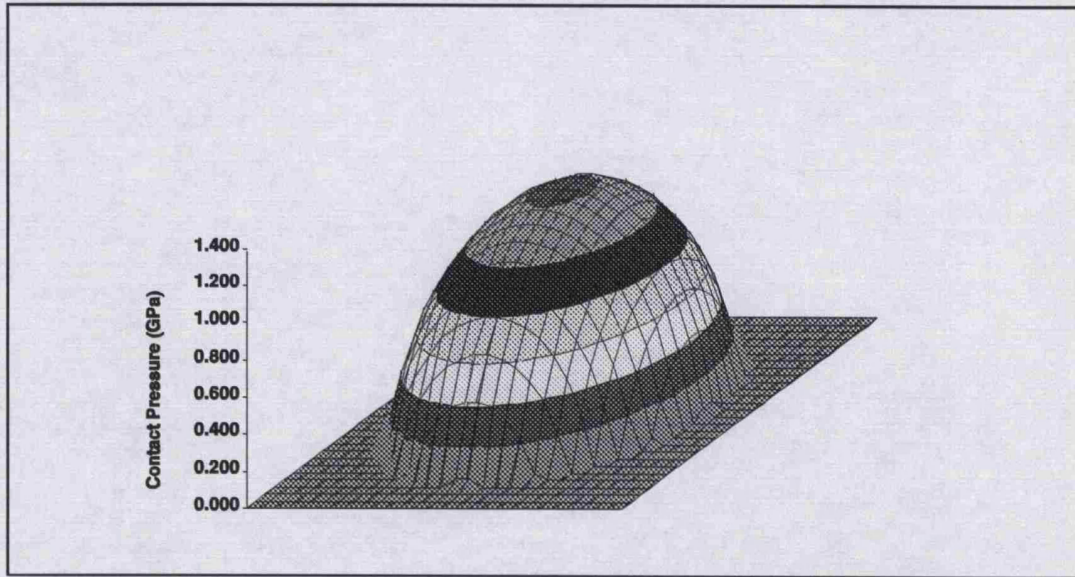


Figure 6.2 Pressure distribution for the contact of smooth spheres

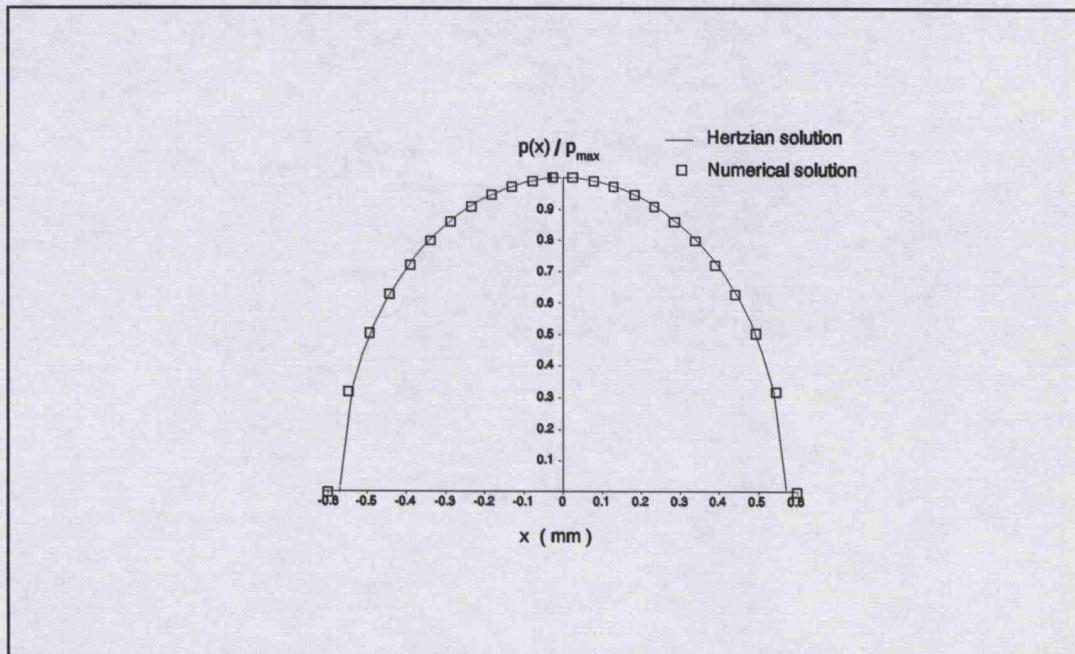


Figure 6.3 Comparison of pressure distribution for the contact of smooth spheres

CHAPTER 6.

6.4.2 Contact of Rough Surfaces

The three-dimensional numerical contact model has been applied to the contact analysis of rough surfaces for Case 2. A series of test cases were studied. Since the model uses the actual digitized surface topography, it can yield the results about the real pressure distribution and the deformed shape. Two of simulated results about the distribution of the contact pressure have been plotted in Figure 6.4, where the two rough surfaces used are same statistics parameters (σ and λ^*) but are generated by simulation with different surface forms. As can be seen from Figure 6.4, local pressure can vary from asperity to asperity; even if the rough surfaces have same statistics parameters, the distribution of contact pressure would have the different form. According to the boundary contact condition defined by Equation (4.13), the contact points corresponds to those points having non-zero contact pressure, whereas the non-contacting points corresponds to those points having zero contact pressure. Therefore, the simulated result of the distribution of contact pressure implies the contact situation at the interface, which provides important information for the simulation analysis of leakage of static sealed joints.

The program **3DNECM** can also be applied to predict contact parameters such as the mean contact area and the mean contact pressure etc., where these will vary with applied load, material properties and surface roughness. The relationship between the real area of contact and applied load is great interest to the leakage analysis of static sealed joints. Two of the simulated results have been plotted in Figure 6.5, showing the effect of rough surfaces. As can be seen from Figure 6.5, the variation of contact area is

CHAPTER 6.

approximately linear, the variations away from this being attributed to the random nature in which new contacts can be formed.

CHAPTER 6.

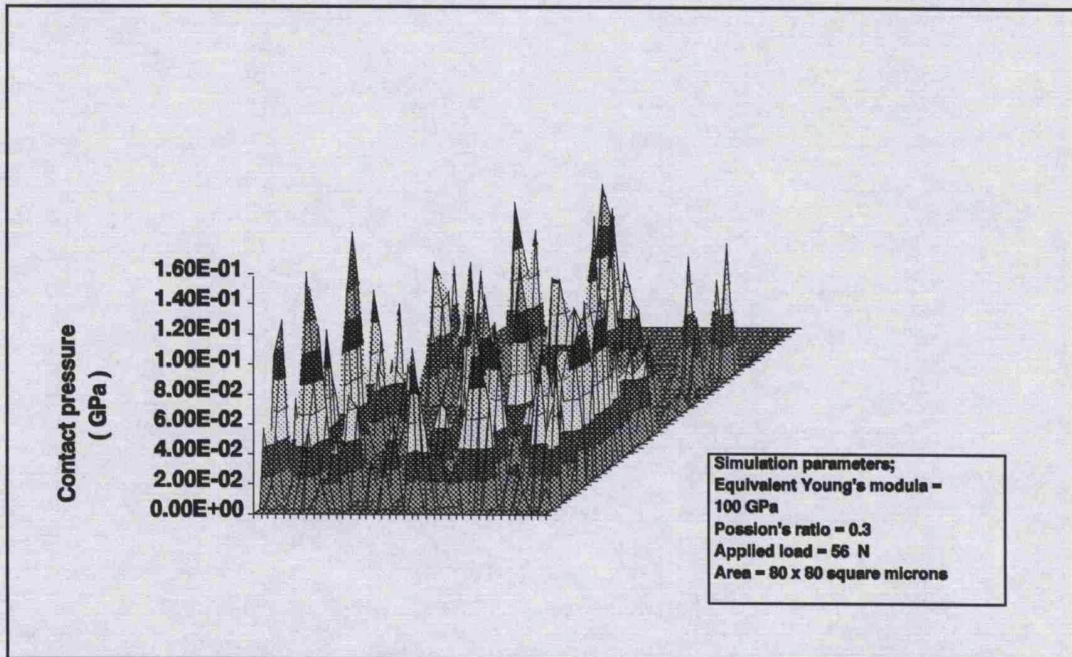
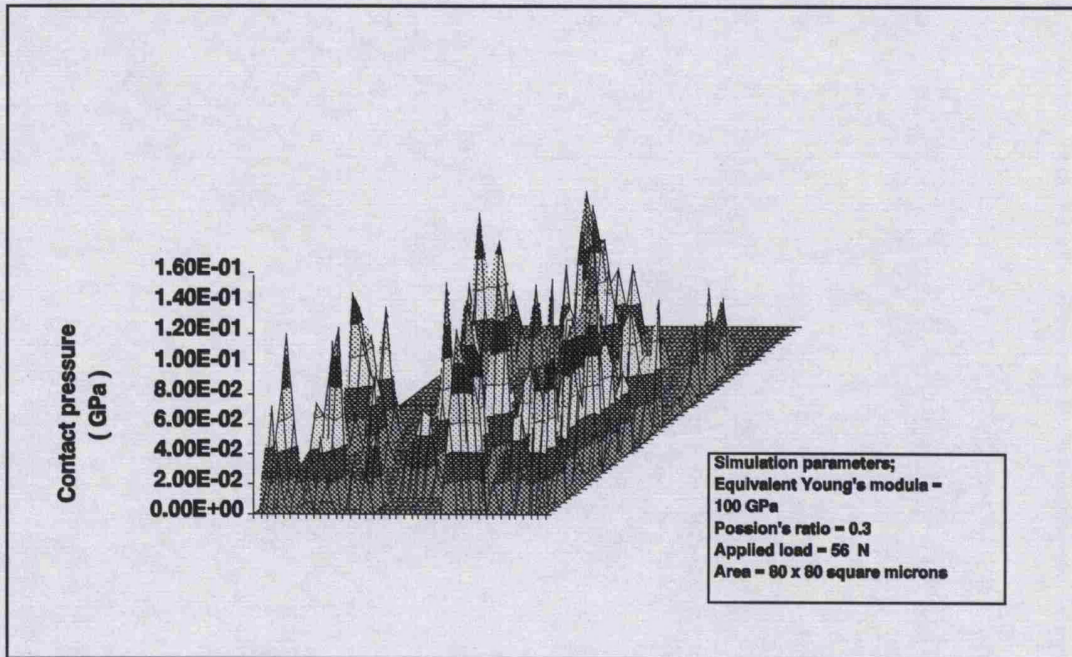


Figure 6.4 Pressure distribution for the contact of rough surfaces

CHAPTER 6.

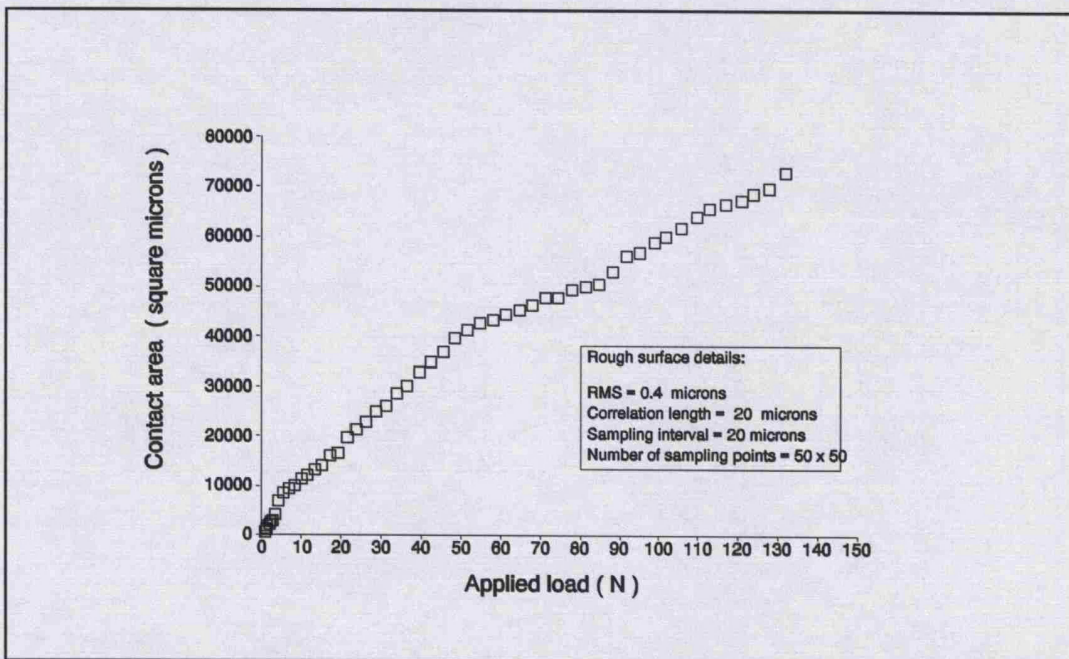
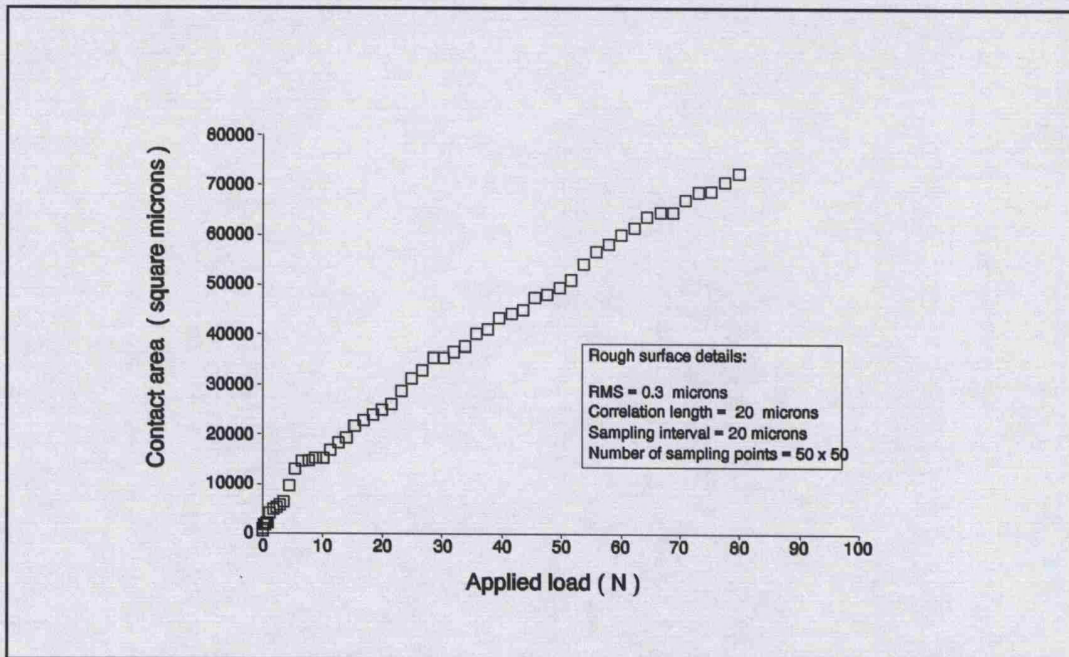


Figure 6.5 Predicted variation of the real contact area with applied load, showing the effect of rough surfaces

CHAPTER 6.

6.5 Comparison of Numerical and Stochastic Results

To confirm the ability of the analysis to deal with the contact of rough surfaces, it is necessary to compare the present contact model with the existing stochastic models. The comparison of stochastic models for the contact of rough surfaces had been done by McCool (1986). He suggested that the GW model would give good order of magnitude estimates of the number of contacts, real contact area fraction and nominal pressure that result at a given separation of a rough and a smooth flat plane. Therefore, the GW model is chosen as a suitable model for comparison.

In order to compare, McCool related the three parameters of the GW model, i.e. β , the assumed constant radius of the spherical summits, σ_s , the standard deviation of the summit height (assumed to be Gaussian) and D_{sum} , the area density of summits, to the three spectral moments m_0 , m_2 and m_4 of rough surfaces. He shown that the real contact area for the GW model at a given mean plane separation depends only on the bandwidth parameter α , defined as:

$$\alpha = \frac{m_0 m_4}{m_2^2} \quad (6.16)$$

and the ratio A_c / A_n of the contact area to the apparent area is given by:

CHAPTER 6.

$$\frac{A_c}{A_n} = 0.0640(\alpha - 0.8968)^{1/2} F_1\left(\frac{d}{\sigma_s}\right) \quad (6.17)$$

where $F_1(t)$ is the integral

$$F_1(t) = \int_t^{\infty} (x - t) \phi(x) dx \quad (6.18)$$

and was evaluated using tables by McCool, where $\phi(x)$ is standard normal density function.

With the same substitutions, the expression for P_a/A_n in the GW model is reduced by McCool to:

$$\frac{P_a}{A_n} = 0.0333 E' m_2^{1/2} (\alpha - 0.8968)^{3/4} F_{3/2}\left(\frac{d}{\sigma_s}\right) \quad (6.19)$$

where $F_{3/2}(t)$ is the integral

$$F_{3/2}(t) = \int_t^{\infty} (x - t)^{3/2} \phi(x) dx \quad (6.20)$$

and is tabulated by McCool.

The computer simulated rough surfaces used in comparison are isotropic having 50×50 sampling points with the sampling interval $\Delta x = \Delta y = \lambda^*$. For the rough surfaces used in the comparison, the bandwidth

CHAPTER 6.

parameters and the second moment of the power spectral density function were calculated by Appendix B. and were tabulated in Table 6.1.

Table 6.1 Bandwidth parameters and second moment of PSD

Roughness parameters σ , λ_x^*	Bandwidth parameter $\bar{\alpha}$	Second moment of PSD \bar{m}_2
$\sigma = 0.2$, $\lambda_x^* = 20$	2.14267	1.44×10^{-4}
$\sigma = 0.3$, $\lambda_x^* = 20$	2.14267	3.24×10^{-4}
$\sigma = 0.4$, $\lambda_x^* = 20$	2.14267	5.75×10^{-4}
$\sigma = 0.2$, $\lambda_x^* = 30$	2.14267	6.39×10^{-5}
$\sigma = 0.2$, $\lambda_x^* = 40$	2.14267	3.61×10^{-5}

Table 6.2 gives the values of P_a/A_c from the GW model and the present numerical model, which are both calculated from the least squares through the calculated results and simulated results. The numerical results are consistently higher than the stochastic results. No straightforward explanations were found. However, when considering the differences between the two analysis techniques, the agreement is generally encouraging.

CHAPTER 6.

Table 6.2 Results comparing numerical and stochastic values of P_a/A_c

Roughness parameters (μm)	P_a/A_c ($\text{N} / \mu\text{m}^2$)	
	GW model	Numerical model
$\sigma = 0.2$, $\lambda_x^* = 20$	0.707×10^{-3}	1.031×10^{-3}
$\sigma = 0.3$, $\lambda_x^* = 20$	1.061×10^{-3}	1.108×10^{-3}
$\sigma = 0.4$, $\lambda_x^* = 20$	1.415×10^{-3}	1.802×10^{-3}
$\sigma = 0.2$, $\lambda_x^* = 30$	0.472×10^{-3}	0.665×10^{-3}
$\sigma = 0.2$, $\lambda_x^* = 40$	0.354×10^{-3}	0.631×10^{-3}

The effect of altering the pressure element size on the load-contact area relationship has also been studied. The size of pressure element size depends on the sampling interval. The isotropic rough surfaces used in comparison are generated to have 50×50 grid points with two sets of sampling interval: $\Delta x = \Delta y = \lambda^*$ and $\Delta x = \Delta y = 1/2\lambda^*$. The parameters in GW model were calculated and were tabulated in Table 6.3.

CHAPTER 6.

Table 6.3 Parameters used in GW model

Parameters	Sampling interval $\Delta x = \Delta y$	
	$\Delta x = \Delta y = \lambda_x^*$	$\Delta x = \Delta y = 1/2 \lambda_x^*$
r_t / λ_x^*	50.0	50.0
r_s / λ_x^*	1.0	0.5
\bar{m}_0 / m_0	0.575954	0.754875
$\bar{m}_2 \beta^2 / m_0$	0.271872	0.962516
$\bar{m}_4 \beta^4 / m_0$	0.268905	3.363759
$\bar{\alpha}$	2.095367	2.740842

Table 6.4 gives the results comparing the numerical and stochastic values of P_a / A_c showing the effect of changing the pressure element size. As can be seen from the results, the stochastic model predicts decreasing values of P_a / A_c as the pressure element size increases, which agrees with the trend observe from the numerical results. This means that the predicted area of real contact increases with increasing sampling interval. This is caused by the lost of information on the small scale asperities. For a particular asperities contact at a large sampling interval, a large continuous contact is predicted; for a smaller sampling interval the equivalent region may well consist of a number of smaller asperity contacts, thus reducing the predicted contact area.

CHAPTER 6.

Table 6.4 Results comparing numerical and stochastic values of P_a/A_c showing the effect of the sampling interval

$\sigma = 0.3 \mu\text{m}$ $\lambda_x^* = 30 \mu\text{m}$	$P_a/A_c \text{ (N / mm}^2 \text{)}$	
	GW model	Numerical model
$\Delta x' = 1/2 \lambda_x^*$	1.691×10^{-3}	2.092×10^{-3}
$\Delta x' = \lambda_x^*$	0.923×10^{-3}	1.214×10^{-3}

The contact boundary condition defined by Equation (4.13) has been examined point by point for all of test cases, the results show that there is no distortion of solutions in the contact simulation of rough surfaces by using the numerical solution technique of the variational method.

CHAPTER 6.

6.6 Conclusions

The numerical solution technique based on variational principles has been applied successfully to the elastic contact of three-dimensional real rough surfaces. The computer algorithm and program in FORTRAN have completed, and have been applied to a series of test cases. The simulated results have confirmed that there is no difficulty in the convergence of the solution. The application of the variational method eliminates the iteration involved in the Matrix Inversion Method for cases of frictionless contact. This facility known as a warm start in the E04NAF routine also leads to significant saving in computational effort when solving a sequence of related problems. Therefore, the program has the characteristics of good robustness as well as higher efficiency.

To verify the computer program and confirm the accuracy of the present model, for the contact of two smooth spheres, the numerical results are compared with the theoretical Hertzian results. The comparison shows that the numerical model produces excellent agreement with the Hertzian theory. The accuracy of the numerical model can be improved by using a finer element size.

The analysis ability of the numerical model to the contact of rough surface profile is also confirmed. The model uses the actual digitized rough surface profiles produced by NSRRS and can yield important results about the real contact situation at interface, which make a good condition to develop a simulation model of leakage. The model is also capable of yielding results

CHAPTER 6.

about the real pressure distribution and the real contact area, and predicting contact parameters such as the mean contact area and the mean contact pressure etc., where these will all vary with applied load, material properties and surface roughness. Therefore it may be applied to a variety of contact problems. Comparison with an existing stochastic contact model for isotropic rough surfaces has been attempted. The results obtained from the stochastic and numerical models show an encouraging agreement considering the many differences between the two techniques.

CHAPTER 7.

Prediction of Leakage Probability and Criteria for Identifying Reliability of Static Sealed Joints

7.1 Introduction

Although perfect sealing may be the general aim, in practice for apparently identical seals in the same application, some may seal while some not. This is due to random variations between apparently identical situations. This thesis concentrates on the effects of random surfaces, but a full analysis of seal reliability would also include variability of materials, loading, etc. Therefore, the important of the reliability of sealed joints cannot be overemphasized. It is the most reasonable to apply the statistical concepts in discussing sealing reliability. However, the statistical analysis of leakage by computer simulation is much simpler and more economic than by experiments. The result of variation in parameters that would affect the sealing performance can be studied without costly and length experimental efforts.

CHAPTER 7.

The numerical simulation model of random rough surfaces presented in Chapter 3 and the numerical elastic contact model of rough surfaces presented in chapter 5 and chapter 6 reveal the effect of the random properties of rough surfaces on the contact state, hence this facilitates the leakage simulation of surface-related random phenomena. In this chapter, the simulation model for the leakage analysis of static sealed joints will be developed. The relationship between the leakage probability and the applied load, which is of great interest to the designers of static sealed joints, will be predicted by the leakage simulation model. Furthermore, the contact area criterion for identifying the reliability of static sealed joints will also be obtained, which provides a simple, inexpensive and useful criterion to evaluate the effects of rough surfaces, material properties and applied load on the sealing reliability of static sealed joints.

7.2 Theoretical Background - Percolation Theory

Percolation theory provides an insight into leakage simulation. What is percolation? Stauffer (1985) have described it in "*Introduction to Percolation Theory*" as:

"Imagine a large array of squares as shown in Figure 7.1 (a). We imagine this array to be so large that any effects from its boundaries are negligible. Physicists call such an array a square lattice, mathematicians denote it by \mathbb{R}^2 ; common sense identifies it with a big sheet of ruled paper. Now a certain fraction of squares are filled with a big dot in the centre,

CHAPTER 7.

whereas the other squares are left empty, as in Figure 7.1 (b). We now define a *cluster* as a group of neighbour squares occupied by these big dots; these clusters are encircled in Figure 7.1 (c). From this picture we see that squares are called neighbours if they have one side in common but not if they only touch at one corner. Physicists call squares with one common side "nearest neighbour sites on the square lattice", whereas squares touching at one corner only are "next nearest neighbours". All sites within one cluster are thus connected to each other by one unbroken chain of nearest neighbour links from one occupied square to a neighbour square also occupied by a big dot. The graphical "cluster" explanation through Figure 7.1 (c) seems more appropriate for our purposes here than a precise mathematical definition. Percolation theory now deals with the number and properties of these clusters."

"How are the dots distributed among the squares in Figure 7.1 (a). One may assume that the dots love to cling together, or that they hate each other and try to move as far away from each other as possible. But the simplest assumption is that they ignore each other. Then the occupation of the squares is random, that is each square is occupied or empty independent of the occupation status of its neighbours. We call p_c as the concentration of a system, i.e the probability of a site being occupied by a big dot; that means that is we have N squares and N is a very large number, then $p_c N$ of these squares are occupied, and the remaining $(1-p_c)N$ of these squares are empty. This case of random percolation is what we concentrated on here:

Each site of a very large lattice is occupied randomly with probability

CHAPTER 7.

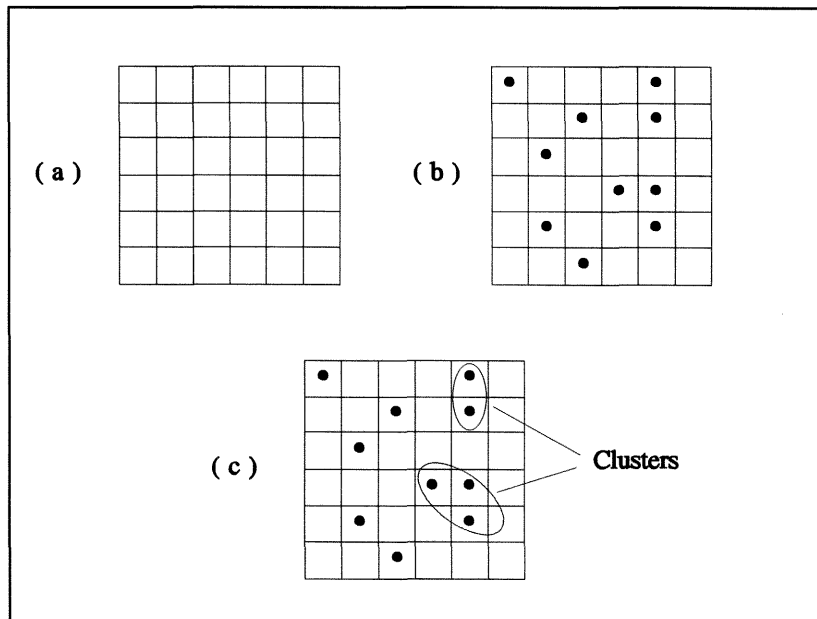


Figure 7.1 Definition of percolation and its cluster.

p_c , independent of its neighbours. Percolation theory deals with the clusters thus formed, in other words the groups of neighbouring occupied sites."

"In such an infinite square lattice, there would be a critical value of the concentration, defined as the percolation threshold p_{c0} , where for the first time one cluster extends from top to bottom and from left to right of the system, the cluster is called as percolating cluster. Furthermore, for all $p_c > p_{c0}$ one has a cluster extending from one side of the system to the other, whereas for all $p_c < p_{c0}$ no such infinite cluster exists. The value of percolation threshold p_{c0} dependent upon the shape of lattice. Table 7.1 lists the selected percolation thresholds for two-dimensional and three-dimensional lattices. In all cases, only nearest neighbours form clusters and no correlations are

CHAPTER 7.

allowed between different sites."

Table 7.1 Selected percolation thresholds for two- and three-dimensional lattices

Lattice	Percolation threshold p_{c0}
Honeycomb	0.6962
Square	0.5928
Triangular	0.5000
Diamond	0.4280
Simple cubic	0.3117

Percolation theory (Stauffer 1985) only really considered cases where each points was statistically independent of all others, whereas in the contact of rough surfaces, there is a certain correlation between points. However, we expect that this may not affect the principle conclusions. That is that there would be a critical value of the proportion of points in contact and that all maps below that value would leak and all those above it would form a seal. This is the motivation for the simulation analysis of leakage of static sealed joints.

CHAPTER 7.

7.3 Simulation Analysis of Leakage of Static Sealed Joints

7.3.1 Simulation Model of Static Sealed Joints

The simulation model for static sealed joints is shown in Figure 7.2, considering a sealed joint with base area $L_x L_y$. Assume $L_x L_y$ is large enough to include a large number of asperities and to be representative of the surfaces but small enough to be handled economically in the computer. The simulation model has been used by Pair and Cheng (1978) for determining effects of three-dimensional roughness on the pressure flow.

Some other assumptions used to develop a simulation method for the leakage analysis of static sealed joints are presented:

- (1) Leakage occurs by fluid flow at the interface and not through the material and the seal formed by the contact between surfaces is defined by zero-leakage;
- (2) The sealed surfaces are geometrically perfect on the large scale: the surfaces are nominally flat and the surface planes in contact are parallel; the only divergences from the plane are superficial roughness with Gaussian statistics;
- (3) The material properties are uniform throughout the material;

CHAPTER 7.

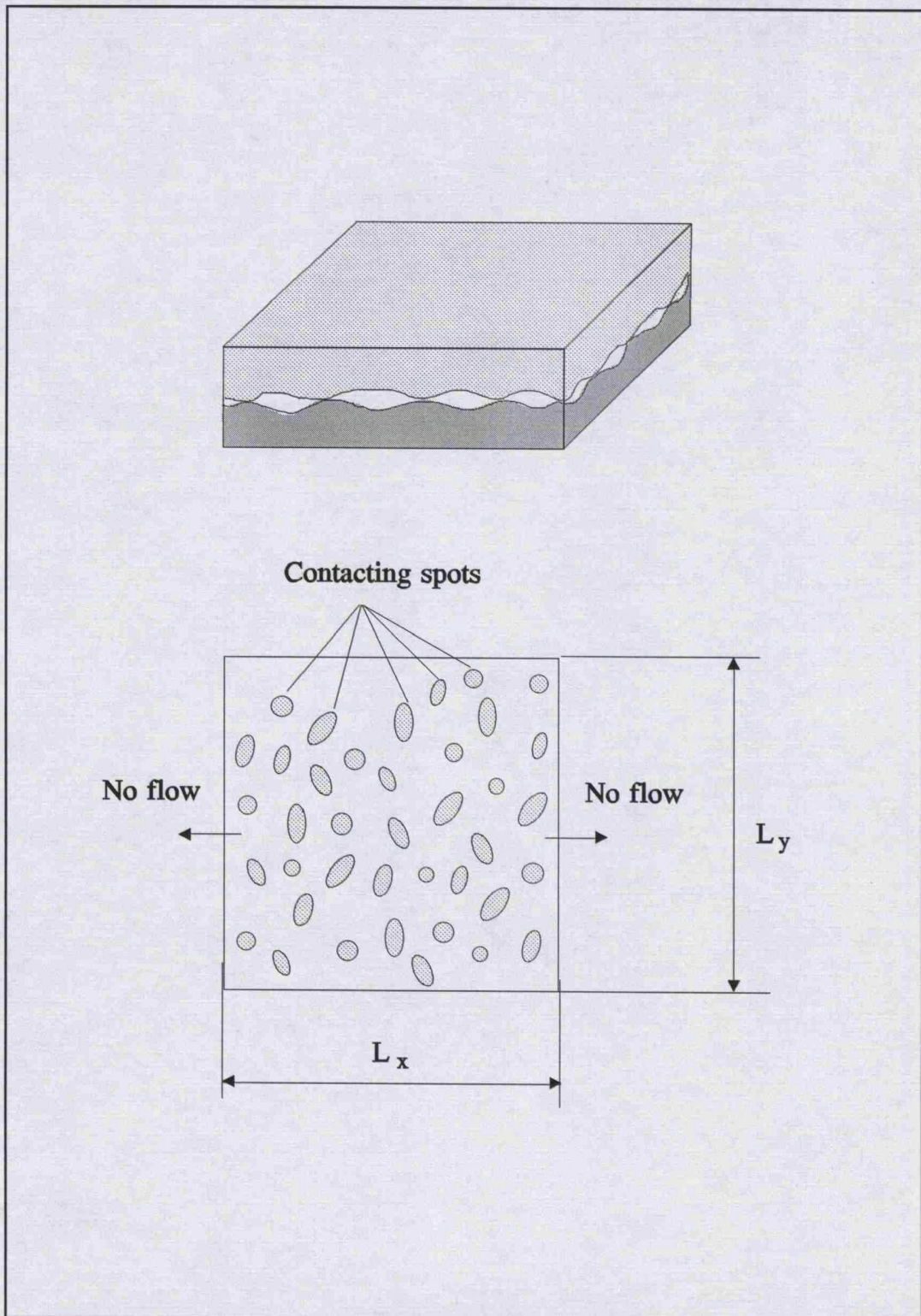


Figure 7.2 Simulation model for static sealed joints

CHAPTER 7.

- (4) The applied load acted the sealed surfaces will not vary with time.

The zero-leakage means that leakage paths at the interface are effectively blocked and no fluid appears on the outer edge of the sealing surfaces over a prescribed period of time. The use of a zero-leakage criterion in conjunction with a map of discrete contacting and non-contacting points provides a practicable means of looking at a sealing problem. It only guarantees that leakage paths, if they exist, are smaller than a certain size, but it make it is possible to use the simulated method to analyze the leakage of static sealed joints.

A simulation of the fluid flow in a leaking joint would be more complex and is beyond the scope of this thesis and would still be limited by hand to be conducted in terms of a finite set of points or elements.

7.3.2 Production of Contact Map

When two surfaces are in contact, the roughness provides a path through which fluid flow may take place. The leakage route is inevitably affected by the way in which the surface roughness asperities are deformed when the two surfaces are loaded together. The contact analysis of rough surfaces can provide important information about the contact situation at the interface.

CHAPTER 7.

In order to make use of the advantage of the numerical simulation, the sealed surfaces are discretized into a number of area elements $\Delta x \Delta y$, whose centres are the sampling points in the numerical simulation of random rough surfaces and the numerical contact model of rough surfaces. Therefore the surfaces and their contacts can be modelled by a series of discrete points and a chain of such points in contact implies a seal. The leakage path is a passage such that non-contacting points connect the inside of sealing surface to outside. The information about the contact situation at the interface is recorded in a map consisting of contacting and non-contacting points. Such a map is called a contact map. The three-dimensional numerical model for the elastic contact of rough surfaces presented in Chapter 6 can produce such contact maps. According to the condition of boundary contact defined by Equation (4.13), the contact points correspond to those points having non-zero contact pressure, whereas the non-contacting points correspond to those points having zero contact pressure. Therefore, the simulated result of the distribution of contact pressure really implies a contact map.

For a given applied load and rough surface characteristics, the contact map obtained is unique to the real topography, which can vary from surface to surface. Therefore the leakage analysis based on the contact maps can reveal the random properties of rough surfaces and model the possible variation between rough surfaces which have the same statistical properties, but a different detailed form. Furthermore, the production of contact maps make it is possible to analyze leakage of static sealed joints using the leakage paths instead of the leakage clearance.

CHAPTER 7.

7.3.3 Computer Check of Leakage Paths

The contact map itself, however, does not provide the readily information whether leakage occurs or not on it. Therefore, for a given contact map, the leakage paths should be checked on these assumptions:

- (1) Fluid flow between two individual elements of the contact map is only in the row or column direction and not across a diagonal;
- (2) A flow path consists of non-contacting points that are adjacent;
- (3) A leakage path is one that connects the top of the contact map to the bottom;
- (4) A blocked flow path contributes nothing to the fluid leakage.

After the production of a contact map, we may analyze it by eye or by computer. If trying to do this visually, we will presumably make some errors in a larger contact map. Therefore, we expect that a computer could do this for us, which is a effective and accurate method. We now explain how to teach the computer to do that for us.

The computer algorithm to determine whether leakage paths exist or not on a given contact map has been devised by the author. The algorithm is that all non-contacting points within the same flow path are given the same label, and different labels are given to non-contacting points belonging to different

CHAPTER 7.

flow paths. Then the flow paths connect throughout the sealing surface if the same label appears in both the first and the last row, and fluid flow may take place. Therefore the joint is considered as leaking. The analysis is carried out row by row, and only two adjacent rows, i.e i th and $(i+1)$ th, need to be written in the program for each time analysis. The i th row is one at which the leakage path has been checked and that all contact information obtained from the previous analysis is recorded in it. The information is how many flow paths appearing in the first row have reached at the current row and if there is not one, which means that the leakage paths have been effectively blocked and the check should be stopped; otherwise the leakage may take place and further check should be done. Then the $(i+1)$ th row is written in the program as a new row to be analyzed. The procedure continues until all rows have been checked.

The advantage of the algorithm is that allows the simulation analysis of large contact maps without having to store the whole contact map. Thus computer memory can be saved so that larger systems can be simulated. The computer program based on the algorithm, called **CCLP**, has been written by the author in FORTRAN. The accuracy of the program is verified with manual solutions for artificial contact maps. Two simulated results of leakage paths are presented in Figure 7.3 for both contact maps having 20×20 sampling points and the contact ratio of 42%, where zero presents contact points while non-zero for non-contacting points. For this typical pattern of contact showed in Figure 7.3(a), since the number of leakage paths is zero, all leakage paths are blocked effectively, hence sealing has formed, while for the one shown in Figure 7.3(b), the number of leakage paths equals to 1, hence

CHAPTER 7.

leakage paths exist and sealing does not occur.

Row 1	1	2	0	0	5	0	0	8	0	10	0	0	0	0	0	16	17	18	0	0
Row 2	1	2	3	0	5	6	7	8	0	0	11	12	13	14	15	16	0	18	19	20
Row 3	1	2	0	4	0	0	0	8	9	10	0	12	13	14	0	0	17	0	0	20
Row 4	1	2	0	4	0	6	7	8	0	10	11	12	13	0	0	16	17	0	19	0
Row 5	0	2	0	4	5	6	7	8	9	10	0	12	13	0	15	16	17	0	0	20
Row 6	0	0	0	4	5	6	0	8	9	10	11	12	0	14	15	16	17	18	19	20
Row 7	1	2	0	0	5	0	7	8	9	10	11	0	0	14	15	16	0	18	19	20
Row 8	0	0	0	0	0	0	0	0	9	0	0	0	13	14	0	0	0	18	19	0
Row 9	1	2	0	4	5	6	7	8	9	10	11	12	13	14	15	16	17	18	19	20
Row 10	0	0	3	4	5	6	0	8	9	0	11	12	13	0	15	16	17	18	19	20
Row 11	1	2	3	4	5	0	7	8	9	10	11	12	13	14	0	16	0	18	19	20
Row 12	1	0	3	4	0	6	0	8	0	10	0	0	0	0	0	16	17	0	0	20
Row 13	1	0	3	0	0	6	0	0	9	0	0	0	0	0	0	16	0	0	0	0
Row 14	1	0	3	4	0	6	0	8	9	10	0	12	13	0	0	16	17	18	0	20
Row 15	1	0	3	0	5	6	0	8	9	10	11	0	13	14	15	16	17	18	19	20
Row 16	1	2	3	4	0	6	7	8	9	0	11	12	13	0	15	0	17	0	0	20
Row 17	1	0	0	0	0	0	0	0	0	0	0	0	13	0	0	0	0	0	19	20
Row 18	1	2	3	4	5	0	7	0	9	0	0	0	0	14	15	0	0	18	19	20
Row 19	0	2	0	0	5	6	7	0	9	0	0	0	13	14	0	0	0	18	0	20
Row 20	0	0	3	4	0	0	0	0	9	0	0	0	0	0	0	16	0	0	0	0

Result	0	0	0	0	0	0	0	0	0	0	0	0	0	0	0	0	0	0	0	0
NUMBER OF LEAKAGE PATHS = 0 AT ITERATION 1																				

Figure 7.3 Results of computer check of leakage paths for typical patterns of contact, where the contact map have 20×20 sampling points and the contact ratio is 42%.

CHAPTER 7.

Row 1	0	2	3	4	0	0	7	8	9	0	11	12	13	14	15	16	0	18	19	20
Row 2	1	2	0	4	5	0	7	8	9	10	11	12	13	14	15	16	17	18	19	20
Row 3	1	2	0	0	0	0	7	8	9	0	0	0	13	14	15	16	17	0	0	20
Row 4	0	0	0	0	0	0	7	0	9	10	0	0	0	14	15	0	17	0	0	0
Row 5	0	2	3	4	5	6	0	8	0	0	11	12	0	0	15	16	0	0	0	20
Row 6	0	0	0	4	0	0	7	0	0	0	0	0	0	0	16	17	0	0	0	0
Row 7	1	2	3	4	0	6	0	8	9	0	11	12	13	14	15	16	0	18	19	20
Row 8	0	2	0	0	0	0	0	0	0	0	0	0	0	14	15	0	17	18	19	20
Row 9	1	2	3	4	0	6	0	8	9	10	0	12	13	14	15	0	17	0	19	20
Row 10	1	0	0	4	0	0	0	8	0	10	0	12	0	0	0	16	0	0	0	0
Row 11	1	0	3	0	0	6	7	8	9	0	11	12	0	0	15	16	0	18	19	20
Row 12	1	2	3	4	5	6	7	0	9	10	11	12	13	14	15	16	17	18	19	20
Row 13	1	2	3	4	5	6	7	8	9	10	11	12	13	14	15	0	17	18	19	20
Row 14	1	0	0	0	0	0	7	8	9	0	0	12	13	0	15	0	0	0	19	20
Row 15	1	0	3	4	5	0	7	0	9	10	11	0	0	0	15	0	0	18	19	0
Row 16	1	0	3	0	0	6	0	0	0	0	0	12	0	14	0	16	17	18	19	20
Row 17	1	0	3	0	0	0	7	8	0	0	11	12	0	0	15	0	0	18	0	0
Row 18	1	2	3	4	5	6	7	8	9	10	11	12	13	14	15	16	17	18	19	20
Row 19	1	0	0	0	0	6	0	8	0	0	0	12	0	14	15	0	17	0	0	20
Row 20	0	2	3	0	0	6	7	0	0	0	0	12	13	0	0	0	0	18	0	0

Result	0	0	0	0	0	6	7	0	0	0	0	12	13	0	0	0	0	0	0	0
NUMBER OF LEAKAGE PATHS = 1 AT ITERATION 43																				

Figure 7.3 (continued) Results of computer check of leakage paths for typical patterns of contact, where the contact map have 20 × 20 sampling points and the contact ratio is 42%.

CHAPTER 7.

Therefore, identifying a joint for which sealing occurs or not in the condition of zero-leakage aims to check if the leakage paths at the interface have been effectively blocked. The computer check of leakage paths along with the numerical simulation of random rough surfaces and the numerical contact model of rough surfaces make it is possible to develop a simulation method for the leakage analysis of static seal joints. Figure 7.4 shows the simulation procedure for the leakage analysis of static sealed joints.

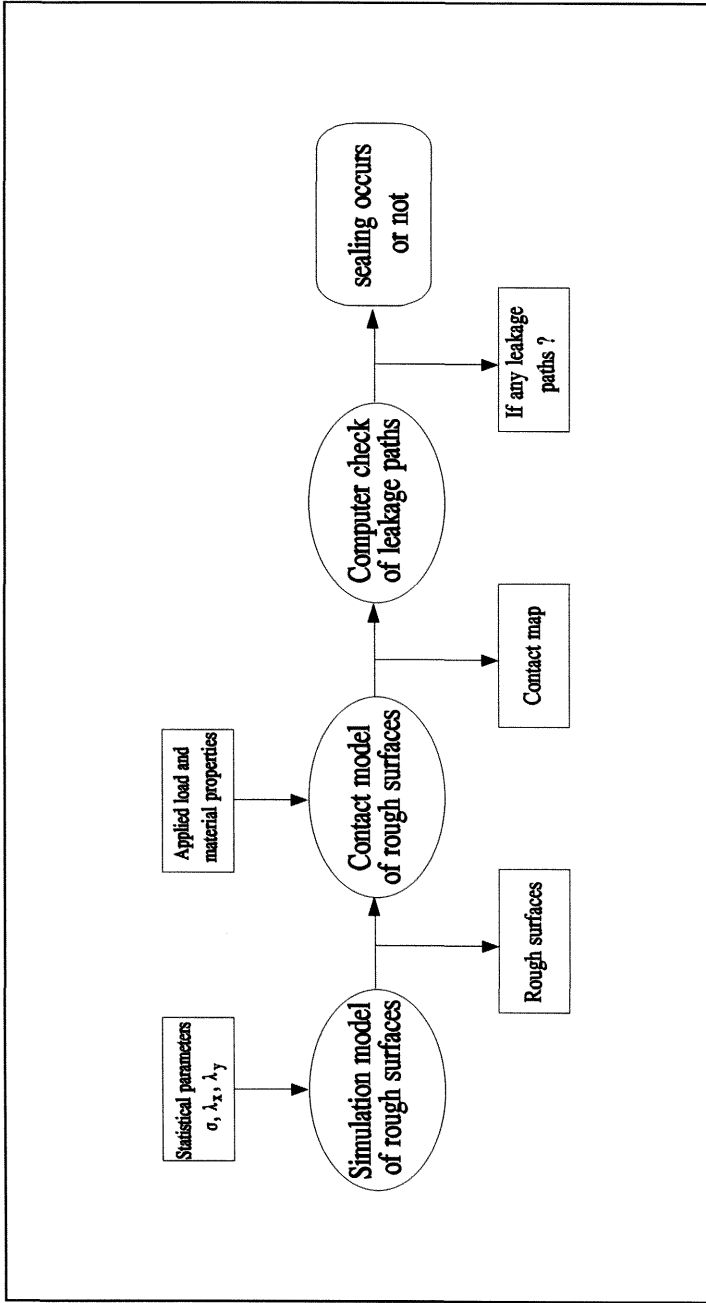


Figure 7.4 Simulation procedure of leakage analysis of static sealed joints

CHAPTER 7.

7.4 Prediction of Leakage and Sealing Probability

7.4.1 Simulation Procedure of Prediction of Leakage Probability

As can be seen from the numerical simulation of random rough surfaces, for each set of values of RMS height σ and correlation length λ^* , there are an infinite number of possible different surfaces, which demonstrates the characteristics of random surfaces. The random characteristics result that for same sealed joints under identical operating conditions, some may leak while some not. Because of this, it is appropriate to apply statistical concepts in discussing seal reliability. The following two statistics have been applied to the reliability analysis of static sealed joints; they are the leakage probability P_L and the sealing probability P_S .

The simulation analysis of leakage, as described in Figure 7.4, makes it possible to predict the leakage probability of static sealed joints. Individual simulation analysis of leakage will show a typical pattern of contact at which sealing occurs or not. Large number of repeated simulation of the same problem will give the leakage probability P_L for such a seal under the given applied load. Thus, the leakage probability of static sealed joints is defined by:

$$P_L = \frac{n_L}{n_S} \quad (7.1)$$

CHAPTER 7.

where n_s is a population and n_L is the number of failure seals in a population. (Note, "population" here is used in the statistical sense of a number of nominally identical sealed joints subjected to identical operating conditions.)

The sealing probability P_s is related to the leakage probability P_L by:

$$P_s = 1 - P_L \quad (7.2)$$

Figure 7.5 shows the simulation procedure for the prediction of leakage probability of static sealed joints.

CHAPTER 7.

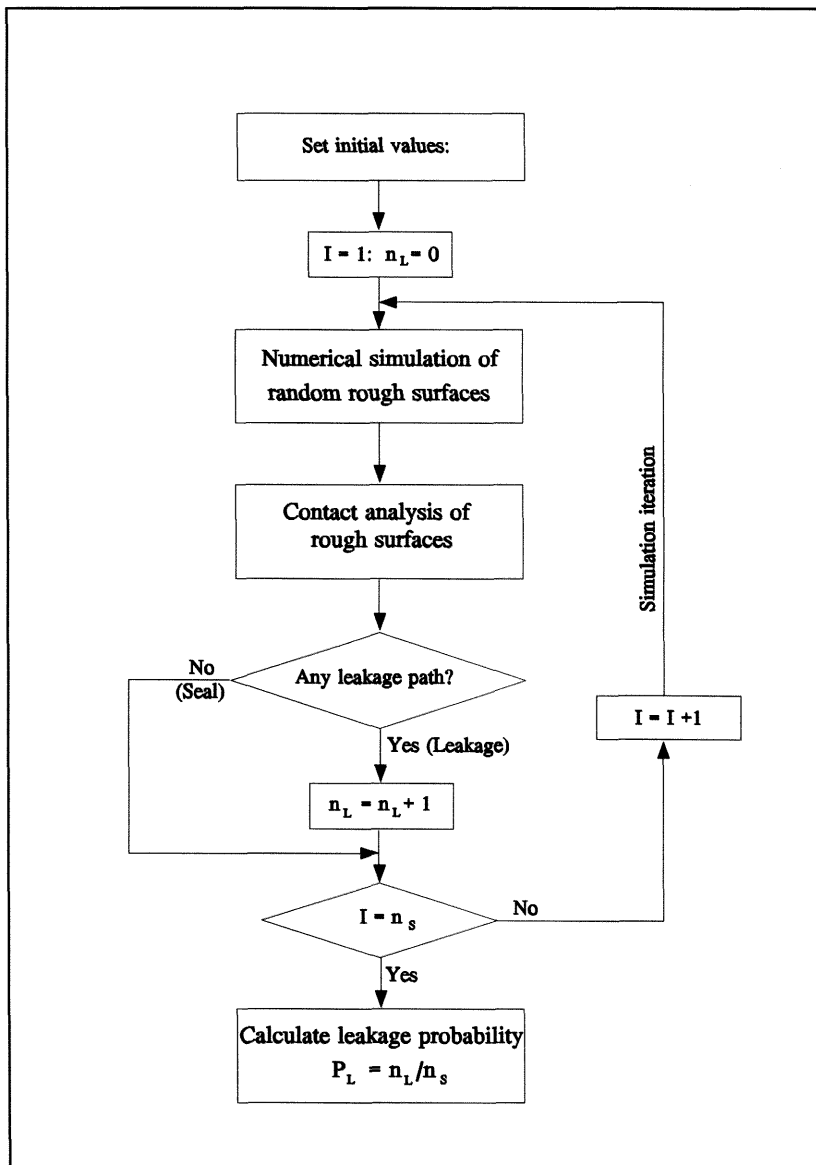


Figure 7.5 Simulation procedure for the prediction of leakage probability

CHAPTER 7.

7.4.2 Leakage Probability-v-Load Relationship

To prevent leakage of static sealed joints, a certain level of contact stress must be maintained between two sealed surfaces. Therefore, the relationship between the leakage probability and the applied load is of great general interest to the designers of static sealed joints. With only a few minor modifications to the original simulation procedure of prediction of leakage probability, as show in Figure 7.5, we can predict the variation of leakage probability as a function of applied load.

A dimensionless contact load \bar{P} including the face contact pressure and material properties can be obtained by normalizing the applied load in the form:

$$\bar{P} = \frac{P_a}{A_n E'} \quad (7.3)$$

Where A_n is the nominal contact area, which is much larger than the real contact area, E' is the equivalent elasticity modulus given by Equation (4.1) and P_a is the applied load. In the following analysis, we will study the effect of the dimensionless contact load on the leaking probability and the sealing reliability of static sealed joints. The numerical contact model of rough surfaces used to produce the contact map in analysis is three-dimensional model and the number of simulation iteration is set to be 100.

CHAPTER 7.

7.4.2.1 Effect of Rough Surfaces

Random isotropic rough surfaces with Gaussian statistics, as considered in this section, may be characterized by two statistical parameters: the RMS height, σ , and the correlation length, λ^* . The first parameter is a measure of the deviation of the surface from smooth, the correlation length measures the rate of change of roughness along the surface. From the contact analysis of rough surfaces in Chapter 6, the contact state is related to the two parameters. In practice, the two parameters themselves, however, will affect the contact properties and hence sealing performance. In the following, we will study how variations in either the RMS height or in the correlation lengths affect the leakage probability and hence reliability of static sealed joints.

The isotropic random rough surfaces used in the analysis are generated by using the computer simulation program NSRRS to have 50×50 sampling points with the sampling interval of $\Delta x = \Delta y = \lambda^*$, which has been used in the leakage analysis by Thomas 1973. The effect of RMS height σ and correlation length λ^* on the leakage probability has been studied for values of RMS height $\sigma = 0.1, 0.3$ and $0.5 \mu\text{m}$ and for different values of correlation lengths $\lambda^* = 20, 30, 40$ and $50 \mu\text{m}$. The data results representing leakage probability-v-applied load relationship have also been tabulated in Table B.1 ~ Table B.4 in Appendix C.

Figure 7.6 presents the predicted variation of leakage probability as a function of dimensionless contact load, showing the effect of RMS height σ , where the set of rough surfaces are generated by simulation for the condition:

CHAPTER 7.

three values of RMS height: $\sigma = 0.1, 0.3$ and $0.5 \mu\text{m}$ at the correlation length $\lambda^* = 20 \mu\text{m}$. The sealing probability can be obtained by the relationship defined in Equation (7.2). Figure 7.7 shows the variation of sealing probability as a function of load for the same surface parameters as Figure 7.6. As can be seen from Figure 7.6 and Figure 7.7, for a given leakage probability or sealing probability, the required load will increase as the RMS height increases. In other words, the leakage probability increases or the sealing probability decreases as the RMS height increases at a given load.

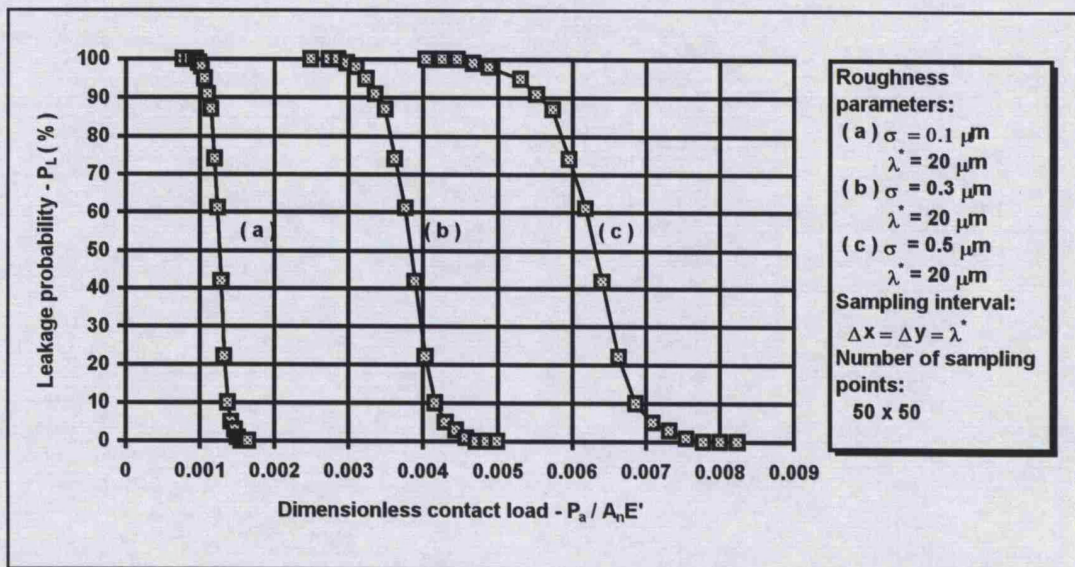


Figure 7.6 Predicted variation of leakage probability as a function of load, showing the effect of RMS height σ

CHAPTER 7.

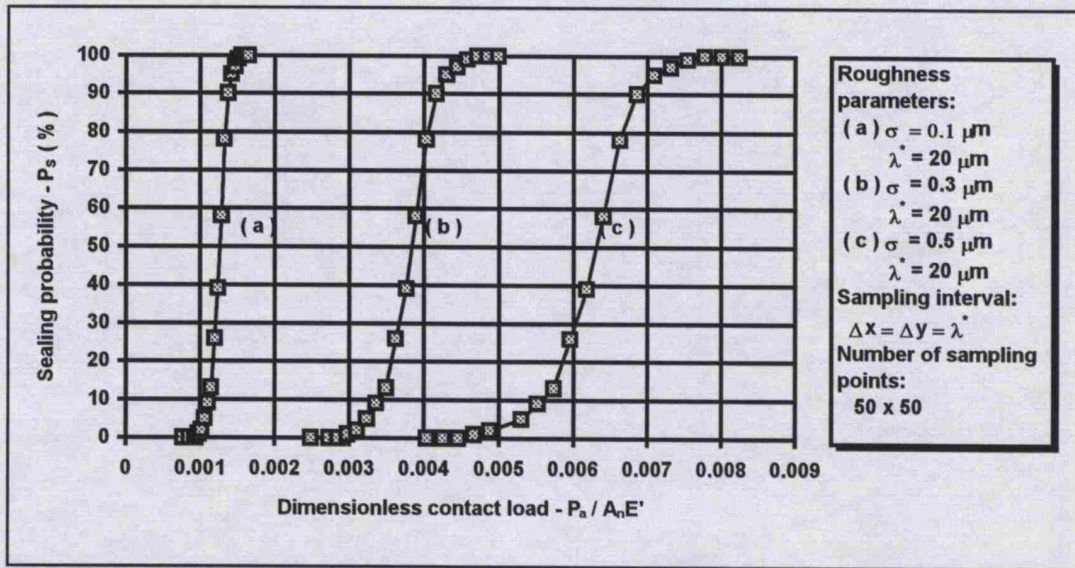


Figure 7.7 Predicted variation of sealing probability as a function of load, showing the effect of RMS height σ

A simple model may illuminate the problem. For contact between a plane and a peak with spherical symmetry, Hertzian theory gives the load at each contact point as (Greenwood and Williamson 1966):

$$P_i = \frac{4}{3} E' \delta^{3/2} \beta^{1/2} \quad (7.4)$$

where β is the radius of curvature of the peak which is contacting and δ is the indentation of the peak. As the RMS height is increased, for a fixed value of the correlation length, the radius of curvature of any peak will decrease. However, the height of that peak will increase, leading to a greater absolute indentation δ , for a given value of the mean separation. Each contacting peak will therefore be able to support a greater load, (see Equation (7.4)) and will suffer greater indentation before adjacent peaks come into

CHAPTER 7.

contact. The mean surface separation therefore increases, contact occurs at fewer points and the real contact area is reduced as the RMS height increases, hence the leakage probability will increase or the sealing probability will decrease.

Furthermore, three distinct regions are apparent in Figure 7.6 and Figure 7.7. In the middle portion of simulated results, the probability variation is an approximated linearity and is very sensitive to small changes in load; while at two ends, the probability is insensitive to variation in the load, although there is an approximated linearity between normal load and real contact area obtained in Chapter 6. No straightforward explanation were found.

To study the effect of correlation length on sealing performance, the RMS height is kept constant but the correlation length will vary. Figure 7.8 and Figure 7.9 summarize the results, representing the predicted variation of leakage probability and sealing probability as a function of dimensionless contact load for different values of correlation length $\lambda^* = 20, 30$ and $40 \mu\text{m}$ at the values of RMS height $\sigma = 0.5 \mu\text{m}$.

CHAPTER 7.

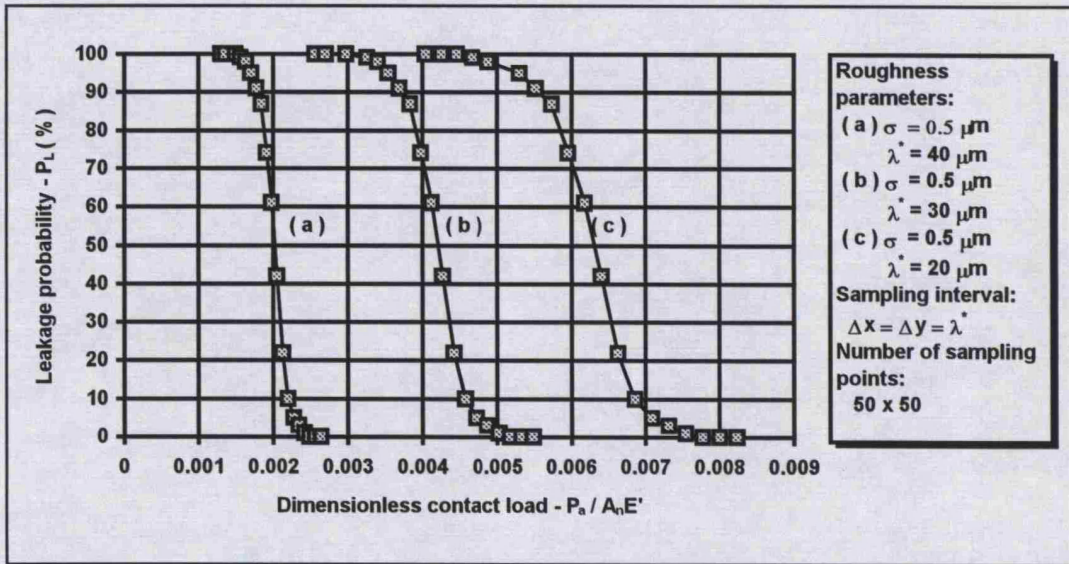


Figure 7.8 Predicted variation of leakage probability as a function of load, showing the effect of correlation length λ^*

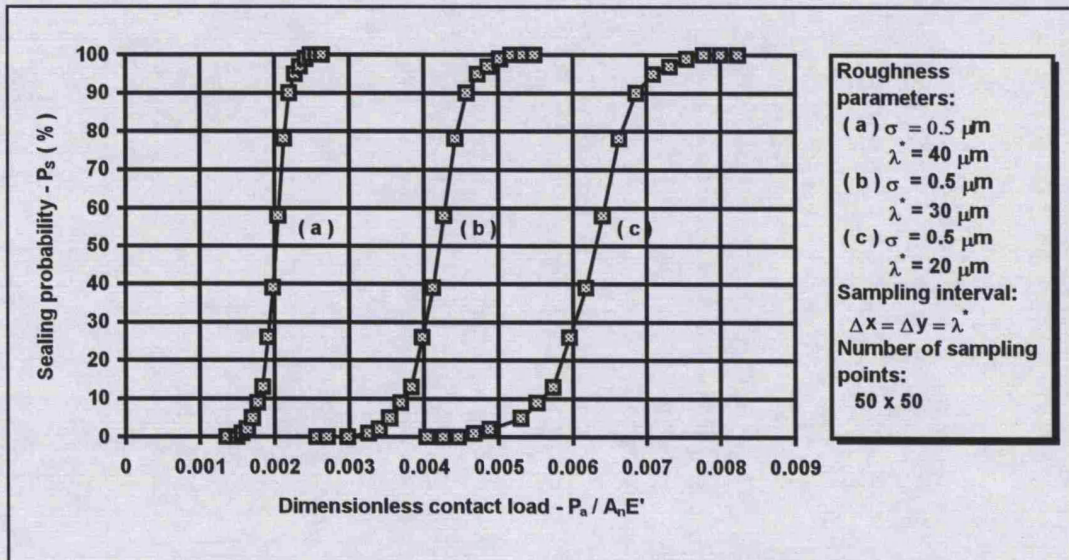


Figure 7.9 Predicted variation of sealing probability as a function of load, showing the effect of correlation length λ^*

CHAPTER 7.

Results show that for a given leakage probability or sealing probability, the required load will decrease as the correlation length increases, which means that for a given load the leakage probability decreases with increasing correlation length, whereas the sealing probability increases. In other words, the longer the main structure of a surface, the more easily it will deform elastically. At first sight this seems contrary to common experience. Surely an asperity of large radius of curvature will be more resistant to deformation than a smaller one? A simple model presented by Thomas (1973) may illuminate the problem. Consider a rectangular array of asperities of equal radius of curvature β and equal height h , whose centres are separated by a distance λ^* , as shown in Figure 7.10. By simple geometry, $\beta \propto \lambda^{*2}$ if $h \ll \lambda^*$. Also, for a given nominal pressure the load P_a per asperity is proportional to λ^{*2} . If the asperities deform elastically against a plane surface, the Hertzian equation relates P_a , β and the mean plane separation h by:

$$P_a \propto (-h)^{3/2} \beta^{1/2} \quad (7.5)$$

whence

$$-h \propto \lambda^{*2/3}$$

i.e. as λ^* increases the surfaces come closer together; in other words, the increase in strength of individually asperities with their size is more than offset by the decrease in their number.

CHAPTER 7.

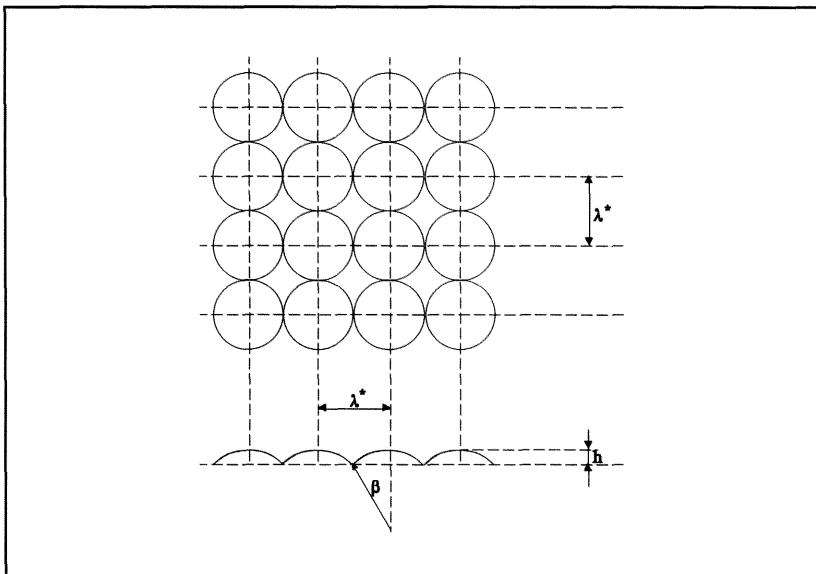


Figure 7.10 Surface model to show relation separation and correlation length at constant normal stress

7.4.2.2 Effect of Simulation Parameters

As can be seen from the analysis above, the variation of leakage probability as a function of load is predicted by numerical simulation based on finite contact maps. Changing the sampling interval and number of sampling points would affect the size of contact map, hence the predicted results of leakage probability. In the following, the effect of sampling interval and number of sampling points on the relationship between leakage probability and load are studied.

CHAPTER 7.

7.4.2.2.1 Effect of Sampling Interval

In the numerical simulation of random rough surfaces, the sampling interval will vary as a result of choosing different values of n_x and n_y , defined as in Equation (3.13). The sampling interval would decrease with increasing values of n_x and n_y , hence more fine structure of roughness can be revealed. Furthermore, the correlation degree of the surface heights at neighbouring grid points is related to the sampling interval. As can be seen from Figure 3.1, the correlation of the surface heights at neighbouring grid points increases as the sampling interval decreases. Choosing $n_x = n_y = 1$, the sampling interval is equal to the correlation length and the surface heights at neighbouring grid points have a correlation of only 0.1; while choosing $n_x = n_y = 2$, the sampling interval is equal to the half of the correlation length and the surface heights at neighbouring grid points have higher correlation.

The effect of the sampling interval on the leakage probability -v- applied load relationship has been investigated, where the random rough surfaces used in comparison are generated for two sets of sampling intervals: $n_x = n_y = 1$, i.e the sampling interval $\Delta x = \Delta y = \lambda^*$ and $n_x = n_y = 2$, i.e the sampling interval $\Delta x = \Delta y = 1/2\lambda^*$. The simulated results of leakage probability and sealing probability have been presented in Figure 7.11 and Figure 7.12 for the following condition: $\sigma = 0.3 \mu\text{m}$, $\lambda^* = 40 \mu\text{m}$ and 50×50 sampling points. As can be seen from Figure 7.11 and Figure 7.12, the variation of leakage probability or sealing probability with the load is sensitive to varying the sampling interval. There is one apparent explanation at least

CHAPTER 7.

for why it is the case. This reason is that the value of P_a/A_c would increase as the sampling interval decreases, which means that for a given load the predicted area of real contact would decrease with decreasing the sampling interval, thus the leakage paths are not easy blocked by the contacting asperities, hence the probability of leakage would increase.

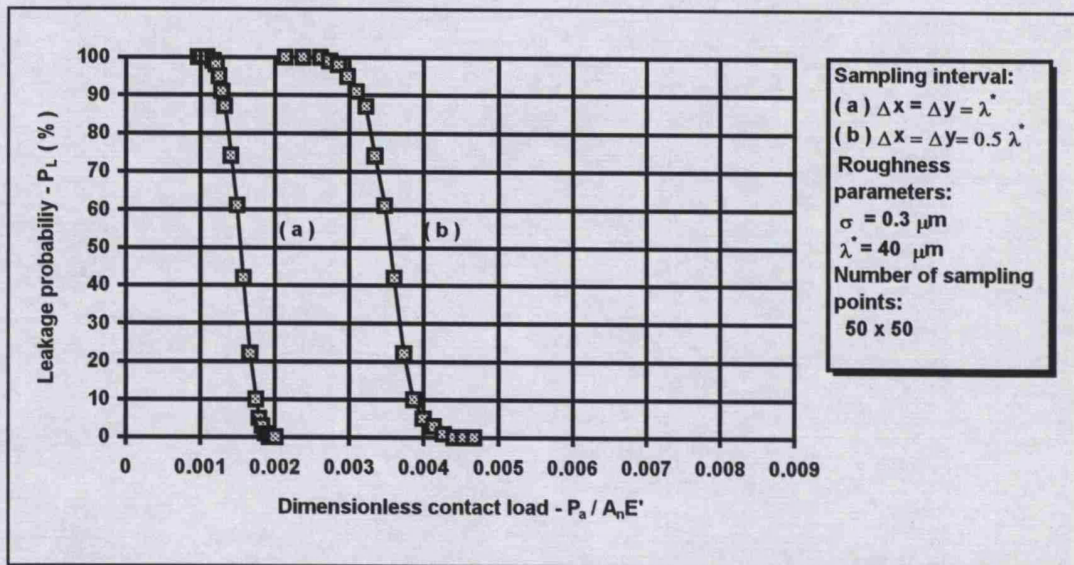


Figure 7.11 Predicted variation of leakage probability as a function of load, showing the effect of sampling interval

CHAPTER 7.

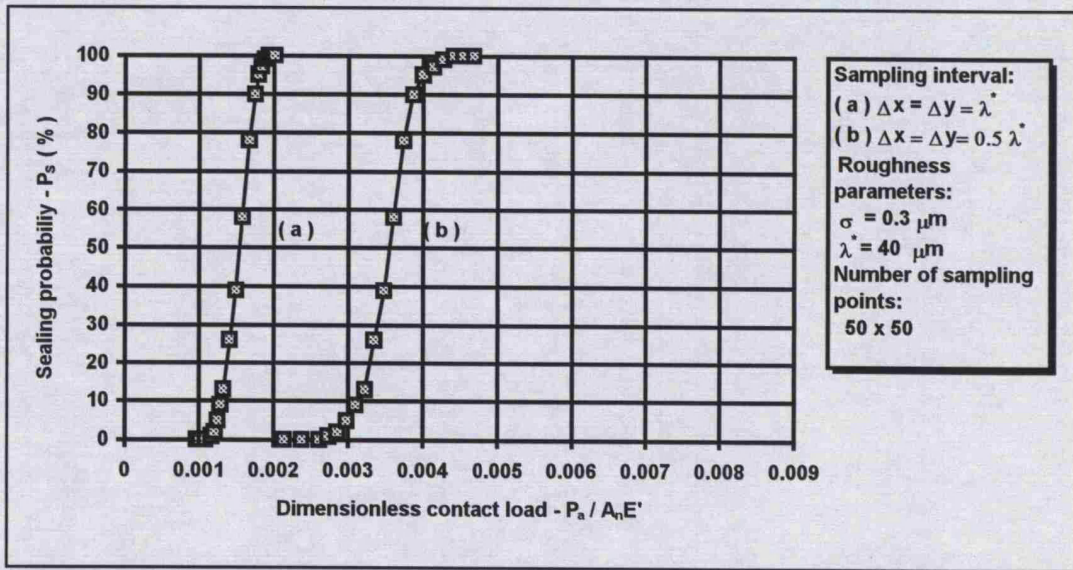


Figure 7.12 Predicted variation of sealing probability as a function of load, showing the effect of sampling interval

7.4.2.2.2 Effect of Number of Sampling Points

The simulation analysis of leakage probability above is based on the contact maps with a finite number of sampling points. Therefore, it is important to see the effect of number of sampling points in contact maps on the variation of leakage probability. The computer simulated rough surfaces used in the comparison are for the following condition: $\sigma = 0.5 \mu\text{m}$, $\lambda^* = 20 \mu\text{m}$ and $\Delta x = \Delta y = \lambda^*$, i.e. $n_x = n_y = 1$. Three sets of number of sampling points used are: 50×50 , 30×30 and 20×20 . The simulated results of leakage probability and sealing probability have been presented in Figure 7.13 and Figure 7.14. As can be seen from Figure 7.13 and Figure 7.14, the predicted variation of leakage probability and sealing probability with load is relative to

CHAPTER 7.

the number of sampling points in contact map, and the curves of probability would become slightly steeper as the number of sampling points is increased, which agrees with the trend observe from the percolation theory. And the curves of probability would be smoother as the number of sampling points increases.

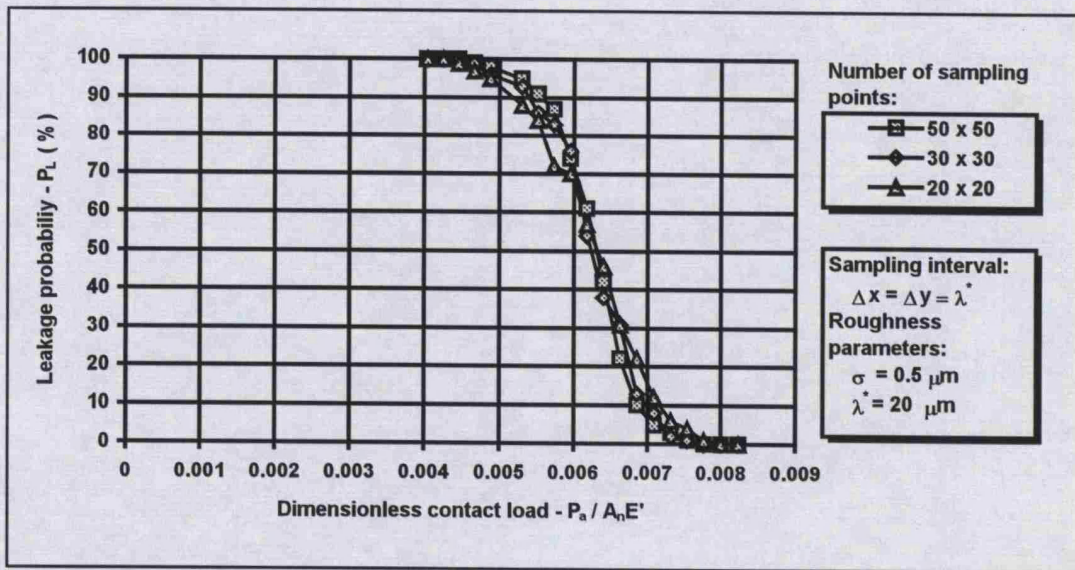


Figure 7.13 Predicted variation of leakage probability as a function of load, showing the effect of number of sampling points

CHAPTER 7.

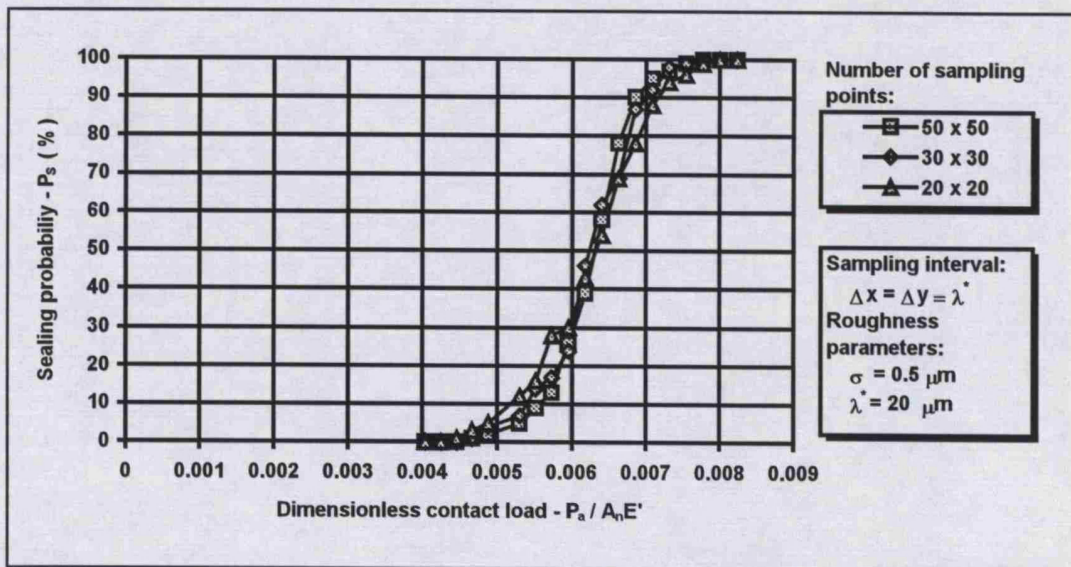


Figure 7.14 Predicted variation of sealing probability as a function of load, showing the effect of number of sampling points

7.5 Criteria for Identifying Sealing Reliability of Static Sealed Joints

7.5.1 Relationship between Sealing Reliability and Sealing Probability

To evaluate the effects of important parameters (i.e. surface characteristics, applied load and mechanical properties of the mating faces) on the sealing reliability, criteria for identifying the sealing reliability of static sealed joints should be obtained. As can be seen from the prediction of leakage probability of static sealed joints, the lower the expected leakage

CHAPTER 7.

probability, the larger the required applied load and the smoother the required sealed surfaces. The lower the leakage probability the more reliable the sealed joints. Therefore the sealing probability or the leakage probability is an important influence factor in determining the criteria for identifying the sealing reliability of static sealed joints. It is important for the design of sealed joints to take account not only of the reliability of the seal, but also of the costs of joints etc..

The failure probability of 5%, 1% and 0% is used to identifying the reliability of sealed joints by Summers-Smith (1988). A 5% failure probability means that from a sample population of sealed joints, if there are only less than or equal to 5 percent sealed joints which leakage occurs the sealed joints are considered as reliability. Static sealed joints are widely used in many fields. Therefore, the value of failure probability will depend very much on the characteristics of the sealed product and the environment in which the sealed joints is operating. As a general rule it may be said that the value of failure probability should be as low as possible, for high technology applications, dangerous chemicals, nuclear radiation etc., because the failure of sealed joints applied in such environments may imply a dangerous accident.

CHAPTER 7.

7.5.2 Criteria for Identifying Sealing Reliability of Static Sealed Joints with Isotropic Surfaces

What can be used for the criteria for identifying sealing reliability? From the introduction of percolation theory in Section 7.2, we know that there is the percolation threshold p_{c0} for infinite systems. If one knows the concentration of a system, one can predict whether percolation phenomena in the system occurs or not according to the condition: for all $p_c > p_{c0}$ percolating clusters are formed, whereas for all $p_c < p_{c0}$ no such a percolating cluster exists. In finite systems, there is not such a sharply defined threshold, which has been observed in the prediction of leakage probability above. However, we still expect to find a criteria used to identify the sealing reliability.

The contact map in the leakage analysis can be considered as a finite square lattice, as shown in Figure 7.1. Each square is either occupied by the non-contacting points or it is empty for all contacting points. Therefore, the proportion of non-contacting points on a contact map is equivalent to the concentration p_c defined in percolation theory by (Stauffer 1985). The contact area ratio equals numerically to $(1-p_c)$ and the leakage paths may be considered as the percolating clusters. From the leakage analysis above, we also observe that the leakage probability is relative to the real contact area; the larger the real contact area, the more easily the leakage paths at the interface are blocked, hence the leakage probability would decrease with increasing the real contact area. The following section discusses whether there is a consistent relationship between the contact area ratio and whether or not a seal occurs. If yes, then the contact area ratio may be used for the criteria to

CHAPTER 7.

identify the sealing reliability of static sealed joints.

Table 7.2 gives the values of average contact ratio for different values of sealing probability: $P_s = 95\%$, 99% and 100% , where the average contact area ratio is calculated by averaging the values over all these different sequences of leakage simulations at a given leakage probability. The data listed in Table 7.2 comes from the simulated results of leakage probability presented in Table B.1(a) ~ Table B.1(d), which shows the effect of roughness parameters on the average contact area ratio, where the rough surface are generated having the sampling points of 50×50 and the sampling interval of $\Delta x = \Delta y = \lambda^*$. As can be seen from Table 7.2, the difference among the average contact ratio for a given sealing probability P_s is surprisingly small. The mean values of average contact ratio at a given confidence level (i.e the sealing probability) are listed in Table 7.3 and the error of one standard deviation above and below the mean are calculated about $\pm 0.17\%$. Therefore, the results confirm that using the contact area ratio as the criteria for identifying the reliability of static sealed joints is reasonable.

CHAPTER 7.

Table 7.2 Average contact area ratio for different values of sealing probability, showing the effect of rough surfaces†

Roughness parameters (μm)	Average contact area ratio		
	$P_s = 95\%$	$P_s = 99\%$	$P_s = 100\%$
$\sigma = 0.1, \lambda^* = 20$	0.398	0.412	0.421
$\sigma = 0.3, \lambda^* = 20$	0.396	0.416	0.423
$\sigma = 0.5, \lambda^* = 20$	0.399	0.412	0.420
$\sigma = 0.1, \lambda^* = 30$	0.401	0.410	0.419
$\sigma = 0.3, \lambda^* = 30$	0.395	0.415	0.422
$\sigma = 0.5, \lambda^* = 30$	0.398	0.414	0.424
$\sigma = 0.1, \lambda^* = 40$	0.400	0.416	0.423
$\sigma = 0.3, \lambda^* = 40$	0.397	0.413	0.421
$\sigma = 0.5, \lambda^* = 40$	0.396	0.415	0.420
$\sigma = 0.1, \lambda^* = 50$	0.399	0.410	0.419
$\sigma = 0.3, \lambda^* = 50$	0.402	0.413	0.422
$\sigma = 0.5, \lambda^* = 50$	0.397	0.411	0.420

†where the rough surfaces are generated to have the sampling points of 50×50 and the sampling interval of $\Delta x = \Delta y = \lambda^*$.

CHAPTER 7.

Table 7.3 Contact ratio criteria for different values of sealing probability

Sealing probability P_s	Contact ratio criteria
95%	0.398
99%	0.413
100%	0.421

The effect of sampling interval on the average contact ratios has been investigated. The average contact ratios coming from the simulated results listed in Table B.2 are listed in Table 7.4 for different values of sampling interval: $\Delta x = \Delta y = \lambda^*$ and $\Delta x = \Delta y = 1/2\lambda^*$, where the rough surfaces used are generated to have 50×50 sampling points and the roughness parameters of $\sigma = 0.3 \mu\text{m}$, $\lambda^* = 40 \mu\text{m}$. The simulated results show that for a given sealing probability the average contact ratios for smaller interval intervals are consistently higher than for larger sampling intervals. The results may present the trend that the average contact ratio would increase as the correlation degree of the surface heights increase, i.e the sampling interval decrease. However, the increment in contact area ratio with decreasing the sampling interval is slight although the predicted variation of leakage probability and sealing probability with load is very sensitive to the variation of the sampling interval. The errors of above the mean of the average contact ratio listed in Table 7.4 are about $\pm 4\%$. Since the leakage analysis is dealing with a surface discretized into a finite number of sampling points, the sampling interval should be chosen carefully so that any required degree of sealing can be predicted in practice.

CHAPTER 7.

Table 7.4 Average contact area ratio for different values of sealing probability, showing the effect of sampling interval†

Sampling interval	Average contact area ratio		
	$P_s = 95\%$	$P_s = 99\%$	$P_s = 100\%$
$\Delta x = \Delta y = \lambda^*$	0.397	0.413	0.421
$\Delta x = \Delta y = 1/2\lambda^*$	0.403	0.417	0.428

†where the rough surfaces are generated to have 50×50 sampling points and the roughness parameters of $\sigma = 0.3 \mu\text{m}$ and $\lambda^* = 40 \mu\text{m}$.

Stochastic contact models have demonstrated that the real area of contact is virtually independent of the nominal area of contact, for example Greenwood and Williamson (1966) show that the load-v-area results obtained for a nominal surface area of 10cm² are almost identical to those obtained for 1cm². Similar conclusions have been obtained in the numerical contact models by Webster (1986). What is the effect of changing the number of sampling points on the average area ratio related to the sealing probability? Table 7.5 presents the results showing the effect of number of sampling points on the average contact ratio for three sets of number of sampling points: 50×50, 30×30 and 20×20, where the rough surfaces are generated to have $\sigma = 0.3 \mu\text{m}$, $\lambda^* = 40 \mu\text{m}$ and $\Delta x = \Delta y = \lambda^*$. The simulated results show this trend that for a given sealing probability the contact maps with larger number of sampling points would predict a slight lower values of average contact ratio than ones with smaller ones. Comparing the value of average contact ratio 0.421 obtained from

CHAPTER 7.

finite system of 50×50 sampling points with the value of 0.4072 (i.e (1-0.5928) listed in Table 7.1) obtained from infinite system, we expect that it would not lead to larger predicted errors to apply the contact ratio criteria derived from finite number of sampling points for general sizes of static sealed joints.

Table 7.5 Average contact area ratio for different values of sealing probability, showing the effect of number of sampling points†

Number of sampling points	Average contact area ratio		
	$P_s = 95 \%$	$P_s = 99 \%$	$P_s = 100 \%$
50×50	0.399	0.412	0.420
30×30	0.402	0.411	0.421
20×20	0.405	0.422	0.438

†where the rough surfaces are generated to have the roughness parameters of $\sigma = 0.3 \mu\text{m}$ and $\lambda^* = 40 \mu\text{m}$ and the sampling interval of $\Delta x = \Delta y = \lambda^*$.

The analysis above shows that the reliability of static sealed joints depends very much on the contact area ratio, hence using the contact ratio criteria for identifying the reliability of static sealed joints is reasonable and does not lead to larger predicted errors.

CHAPTER 7.

7.5.3 Effect of Surface Anisotropy on Contact Ratio Criteria

For the static sealed joints with isotropic rough surfaces, the contact ratio criteria for identifying the sealing reliability has been obtained above. How about the effect of surface anisotropy on the contact ratio criteria?

The effect of surface anisotropy on the contact ratio criteria has been investigated, showing the effect of surface anisotropy on the sealing reliability. The anisotropic rough surfaces used are generated to have an infinite degree of anisotropy, i.e two-dimensional longitudinal ridges in the direction of fluid flow. Thus, identifying a joint with longitudinal ridges in the direction of fluid flow for which sealing occurs or not in the condition of zero-leakage is simplified to check if the mean gap at the interface equals to zero. The zero mean gap means that all leakage paths are blocked effectively and leakage cannot take place. Instead of three-dimensional numerical contact model for the isotropic rough surfaces in leakage simulation, the two-dimensional model is used to provide required information for surfaces with an infinite degree of anisotropy. The simulated results of average contact ratio obtained from the surfaces with an infinite degree of anisotropy for different values of sealing probability are presented in Table 7.6, where the rough surfaces are generated by numerical simulation to have 1000 sampling points and the sampling interval of $\Delta x = \lambda_x^*$.

CHAPTER 7.

Table 7.6 Average contact ratio obtained from surfaces with an infinite degree of anisotropy for different values of sealing probability

Roughness parameters (μm)	Average contact ratio		
	$P_s = 95 \%$	$P_s = 99 \%$	$P_s = 100 \%$
$\sigma = 0.2, \lambda_x^* = 20$	0.910	0.970	1.00
$\sigma = 0.3, \lambda_x^* = 30$	0.870	0.950	1.00

Comparing the values of average contact ratio in Table 7.6 for the anisotropic surfaces with ones in Table 7.2 for isotropic ones, the contact ratio criteria would increase apparently with the degree of surface anisotropy. Therefore, the surface anisotropy is an important parameter for the sealing performance, and to insure a good performance of a static sealed joint, it may be more important to control and inspect the surface-finish profile across the direction of fluid flow than in the direction of fluid flow.

Pair and Cheng (1978) has also demonstrated that the surface anisotropy would affect the pressure flow factor, which are obtained by comparing the average pressure flow in a rough bearing to that of a smooth bearing. The results show that for surfaces having larger correlation lengths in the direction of fluid flow, the pressure flow factor is greater than 1; while larger correlation lengths in the transverse direction of flow yield pressure flow factor smaller than 1. The flow factors are a function

CHAPTER 7.

of h/σ and would approach to 1 asymptotically as h/σ , where h is the nominal file thickness (compliance) defined as the distance between the mean planes of rough surfaces. But as h/σ decreases below 3, the flow factors become very sensitive to the directional properties of the surface roughness. When the flow factors is applied for estimating the mean flow in static sealed joints, the effect of surface anisotropy on the sealing performance have similar conclusion as same as leakage simulation.

CHAPTER 7.

7.6 Conclusion

The simulation model for the leakage analysis of static sealed joints has been developed based on the percolation theory in this chapter. It consists of the numerical simulation of random rough surfaces and the numerical elastic contact model of rough surfaces along with the computer check of leakage paths. By introducing the concept of contact map, we can describe the leakage phenomenon by leakage path instead of leakage clearance. The assumption of zero-leakage is reasonable in light of the complexity of leakage probability and also make it is possible to use the simulation method to analyze the leakage of static sealed joints. The leakage simulation model reveals the effect of random properties of rough surfaces on the sealing performance and makes it possible to apply the statistical concepts in discussing the sealing reliability of static sealed joints. By the simulation method, the result of variation in parameters that would affect the sealing performance can be studied without costly and length experimental efforts.

The relationship between the leakage probability and the applied load, which is of great general interest to the designers of static sealed joints, has been predicted by the leakage simulation model. The simulated results show that the variation of leakage probability with the load is nonlinear about $P_L < 10\%$, which will be preferred for practical design, although there is an approximate linearity between real contact area and applied load. The variation region of leakage probability depends very much on the roughness parameters: RMS height σ and correlation length λ^* . For a given leakage probability, the required load will increase as the value of RMS height σ increases or the

CHAPTER 7.

value of correlation length λ^* decrease. The influence of variables such as the sampling interval and the number of sampling points has been examined and the simulated results suggest that the sampling interval should be chosen carefully so as to predict the required degree of sealing and the smoother variation of probability is achieved with larger number of sampling points.

To evaluate the effects of important parameters on the sealing reliability, criteria for identifying the sealing reliability of static sealed joints have been set. The simulated results of leakage confirm that using the contact area ratio as the criteria for identifying the reliability of static sealed joints is reasonable and it would seem does not lead to larger prediction errors, although it is derived from certain simulation conditions such as the sampling interval of $\Delta x = \Delta y = \lambda^*$ and the finite size of contact maps. The values of contact ratio criteria depend on the confidence level of reliability prediction, the higher the confidence level, the larger the value of contact ratio. The effect of surface anisotropy on the sealing reliability has been investigated. Comparing the isotropic rough surfaces with the anisotropic ones, the contact ratio criteria would increase apparently. Therefore, the surface anisotropy is an important parameter for the sealing performance, and to insure a good performance of a static sealed joint, it may be more important to control and inspect the surface-finish profile across the direction of fluid flow than in the direction of fluid flow.

The contact ratio criterion provide a simple, inexpensive and useful tool to evaluate the effects of rough surfaces, material properties and applied load on the sealing reliability of static sealed joints. However, the drawback of

CHAPTER 7.

this method is the tedious effort required to obtain the contact ratio criteria through computer simulation. But once they are obtained correctly, they can be utilized to determine the effects of rough surfaces, material properties and applied load on the sealing reliability of static sealed joints.

In order to be of practical use, experimental work is required to evaluate its validity.

CHAPTER 8.

Summary and Further Work

8.1 Conclusion

8.1.1 Overall Conclusions

Leaking, friction and wear of seals are concerns for machine designers and user everywhere. Although perfect sealing may be the general aim, in practice for apparently identical seals in the same application, some may seal while some not. This is due to random variations between apparently identical situations. Therefore, the important of the reliability of sealed joints cannot be overemphasized.

Some previous of work has been done to consider the effect of rough surfaces on the sealing performance of static sealed joints (Rathbun 1963; Tsukizoe and Hisakado 1965; Mitchell and Rowe, 1967/1969; Thomas 1973; Shimomura, Hirabayshi and Nakajima 1989; Etsion and Front 1994), and several surface criteria have been proposed for the effectiveness of such seals. The mean gap or clearance between two sealed surfaces has been considered

CHAPTER 8.

as the main factor controlling the fluid flow, therefore, they have concentrated their attention on analysing the effect of surface roughness on the mean gap or clearance based on two-dimensional individual asperity models or stochastic contact models. All of these researches have achieved certain successes but also with some limitations on each of the solution methods.

The existing work deals only with average properties and cannot therefore model the possible variations of surface-related random phenomena. Up to now, there is not a paper in the published literature about the reliability analysis of static sealed joints. The lack of a reliable model that predicts the effects of influential parameters (i.e surface roughness, material properties and applied load) on the sealing reliability of static sealed joints necessitates the use of tests. This may be a tedious procedure and can not satisfy the need that market competition produces for faster product development.

All of these facts provide the motivation for the current research work. The computer simulation model for the leakage analysis of static sealed joints has been developed firstly based on the percolation theory in this thesis. The leakage simulation model consists of the numerical simulation model of random rough surfaces, the numerical elastic contact model of rough surfaces and the computer check of leakage paths, therefore the computer algorithms and programs corresponding to these have also been developed in FORTRAN. The features of the leakage simulation model can be concluded as follows:

- (1) It reveals the effect of random properties of rough surfaces on the sealing performance and makes it possible to apply statistical concepts

CHAPTER 8.

in discussing the sealing reliability of static sealed joints;

- (2) It provides much simpler and more economic tool for the statistical analysis of leakage by computer simulation than by experiments. Thus the result of variation in parameters that would affect the sealing performance can be studied without costly and length experimental efforts;
- (3) It makes it possible to describe the leakage phenomenon more accurately using the leakage path model instead of the clearance between surface centre-lines, because the pockets or blocked passages contribute nothing on the fluid leakage;
- (4) It eliminates the need for individual asperity model of rough surfaces, because the actual digitized surface profile is used directly, this is the most reasonable in light of the complexity of the leakage problem.

The relationship between the leakage probability and the applied load, which is of great general interest to the designers of static sealed joints, has been predicted by the leakage simulation model. The simulated results show that the variation of leakage probability with the load is nonlinear about $P_L < 10\%$, which will be preferred for practical design, although there is an approximate linearity between real contact area and applied load. The variation of leakage probability depends very much on the roughness parameters: RMS height σ and correlation length λ^* . For a given leakage probability, the required load will increase as the value of RMS height σ

CHAPTER 8.

increases or the value of correlation length λ^* decrease.

The contact ratio criteria which is relative to the confidence level of reliability prediction has been obtained. Although the criteria is derived from certain simulation conditions, the effects of simulation variables such as the sampling interval and the number of sampling points show that it would seem to show that it does not lead to larger prediction errors. The effect of surface anisotropy on the sealing reliability has been investigated. Comparing the isotropic rough surfaces with the anisotropic ones, the contact ratio criteria would increase apparently. Therefore, the surface anisotropy is an important parameter for the sealing performance, and to insure a good performance of a static sealed joint, it may be more important to control and inspect the surface-finish profile across the direction of fluid flow than in the direction of fluid flow.

The contact ratio criteria provide a simple, inexpensive and useful tools to evaluate the effects of rough surfaces, material properties and applied load on the sealing reliability of static sealed joints. However, the drawback of this method is the tedious effort required to obtain the contact ratio criteria through computer simulation. But once they are obtained correctly, they can be utilized to determine the effects of rough surfaces, material properties and applied load on the sealing reliability of static sealed joints.

In order to practical use, experimental work is required to evaluate its validity.

CHAPTER 8.

8.1.2 Numerical Simulation of Random Rough Surface

It is considered that numerical simulation of rough surfaces is an important tool for analysing the effecting of surface roughness on many engineering problems. However, the subject has received very little attention compared with the measurement of rough surfaces in the published literature so far. The only exception is Lai and Cheng's work (1985), which describes the computer simulation of rough surfaces having Gaussian height distribution and bilinear autocorrelation function. The bilinear autocorrelation is only an approximation to the exponential autocorrelation which is typical in many applications. By introducing an autocorrelation function matrix in Chapter 3, the simulation algorithm can, in principle, be extended to deal with the general form autocorrelation function.

The numerical simulation algorithms for randomly generating Gaussian surfaces with predetermined statistical parameters (i.e RMS height σ and correlation length λ) has been devised and the computer program called NSRRS in FORTRAN has been developed in Chapter 3. The numerical simulation model has been verified through a series of comparisons. The close agreement between the theory and simulation validates the use of this procedure for numerical simulation of random surfaces.

Randomly generating rough surfaces by numerical simulation is much simpler and more economic than measurement. The simulation model can substitute surface measurements by artificially creating rough surfaces, so that the result of variation in surface parameters (i.e σ and λ) that affect the seal

CHAPTER 8.

reliability can be studied without costly and length experimental efforts. For each set of statistical parameters, many surface forms can be obtained by only changing the seed values of random number generators. It reveals the random properties of rough surfaces and also facilitates the simulation of surface-related random phenomena.

8.1.3 Numerical Contact Models of Rough Surfaces

Stochastic models for the contact of rough surfaces are numerous, they have been refined over many years. However, these models yield important results about the average properties of the contact of rough surfaces, but the information about the real pressure distribution and the deformed shape is lost due to the type of approach adopted, which are important results for the simulation analysis of leakage. Numerical contact models use the actual digitized surface profiles and can provide important information about the contact situation at the interface. Therefore, the numerical contact model provides a suitable model for simulation analysis of leakage. Some numerical models have been developed to deal with the contact of two elastic or three elastic bodies by Webster and Sayles (1986), Xian and Zheng (1991), Lee and Cheng (1992). The numerical contact models have achieved certain successes in some applications. Applying these existing numerical models to the leakage simulation analysis, the main problem is the numerical solution method. The numerical solution method used widely in the numerical contact models of rough surfaces is one called as Matrix Inversion Method described by Johnson (1985). Although Matrix Inversion method is straight forward and simple for

CHAPTER 8.

the numerical solution in some applications, the iteration to obtain a fully consistent solution and the distortion of solutions for larger systems limit this approach to be unacceptable in simulation analysis of leakage, where the accuracy of solution and the speed of solution procedure are concerns for us. Clearly it might be advantageous to use an alternative method of solution.

A powerful alternative method of numerical solution is called as variational method based on variational principles (Johnson 1985), which has been applied to non-Hertzian contact problems by Kalker (1990) amongst others. The variational method has also been applied successfully the cases of frictionless contact of rough surfaces in Chapter 5 and Chapter 6. The computer algorithm and programs called **2DENCM** and **3DENCM** in FORTRAN based on the numerical solution technique of variational method have been developed for two-dimensional and three-dimensional numerical elastic contact of rough surfaces. The programs **2DENCM** and **3DENCM** can offer the following main advantages:

- (1) No iteration is involved for cases of frictionless contact where only the normal pressure needs to be determined; this facility known as a warm start for quadratic programming routine E04NAF, can lead significant saving in computational effort when solving a sequence of related problems, thus the efficiency of solution procedure is considerably improved;
- (2) There is good computational convergence and robustness, thus the distortion of solutions is eliminated;

CHAPTER 8.

(3) With only simple rewriting to the pressure constraint, i.e. $3Y > p_y > 0$ (Lee and Cheng 1992), thus the plastic deformation on the high asperity peaks are easily taken account into the present contact model without any modification of original program **ENCM**, leading to an approximate elastic-perfectly-plastic contact model.

To confirm the accuracy of program **ENCM**, a series of test cases has been studied. Comparison with existing stochastic contact models (BGK model for two-dimensional contact and GW model for three-dimensional contact) has been attempted. The results obtained for the stochastic and numerical models show an encouraging agreement considering the many difference between the two techniques.

8.1.4 Computer Check of Leakage Paths

The computer algorithm for the computer check of leakage paths has been devised and the computer program called **CCLP** has been developed in FORTRAN in Chapter 8. The program **CCLP** along with the numerical simulation of random rough surfaces and the numerical contact model of rough surfaces make it is possible to develop a simulation method for the leakage analysis of static sealed joints. The accuracy of the program is verified with manual solutions for smaller contact maps. The features of program **CCLP** can be concluded as follows:

CHAPTER 8.

- (1) It provides an effective and accurate method for determining a typical pattern of contact at which sealing occurs or not;
- (2) It not only provides the information if any leakage path exists or not for a given contact map, but also calculates the number of leakage paths, thus the width of leakage paths can be calculated by multiplying the element width by the number of leakage paths;
- (3) It allows the simulation analysis of large contact maps without having to store the whole contact map, thus computer memory can be saved so that larger systems can be simulated.

8.2 Suggestions for Further work

The research contained in this thesis has provided an overall simulation procedure for the reliability analysis of static sealed joints. However, additional research is always required to enable improvements or refinements to the studied topics and enlargements to the practical applications. This section gives a suggestion for further work, resulting from this research, which are outlined within the following three topics.

8.2.1 Numerical Simulation of Random Rough Surfaces

The random rough surfaces considered in the numerical simulation

CHAPTER 8.

model are ones with Gaussian height distribution. This is because linear transformation required for the desired autocorrelation function on independent Gaussian random variables result in Gaussian variables, while most non-Gaussian random variables do not have this property. The linear transformation also would change the probability density of the input matrix. However, the simulation algorithm can, in principle, be extended to deal surfaces with non-Gaussian height distribution provided additional relations can be obtained to relate the probability density of the input matrix and the desired probability density of the roughness heights.

The effect of linear transformations on the probability density function of a random variable can be analyzed by utilizing its characteristic function. The Fourier transform of the probability density function of a random variable is called the characteristic function of the random variable (Davenport 1970). Therefore the generation of roughness heights with non-Gaussian density functions may present more complicated problems.

8.2.2 Numerical Contact of Rough Surfaces

There are many possible improvements to the present numerical contact model. Some are listed below:

- (1) If the numerical contact model used in the leakage analysis is extended to include such as the case where one of the bodies has an elastic surface layer, as shown in Figure 8.1, the reliability of static sealed joints with gasket

CHAPTER 8.

may be analyzed.

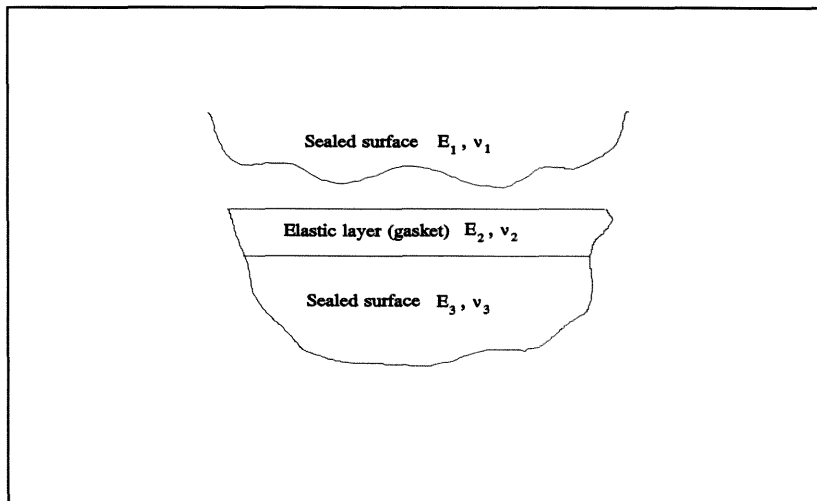


Figure 8.1 Contact model of layer elastic bodies with rough surfaces

The contact problem of layered structures has been of considerable interest in various fields of science and engineering. The Integral transforms are the usual mathematical tool employed in the contact analysis of layered structures and many publications exist in the literature dealing with two and three-dimensional layered elastic bodies subject to normal and transverse surface pressure loading (Chen 1971, Chiu and Hartnett 1983, King and Sullivan 1987, Cole and Sayles 1992).

(2) Elastic deformations of sealed surfaces interact with plastic deformation in a complex way. With a minor modifications of the contact pressure constrains by setting a ceiling on their contact pressure at the material hardness value or three times the uniaxial yield strength, i.e. $3Y > P_{ij} > 0$, as

CHAPTER 8.

done in two-dimensional contact model by Lee and Cheng (1992), the plastic deformations on the high asperity peaks are taken into account and a crude three-dimensional model of plasticity may be included. Although the proposed method is not an accurate model for plastic contact it should reproduce the main features of a mixed elastic-plastic contact model.

(3) The computer program could be installed on a more powerful computer, many of its limitations being due to the relatively small amount of computer memory available, so that an area of more reasonable size can be analyzed.

8.2.3 Reliability Analysis of Static Sealed Joints

There are many further studies that can be done. Some are listed below:

(1) To prevent leakage, a certain level of contact stress must be maintained between sealed surfaces. The contact pressure was assumed to be static in this thesis. However, it is important to realise that this contact stress will vary with time. This time effect arise form several sources:

- changes of fluid pressure and temperature, with associated flange distortions;
- creep in highly stressed regions of the bolts and flanges.
- stress relaxation in the gasket material;

CHAPTER 8.

This variation of contact stress will affect the sealing performance. Therefore, the effect of variation of contact stress on the reliability of static sealed joints should be taken into account.

(2) The contact ratio criteria listed in Table 7.3 is derived for a certain simulation conditions. In order to practical use, more simulations are required to obtain more accurate value of contact ratio criteria , such as:

- (a) the relationship between the contact ratio criteria and the sampling interval;
- (b) the relationship between the contact ratio criteria and the surface anisotropy;
- (c) the effect of plastic deformation on the contact ratio criteria;
- (d) the effect of gasket material on the contact ratio criteria;
- (e) the effect of system pressure and environmental pressure on the contact ratio criteria;
- (f) the effect of fluid viscosity on the contact ratio criteria.

(3) In order to practical use, experimental work is required to evaluate its validity.

APPENDIX A.

Quadratic Programming Routine - E04NAF

E04NAF is designed to solve the quadratic programming (QP) program - the minimization of a quadratic function subject to a set of linear constraints on the variables. The problem is assumed to be stated in the following form:

$$\begin{aligned} & \underset{x \in R^n}{\text{Minimize!}} \quad c^T x + \frac{1}{2} x^T H x \\ & \text{Subject to :} \quad l \leq \begin{pmatrix} x \\ Ax \end{pmatrix} \leq u \end{aligned} \tag{A.1}$$

where c is a constant n -vector and H is a constant $n \times n$ symmetric matrix: Note that H is the Hessian matrix (matrix of second partial derivatives) of the quadratic objective function. The matrix A is $m \times n$, where m may be zero; A is treated as a dense matrix.

The constraints involving A will be called the general constraints. Note that the upper and the lower bounds are specified for all the variables

APPENDIX A.

and for all the general constraints. The form of Equation (A.1) allows full generality in specifying other types of constraints. In particular, an equality constraint is specified by setting $l_i = u_i$.

E04NAF allows the user to provide the indices of the constraints that are believed to be exactly satisfied at the solution. This facility, known as a warm start, can lead to significant saving in computational effort when solving a sequence of related problems.

APPENDIX B.

Calculation of Bandwidth Parameter

Lai and Cheng (1985) have derived the expression for the calculation of bandwidth parameter after the long- and short-wavelength cutoffs.

In order to defined the bandwidth parameter, moments of power spectrum density (PSD) are needed. Nth moment of PSD is defined as

$$M_n = \int_{-\infty}^{\infty} \phi(k) k^n dk \quad (\text{B.1})$$

Assuming exponential autocorrelation function,

$$R(r) = m_0 \exp\left(\frac{-|r|}{\beta}\right) \quad (\text{B.2})$$

the corresponding PDS is

$$\begin{aligned} \phi(k) &= \frac{1}{2\pi} \int_{-\infty}^{\infty} R(r) \exp(-ikr) dr \\ &= \frac{m_0}{\pi} \frac{\beta}{1 + (\beta k)^2} \end{aligned} \quad (\text{B.3})$$

APPENDIX B.

Because of the long- and short-wavelength cutoffs, $\phi(k)$ is modified as

$$\phi(k) = \begin{cases} \frac{m_0}{\pi} \frac{\beta}{1 + (\beta k)^2} & k_l \leq |k| \leq k_h \\ 0 & \text{otherwise} \end{cases} \quad (\text{B.4})$$

where

$$\begin{aligned} k_l &= \frac{2\pi}{\lambda_l} \\ k_h &= \frac{2\pi}{\lambda_h} \end{aligned} \quad (\text{B.5})$$

λ_l is long-wavelength cutoff and λ_h is short-wavelength cutoff.

Accordingly, the zero, second and fourth moment of PSD are obtained as:

$$\begin{aligned} \overline{m_0} &= \frac{2m_0}{\pi} \tan^{-1} \beta k \Big|_{k=k_l}^{k=k_h} \\ \overline{m_2} &= \frac{2m_0}{\pi \beta^2} (\beta k - \tan^{-1} \beta k) \Big|_{k=k_l}^{k=k_h} \\ \overline{m_4} &= \frac{2m_0}{\pi \beta^4} \left[\frac{1}{3} (\beta k)^3 - \beta k + \tan^{-1} \beta k \right] \Big|_{k=k_l}^{k=k_h} \end{aligned} \quad (\text{B.6})$$

APPENDIX B.

and bandwidth parameter is

$$\bar{\alpha} = \frac{\overline{m_0} \overline{m_4}}{\overline{m_2}^2} \quad (\text{B.7})$$

By setting

$$\lambda_t = 2r_t, \quad \lambda_h = 2r_s, \quad \lambda^* = 2.3\beta \quad (\text{B.8})$$

where r_t is the width of the normal region analyzed and r_s is sampling interval.

APPENDIX C.

Simulated Results of Leakage Probability of Static Sealed Joints

Table C.1 (a) Predicted variation of leakage probability as a function of load, showing the effect of rough surfaces†

Leakage probability P_L (%)	Dimensionless contact load - $P_a / A_n E'$		
	$\sigma = 0.1 \mu\text{m}$ $\lambda^* = 20 \mu\text{m}$	$\sigma = 0.3 \mu\text{m}$ $\lambda^* = 20 \mu\text{m}$	$\sigma = 0.5 \mu\text{m}$ $\lambda^* = 20 \mu\text{m}$
100	0.000769	0.002482	0.004042
100	0.000851	0.002728	0.004251
100	0.000935	0.002852	0.004464
99	0.000977	0.002978	0.004673
98	0.001019	0.003105	0.004883
95	0.001062	0.003232	0.005308
91	0.001105	0.003361	0.005523
87	0.001148	0.003493	0.005741
74	0.001192	0.003626	0.005961
61	0.001237	0.003759	0.006183
42	0.001281	0.003894	0.006406
22	0.001326	0.004029	0.006630

APPENDIX C.

10	0.001371	0.004166	0.006856
5	0.001417	0.004302	0.007084
3	0.001462	0.004439	0.007312
1	0.001508	0.004577	0.007541
0	0.001554	0.004715	0.007771
0	0.001600	0.004853	0.008002
0	0.001647	0.004993	0.008235

where the rough surfaces used are generated to have 50×50 sampling points and sampling interval of $\Delta x = \Delta y = \lambda$.

APPENDIX C.

Table C.1 (b) Predicted variation of leakage probability as a function of load, showing the effect of rough surfaces†

Leakage probability P_L (%)	Dimensionless contact load - $P_a / A_n E'$		
	$\sigma = 0.1 \mu\text{m}$ $\lambda^* = 30 \mu\text{m}$	$\sigma = 0.3 \mu\text{m}$ $\lambda^* = 30 \mu\text{m}$	$\sigma = 0.5 \mu\text{m}$ $\lambda^* = 30 \mu\text{m}$
100	0.000486	0.001771	0.002564
100	0.000513	0.001853	0.002700
100	0.000540	0.002019	0.002976
99	0.000568	0.002104	0.003256
98	0.000595	0.002189	0.003397
95	0.000623	0.002275	0.003539
91	0.000651	0.002362	0.003682
87	0.000679	0.002450	0.003827
74	0.000708	0.002628	0.003974
61	0.000736	0.002717	0.004122
42	0.000765	0.002808	0.004270
22	0.000795	0.002989	0.004420
10	0.000824	0.003172	0.004571
5	0.000854	0.003264	0.004722
3	0.000884	0.003356	0.004875
1	0.000914	0.003448	0.005027
0	0.000944	0.003540	0.005181
0	0.000973	0.003727	0.005335
0	0.001005	0.003914	0.005490

†where the rough surfaces used are generated to have 50×50 sampling points and sampling interval of $\Delta x = \Delta y = \lambda^*$.

APPENDIX C.

Table C.1 (c) Predicted variation of leakage probability as a function of load, showing the effect of rough surfaces†

Leakage probability P_L (%)	Dimensionless contact load - $P_a / A_n E'$		
	$\sigma = 0.1 \mu\text{m}$ $\lambda^* = 40 \mu\text{m}$	$\sigma = 0.3 \mu\text{m}$ $\lambda^* = 40 \mu\text{m}$	$\sigma = 0.5 \mu\text{m}$ $\lambda^* = 40 \mu\text{m}$
100	0.000385	0.000968	0.001296
100	0.000426	0.001007	0.001362
100	0.000467	0.001086	0.001495
99	0.000488	0.001165	0.001563
98	0.000510	0.001205	0.001630
95	0.000531	0.001246	0.001699
91	0.000552	0.001287	0.001767
87	0.000574	0.001328	0.001837
74	0.000596	0.001411	0.001908
61	0.000618	0.001495	0.001978
42	0.000641	0.001578	0.002050
22	0.000663	0.001663	0.002122
10	0.000686	0.001748	0.002194
5	0.000708	0.001791	0.002267
3	0.000731	0.001834	0.002340
1	0.000754	0.001877	0.002413
0	0.000777	0.001920	0.002487
0	0.000802	0.001964	0.002561
0	0.000823	0.002008	0.002635

†where the rough surfaces used are generated to have 50×50 sampling points and sampling interval of $\Delta x = \Delta y = \lambda^*$.

APPENDIX C.

Table C.1 (d) Predicted variation of leakage probability as a function of load, showing the effect of rough surfaces†

Leakage probability P_L (%)	Dimensionless contact load - $P_a / A_n E'$		
	$\sigma = 0.1 \mu\text{m}$ $\lambda^* = 50 \mu\text{m}$	$\sigma = 0.3 \mu\text{m}$ $\lambda^* = 50 \mu\text{m}$	$\sigma = 0.5 \mu\text{m}$ $\lambda^* = 50 \mu\text{m}$
100	0.000308	0.000553	0.001538
100	0.000324	0.000626	0.001703
100	0.000357	0.000700	0.001869
99	0.000391	0.000775	0.001953
98	0.000408	0.000852	0.002038
95	0.000425	0.000932	0.002123
91	0.000442	0.001014	0.002209
87	0.000459	0.001096	0.002296
74	0.000477	0.001181	0.002385
61	0.000495	0.001267	0.002473
42	0.000512	0.001353	0.002562
22	0.000530	0.001441	0.002652
10	0.000548	0.001530	0.002742
5	0.000567	0.001621	0.002833
3	0.000585	0.001712	0.002925
1	0.000603	0.001804	0.003016
0	0.000622	0.001897	0.003109
0	0.000640	0.001990	0.003201
0	0.000659	0.002085	0.003294

†where the rough surfaces used are generated to have 50×50 sampling points and sampling interval of $\Delta x = \Delta y = \lambda^*$.

APPENDIX C

Table C.2 Predicted variation of leakage probability as a function of load, showing the effect of sampling interval†

Leakage probability P_L (%)	Dimensionless contact load - $P_a / A_r E'$	
	$\Delta x = \Delta y = 1/2 \lambda^*$	$\Delta x = \Delta y = \lambda^*$
100	0.002139	0.000968
100	0.002373	0.001007
100	0.002611	0.001086
99	0.002731	0.001165
98	0.002852	0.001206
95	0.002974	0.001246
91	0.003098	0.001287
87	0.003222	0.001328
74	0.003347	0.001411
61	0.003474	0.001495
42	0.003603	0.001579
22	0.003734	0.001663
10	0.003865	0.001748
5	0.003999	0.001791
3	0.004133	0.001834
1	0.004268	0.001877
0	0.004403	0.001920
0	0.004539	0.001964
0	0.004677	0.002008

†where the rough surfaces used are generated to have 50×50 sampling points and roughness parameters of $\sigma = 0.3 \mu\text{m}$ and $\lambda^* = 40 \mu\text{m}$

APPENDIX C.

Table C.3 Predicted variation of leakage probability as a function of load, showing the effect of number of sampling points†

Dimensionless contact load $P_a / A_n E'$	Leakage probability - P_L (%)		
	sampling points 50 × 50	sampling points 30 × 30	sampling points 20 × 20
0.004042	100	100	100
0.004251	100	100	100
0.004464	100	100	99
0.004673	99	99	97
0.004883	98	96	95
0.005308	95	93	88
0.005523	91	86	84
0.005741	87	83	72
0.005961	74	76	70
0.006183	61	54	57
0.006406	42	38	46
0.006630	22	31	31
0.006856	10	13	22
0.007084	5	8	12
0.007312	3	2	6
0.007541	1	1	4
0.007771	0	0	1
0.008002	0	0	0
0.008235	0	0	0

†where the rough surfaces used are generated to have the sampling interval of $\Delta x = \Delta y = \lambda$ and the roughness parameters of $\sigma = 0.5 \mu\text{m}$ and $\lambda^* = 20 \mu\text{m}$.

REFERENCES

- [1] Archard, J. F., Hunt, T. R., and Onions, R. A. (1975). "**Stylus profilometry and the analysis of the contact of rough surfaces.**" Proc. UITAM Symp. on the Mechanics of the contact of deformable bodies, Delft Univ. Press, Delft.
- [2] Azarkhin, A. (1988) "**Some history-dependent problems for dissimilar cylinders with finite friction.**" ASME Journal of Applied Mechanics, Vol. 55, 81-86.
- [3] Bentall, R. H., and Johnson, K. L. (1967) "**Slip in the rolling contact of two dissimilar elastic rollers.**" Int. J. Mech. Sci., 9, 389-404.
- [4] Bush, A. W., Gibson, R. D., and Thomas, T. R. (1975). "**The elastic contact of a rough surface,**" Wear, Vol. 35, 87-111.
- [5] Bush, A. W., Gibson, R. D., and Keogh, G. P. (1979). "**Strongly anisotropic rough surfaces.**" ASME Journal of Lubrication Technology, Vol. 101, 15-20.
- [6] Chang, W. R., Etsion, I., and Bogy, D. B. (1987) "**An elastic-plastic model for the contact of rough surfaces.**" Journal of Tribology, vol. 109, 257-263.
- [7] Chen, W. T. (1971) "**Computation of stresses and displacements in a layered elastic medium.**" International Journal of Engineering Science, Vol. 9, 775-800.

REFERENCES

- [8] Childs, T. H. C., (1973) "**The persistence of asperities in indentation experiments,**" *Wear*, Vol. 25, 3-16.
- [9] Chiu, Y. R., and Hartnett, M. J. (1983) "**A numerical solution for layered solid contact problems with application to bearings.**" *ASME Journal of Lubrication Technology*, Vol. 105, 585-590.
- [10] Cole, S. J., and Sayles, R. S. (1992) "**A numerical model for the contact of layered elastic bodies with real rough surfaces.**" *Transactions of the ASME, Journal of Tribology*, vol. 114, 334-340.
- [11] Davenport, W. B. (ed.) (1970). "**Probability and random processes.**" McGraw-Hill, New York.
- [12] de Mul, J. M., Kalker, J. J. and Fredriksson, B. (1986) "**The contact between arbitrarily curved bodies of finite dimensions.**" *Transactions of the ASME, Journal of Tribology*, vol. 108, 140-148.
- [13] Etsion, I. and Front, I. (1994). "**A model for Static Sealing Performance of End Face Seals.**" *Tribology Transactions*, Vol.37, 1, 111-119.
- [14] Fichera, G. (1964) "**Problemi elastostatici con vincoli unilaterale: il problema di signorini con ambigue condizioni al contorno.**" *Mem. Accad. Naz. Lincei, Series 8*, 7, 91.
- [15] Flamant. (1892) *Compt. Rend.*, 114, pp1465, Paris.
- [16] Flitney, R. K., Nau, B. S., and Reddy, D. (1984). "**The Seal Users Handbooks.**" RHRA, The Fluid Engineering Centre.
- [17] Gill, P. E., Murray, W., Saunders, M. A., and Wright, M. H. (1983)

REFERENCES

- "User's guide or SOL/QPSOL."** Report SOL 83-7. Department of Operations Research, Stanford University, California, 1983.
- [18] Greenwood, J. A. and Williamson, J. B. P. (1966). **"Contact of nominally flat surfaces,"** Proc. Roy. Soc. London, Vol. A 295, 300-319.
- [19] Greenwood, J. A. and Tripp, J. H. (1967). **"The elastic contact of rough surfaces,"** ASME Journal of Applied Mechanics, Vol. 34, 153-159..
- [20] Greenwood, J. A. (1967) **"The area of contact between rough surfaces and flats,"** ASME Journal of Lubrication Technology, Vol. 89, 81-91.
- [21] Greenwood, J. A. and Tripp, J. H. (1971). **"The contact of two nominally flat rough surfaces."** Proc. Instn. Mech. Engrs., Vol. 185, 625-633.
- [22] Greenwood, J. A. (1984). **"A unified theory of surface roughness."** Proc. Roy. Soc. A393, 133-157.
- [23] Hartnett, M. J. (1980) **"A general numerical solution for elastic body contact problems,"** ASME Solid contact and Lubrication, Cheng and Kerr, ed., 51-66, AMD-39.
- [24] Hertz, H. (1896). **"On the contact of rigid elastic solids and on hardness,"** Miscellaneous papers, Macmillian, London.
- [25] Hutchings, I. M. (ed.) (1992). **"Friction and wear of engineering materials."** Edward Arnold, A division of Hodder & Stoughton , London.

REFERENCES

- [26] Johnson, K. L. (1982). "**One hundred years of Hertz contact,**" Proc. I. Mech. Eng., Vol.196, No 39, 363-378.
- [27] Johnson, K. L. (1985) "**Contact mechanics.**" Cambridge University Press.
- [28] Kalker, J. J. (1971) "**A minimum principle for the law of dry friction with application to elastic cylinders in rolling contact (part. 1).**" ASME Journal of Applied Mechanics, Vol. 38, 875-880.
- [29] Kalker, J. J. (1977) "**Variational principles of contact elastostatics.**" Journal Inst. Math. & Appl. Vol 20, 199.
- [30] Kalker, J. J. (1978) "**Numerical contact elastostatics.**" In contact problems and load transfer in mechanics assemblages, Proc.Euromech Coll. No. 10, Sweden.
- [31] Kalker, J. J. (1990) "**Three-dimensional elastic bodies in rolling contact.**" Kluwer, Dordrecht.
- [32] King, R. B., and Sullivan, T. C. (1987) "**Sliding contact stresses in a two-dimensional layered elastic half-space.**" International Journal of Solids and structures, Vol. 23, No. 5, 581-597.
- [33] Lai, W. T., and Cheng, H. S. (1985). "**Computer simulation of elastic rough contact.**" ASME Transactions, Vol. 28, 2, 172-180.
- [34] Lee. S. C. and Cheng. H. S. (1992). "**On the relation of load to average gap in the contact between surfaces with longitudinal roughness,** Tribology Transactions, Vol. 35, No. 3, 523-529.
- [35] Longuet-Higgins, M. S. (1957a). "**The statistical analysis of a**

REFERENCES

- random, moving surface,"** Phil. Trans. Roy. Soc. Vol. A249, 321-387.
- [36] Longuet-Higgins, M. S. (1957b). "**Statistical properties of an isotropic random surface,**" Phil. Trans. Roy. Soc. Vol. A250, 157-174.
- [37] Love, A. E. H. (1927). "**A treatise on the mathematical theory of elasticity.**" Cambridge University Press. Cambridge.
- [38] McCool, J. I. (1986). "**Comparison of models for the contact of rough surfaces.**" Wear, Vol. 107, 37-60.
- [39] Merriman, T. and Kannel, J. (1989). "**Analysis of the role of surface roughness on contact stresses between elastic cylinders with and without soft surface coating,**" ASME Journal of Tribology, Vol. 111, 87-94.
- [40] Mitchell, L. A., and Rowe, M. D. (1967/1968). "**Assessment of face seal performance based on the parameters of a statistical representation of surface roughness.**" The Institution of Mechanical Engineering Proceeding. 182, part 3K, 101-107.
- [41] Mitchell, L. A., and Rowe, M. D. (1969). "**Influence of asperity deformation mode on gas leakage between contacting surfaces.**" J. Mech. Eng. Sci., 11, 534-545.
- [42] Mostofi, A. and Gohar, R. (1984). "**The use of various types of pressures element in some elastic contact problems.**" Proc. Instn. Mech. Engrs., Vol. 198C, No. 12, 189-196.
- [43] Nayak, P. R. (1971). "**Random process model of rough surfaces.**" Transactions of the ASME, July, 1971, 398-406.

REFERENCES

- [44] Ogilvy, J. A. (1991). "**Theory of wave scattering from random rough surfaces**", Bristol: Adam Hilger.
- [45] Ogilvy, J. A. (1992). "**Numerical simulation of elastic-plastic contact between anisotropic rough surfaces.**", Journal of Physics, D: Applied physics. Vol. 25, 1798-1809.
- [46] Onions, R. A. and Archard, J. F. (1973). "**The contact of surfaces having a random structure.**" Journal of Physics, D: Applied physics. Vol. 6, 289-304.
- [47] Patir, N. (1978) "**A numerical procedure for random generation of rough surfaces**", Wear, Vol. 47, 263-277.
- [48] Patir, N. and Cheng, H. S. (1978). "**A average flow model for determining effects of three dimensional roughness on partial hydrodynamic lubrication.**" ASME Journal of Lubrication Technology, Vol. 100, 2. 12-17.
- [49] Peklenik, J. (1967/1968). "**New developments in surface characterization and measurements by means of random process analysis.**" Proceeding of Institute of Mechanical engineer, 182, Part 3K, 108-126.
- [50] Rathbun, F. O. (ed.) (1963). "**Design criteria for zero-leakage connectors for launch vehicles.**" No. 3, NASA, contract report N63-18159, CR-50559.
- [51] Rektoys, K. (1969). "**Survey of applicable mathematics.**" London.
- [52] Sainsot, P. (1989). "**Effect of surface coatings in a rough normally loaded contact.**" Mechanics of coatings, Proceedings of the 16th

REFERENCES

- leeds-lyon Symposium on Tribology held at INSA, Lyon, France.
- [53] Sayles, R. S. and Thomas, T. R. (1979). "**Measurements of the statistical microgeometry of engineering surfaces.**" ASME Journal of Lubrication Technology, Vol. 101, 409-417.
- [54] SEA Gasket Subcommittee of SAE Seal Committee (ed.), "**Gasket and joint design manual for engine and transmission systems.**"
- [55] Shimomura, T., Kiryu, K., Hirabayashi, H. and Nakajima, T. (1989). "**A Study of The Relationship Between Sealing Performance and Surface Characteristics of End Face Seals.**" Lubrication Engineering, Vol. 45, 12, 785-791.
- [56] Sigh, K. P. and Paul, B. (1974). "**Numerical solution of non-Hertzian elastic contact problems,**" ASME Journal of Applied Mechanics, Vol. 41, 484-490.
- [57] Stauffer, D. (1985). "**Introduction to percolation theory.**" Taylor & Francis.
- [58] Summers-Smith, J. D. (ed.) (1988). "**Mechanical seal practice for improved performance.**" I.Mech.E., London.
- [59] Tabor, D. (1951). "**The hardness of metals.**" Oxford University Press, Oxford, England.
- [60] Thomas, T. R. (1973). "**Influence of roughness on the deformation of metal surfaces in static contact.**" Proc. 6th International Conference on Fluid Sealing, Munich, German, B3, 33-48.
- [61] Thomas, T. R. (1982). "**Rough surfaces.**" Longman, London.

REFERENCES

- [62] Timoshenko, S. (1951) "**Theory of Elasticity.**" McGraw-Hill, London.
- [63] Tsukizoe, T., and Hisakado, T. (1965). "**On the mechanism of contact between metal surfaces - the penetrating depth and the average clearance.**" Trans. Am. Soc. Mech. Engrs. 87D, 666-672.
- [64] Webster, N. M., West, M. A., and Sayles, R. S. (1986). "**A method of three-dimensional topography measurement and analysis of arcuate surfaces.**" Wear, 109, 385-399.
- [65] Webster, M. N. and Sayles, R. S. (1986). "**A numerical model for the elastic frictionless contact of real rough surfaces,**" ASME Journal of Tribology, Vol. 108, 314-320.
- [66] West, M. A. and Sayles, R. S. (1988). "**A 3-dimensional method of studying 3-body contact geometry and stress on real rough surfaces.**" In interface Dynamics, Proc. 14th Leeds-Lyon Symposium on Tribology (eds. Dowson, D., Taylor, C. M., Godet, M., and Berthe, D.), Elsevier, Amsterdam, 195-200.
- [67] Whitehouse, D. J. and Archard, J. F. (1970). "**The properties of random surfaces of significance in their contact**", Proc. R. Soc. London, Vol. A316, 97-121.
- [68] William, H. P. (1992). "**Numerical recipes in Fortran - the art of scientific computing.**" Cambridge University.
- [69] Williamson, J. B. P. (1967/1968). "**The microtopography of solid surfaces.**" Proc. Inst. Mech. Engrs., 182, Part 3K, 21-30.
- [70] Williamson, J. B. P., Pullen, J., and Hunt, R. T. (1970). "**The shape**

REFERENCES

- of solid surfaces.**" in "Surface Mechanics.", ASME., New York, 24-35.
- [71] Xian Liang and Zheng Linqing (1991). "A numerical model for the elastic contact of three-dimensional real rough surfaces." *Wear*, Vol., 91-100.